REPORT DOCUMENTATION PAGE

Form Approved OMB NO. 0704-0188

1. REPORT DATE (DD-MM-YYYY)	2. REPORT TYPE	3. DATES COVERED (From - To)
22-04-2019	Final Report	1-Nov-2013 - 30-Apr-2018

4. TITLE AND SUBTITLE

Final Report: Rational Engineering of Reactive Nanolaminates for Tunable Ignition and Power

5a. CONTRACT NUMBER
W911NF-13-1-0493

5b. GRANT NUMBER

5c. PROGRAM ELEMENT NUMBER
611102

6. AUTHORS

5d. PROJECT NUMBER

5e. TASK NUMBER

5f. WORK UNIT NUMBER

7. PERFORMING ORGANIZATION NAMES AND ADDRESSES

North Carolina State University
2701 Sullivan Drive
Admin Srvcs III, Box 7514
Raleigh, NC 27695 -7514

8. PERFORMING ORGANIZATION REPORT NUMBER

9. SPONSORING/MONITORING AGENCY NAME(S) AND ADDRESS (ES)

U.S. Army Research Office
P.O. Box 12211
Research Triangle Park, NC 27709-2211

10. SPONSOR/MONITOR'S ACRONYM(S)
ARO

11. SPONSOR/MONITOR'S REPORT NUMBER(S)
63686-EG.6

12. DISTRIBUTION AVAILIBILITY STATEMENT

Approved for public release; distribution is unlimited.

13. SUPPLEMENTARY NOTES

The views, opinions and/or findings contained in this report are those of the author(s) and should not contrued as an official Department of the Army position, policy or decision, unless so designated by other documentation.

14. ABSTRACT

15. SUBJECT TERMS

16. SECURITY CLASSIFICATION OF:			17. LIMITATION OF ABSTRACT	15. NUMBER OF PAGES	19a. NAME OF RESPONSIBLE PERSON
a. REPORT	b. ABSTRACT	c. THIS PAGE			Jon-Paul Maria
UU	UU	UU	UU		19b. TELEPHONE NUMBER: 919-522-9310

RPPR Final Report
as of 22-Apr-2019

Agency Code:

Proposal Number: 63686EG **Agreement Number: W911NF-13-1-0493**
INVESTIGATOR(S):

Name: Donald Brenner Ph.D.
Email: brenner@ncsu.edu
Phone Number: 9195151338
Principal: N

Name: Douglas L Irving Phd
Email: dlirving@ncsu.edu
Phone Number: 9195156154
Principal: N

Name: Jon-Paul Maria
Email: jpmaria@ncsu.edu
Phone Number: 9195229310
Principal: Y

Organization: **North Carolina State University**
Address: 2701 Sullivan Drive, Raleigh, NC 276957514
Country: USA

DUNS Number: 042092122 EIN: 566000756
Report Date: 31-Jul-2018 Date Received: 22-Apr-2019
Final Report for Period Beginning 01-Nov-2013 and Ending 30-Apr-2018
Title: Rational Engineering of Reactive Nanolaminates for Tunable Ignition and Power
Begin Performance Period: 01-Nov-2013 **End Performance Period:** 30-Apr-2018
Report Term: 0-Other

Submitted By: Donald Brenner Email: brenner@ncsu.edu
Phone: (919) 515-1338

STEM Degrees: 1 **STEM Participants:** 0

Major Goals: The team of Maria, Brenner, and Irving propose a collaborative experimental-computational investigation of reactive nanocomposite structures identified as attractive new energetic materials with the potential for tunable power via engineered ignition. The material combinations belong to a family of metal/metal oxide nanolaminates that are thermodynamically predisposed to the rapid release of chemical energy via ion exchange. The energy densities are up to four times larger than values accessible to conventional organics (i.e., RDX) and there are electrical ignition possibilities that span local to volumetric geometries. Consequently we foresee a new generation of energetic composites that, in conjunction with conventional materials, create a new capability to design and fabricate munitions with tunable lethality.

The nanocomposites comprise oxygen sources like CuO and oxygen sinks like Cr. The exchange of oxygen from source to sink is accompanied by energy liberation in the range of 5 kJ/cc. Material combinations that support this exchange are historically categorized as a thermites, and though known for many years and optimized for temperature generation, opportunities for high power remain underexplored. The intent of this program to build upon the most important lessons from our prior research:

1 Crystallinity, structure, covalency, and relative molar volume of the terminal oxide controls oxygen exchange kinetics and power. This was demonstrated by comparing Zr and Al oxygen sinks, both of which have similar free energies of oxidation, yet Zr stacks are potentially more powerful (at an equivalent thickness) owing to their rapid oxygen transport.
2 The temperature onset of self-sustaining reactions in nanolaminates can be tuned via the interface density, i.e., the number of layers in a stack with total thickness held constant.
3 Multiscale modeling suggests that joule heating of laminates with physical macro/microstructure engineered for regulating heat flow can further tune the reaction profile.

4 First principles calculations that model interface transport via point defect creation suggest a method to evaluate the energy barriers to the initial stages of exothermic reactions.

Guided by these lessons the PIs will continue to explore energetic nanolaminates based on ion exchange with a focus on engineering rates of energy release by combining a detailed understanding of the defect equilibrium chemistry that controls transport with macroscopic design principles that control Joule heating and thermal energy partitioning. These methods are based on understanding, and thus exploiting: 1) the initial barriers to ion exchange; 2) the mechanisms of mass transport; 3) how material properties like electrical and thermal conductivity regulate heat accumulation and dissipation; and 4) how thermal boundary conditions can be used to "shape" self-sustaining reactions.

Accomplishments: PDF file with accomplishments is attached

Training Opportunities:
Evyn Lee, who joined our ARO program as a new graduate student in July 2016 finished her Masters degree on this program in May of 2018. She continued to develop skills in materials preparation, materials characterization, and disseminating her work in a written thesis.

Results Dissemination: There is a complete Masters Thesis of Evyn Lee available on the NCSU library public website. It is attached to this final report.

Honors and Awards: Nothing to Report

Protocol Activity Status:

Technology Transfer: Nothing to Report

PARTICIPANTS:

Participant Type: Graduate Student (research assistant)
Participant: Evyn Lee
Person Months Worked: 9.00 **Funding Support:**
Project Contribution:
International Collaboration:
International Travel:
National Academy Member: N
Other Collaborators:

Participant Type: PD/PI
Participant: Jon-Paul Maria
Person Months Worked: 1.00 **Funding Support:**
Project Contribution:
International Collaboration:
International Travel:
National Academy Member: N
Other Collaborators:

ARTICLES:

RPPR Final Report
as of 22-Apr-2019

Publication Type: Journal Article Peer Reviewed: Y **Publication Status:** 5-Submitted
Journal: Thin Solid Films
Publication Identifier Type: Publication Identifier:
Volume: Issue: First Page #:
Date Submitted: Date Published: 11/7/16 6:09PM
Publication Location:
Article Title: Interfacial Analysis of Multilayered Nanothermite
Authors: Ed Mily, Edward Savhet, Ramon Collazo, Zlatko Sitar, and Jon-Paul Maria
Keywords: thermite, XPS, thin film, sputtering
Abstract: The authors report a series of experiments designed to probe the limits of interface formation in reactive nanolaminate multilayers using an in situ surface science approach. CuO was used as the oxygen source while Al and Zr were used as reactive companion metals. Si substrates were sputter coated with thin CuO films, then loaded into a UHV system for metal deposition and x-ray photoelectron spectroscopy analysis without further atmospheric exposure. Initial XPS analysis confirmed a surface stoichiometry of CuO. Metal films were deposited one monolayer at a time with spectra collected after each layer. The pre-reacted thicknesses of Al2O3 and ZrO2 that formed during deposition were 2 nm and 3 nm respectively. Oxide formation was deposition rate dependent: thicker oxide layers form under slower deposition rates. Complementary thickness analysis was carried out using X-ray reflectivity measurements. For evaporation at slow rates, these measurements indicate the minimum interfacial thickn
Distribution Statement: 1-Approved for public release; distribution is unlimited.
Acknowledged Federal Support: **Y**

DISSERTATIONS:

Publication Type: Thesis or Dissertation
Institution:
Date Received: 15-Sep-2015 Completion Date:
Title: Computational Study of Grain Boundaries and Nano-Reactive Materials
Authors:
Acknowledged Federal Support:

Publication Type: Thesis or Dissertation
Institution:
Date Received: 15-Sep-2015 Completion Date:
Title: Thermite at the Nano-Scale
Authors:
Acknowledged Federal Support:

Technical Summary of Program Results for 2016-2018

Experimental Studies

Exploring Intermetallic formation in Al/CuO System

In the bulk system, the thermite reaction has been traditionally treated as a reduction- oxidation reaction between a metal and a metal oxide. In the nano-regime, this still holds true in the beginning and end of the reaction, but the question arises: what intermediate steps are occurring between the initiation and completion of the reaction? In the bulk reaction, intermediate or secondary reactions that occur on the nano-scale may be negligible. When the morphology of the reaction is decreased to the nano-scale, these secondary reactions begin to play a larger role, and may alter the characteristics of the reaction entirely. Diffusion at the interface begins to govern the reaction.

Traditionally, the main mechanism for nano-scale thermite in the lower activation energy regime is considered to be solid-state ion transport In prior work, it has been observed that exothermic activity was seen below the melting point of aluminum, 660 °C. DSC studies of CuO and passivized Al nano-particles has shown evidence of reaction occurring at 570 °C, with $CuAlO_2$ formation in a 2:1 ratio of Al:CuO at 1000 °C, as well as Cu_2O formation. Al/CuO nano-composites reacted showed evidence of multiple intermetallic constituents forming. The evidence of melting suggests that the reaction mechanism is shifting from a traditional solid-state ion transport to a different mechanism involving a molten state of the metals, as well as parallel reactions occurring.

This program year our group focused on better characterizing this possibility in the Al-CuO system using in situ high temperature x-ray diffraction to monitor phase evolition and exploring the bigger question of what entity moves first across the original metal metal-oxide boundary. Figure 1 shows the different possibilities.

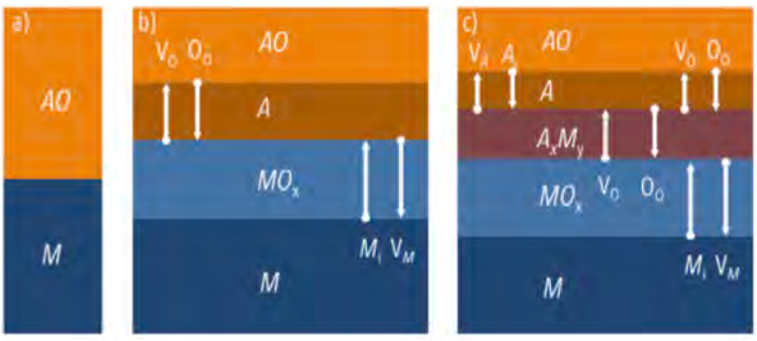

Figure 1: a) The initial geometry of an *AO* and *M* bilayer. **b)** The solid-state ion diffusion model showing movement of the oxygen from *AO* and the metal from *M* to form the final oxide MO_x. **c)**

The proposed model with the formation of an intermetallic A_xM_y between the final constituents of the bilayer.

A twenty-bilayer RNL sample was layered in an alternating geometry on a 2” diameter sapphire substrate via physical vapor deposition using dual beam magnetron sputtering. The total stack thickness was 2 micometers. The sample was allowed to rest for twenty minutes between depositions, and an hour every four bilayers. Deposition rates were determined via X-Ray reflectivity (XRR). Al was deposited at 11 nm/min using DC magnetron sputtering at 4 mTorr. CuO was deposited at 15 nm/min using RF magnetron sputtering at 2 mTorr. The resulting sample contained twenty bilayers of Al/CuO, comprised of 37 nm of Al and 67 nm of CuO, with an overall thickness of approximately 2 microns.

The samples were placed in an XRK 900 Reactor Chamber with an N_2 environment at a flow rate of 20 sccm. The sample was heated at 5 °C/min, and held at 900 °C for 30 minutes, and cooled at 5 °C/min. The sample was analyzed at a 2theta range of 30°- 60° with an omega offset of 2° to limit the presence of the substrate. The results were analyzed for the existence of the final constituents and the presence of possible intermetallic peaks.

The resulting x-ray pattern shows ignition, as indicated by the presence of two prominent Cu peaks at 42.8° and 50° (indicated by the symbol ¢), seen below in Figure 2

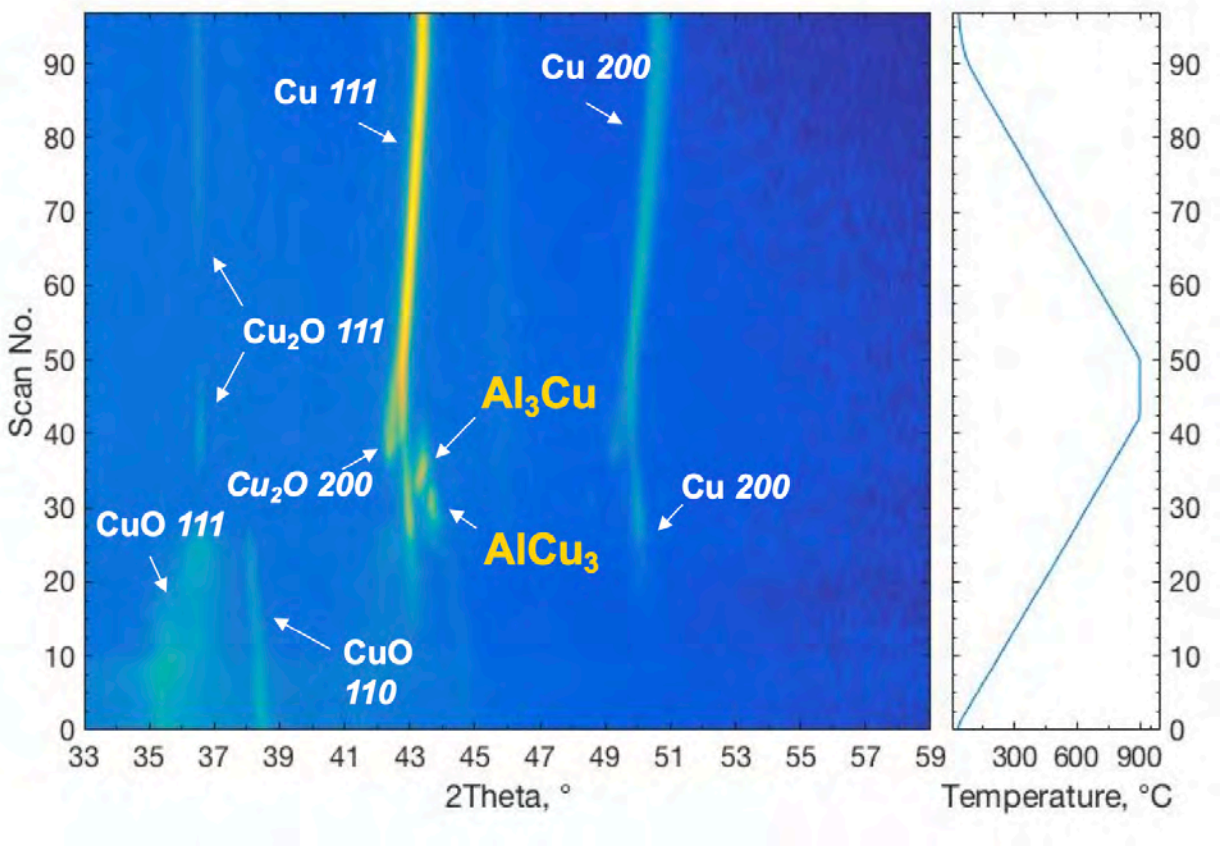

Figure 2: In situ XRD maps for CuO-Al nanolaminates showing intermediate phase formation

There are several areas of interest. Two prominent peaks appear at room temperature, consistent with the presence of monoclinic CuO, 35.38° and 38.56°. The as deposited CuO takes the form of monoclinic CuO, as seen in prior work. A strain of the peaks is expected at low thin film thicknesses. At approximately 423 °C, the 35.38° peak begins to shift towards 36.53°, consistent with the formation of Cu_2O. The most prominent Cu peak begins to appear around 42.48°.

Due to the amorphous nature of sputtered Al, and the forming amorphous Al_2O_3 constituent, the reaction onset and completion is characterized by the formation of Cu. The resulting diffraction pattern shows an end result with Cu peaks present at approximately 42.8° and 50°. The presence of Cu is seen as early as 300 °C, but reaches a prominent intensity around 550 °C, consistent with previous DSC studies. The Cu peaks also undergo a shift during the heating and cooling of the sample, consistent with thermal expansion and relaxation. Through the heating process, Cu metal is observed at (111) and (200).

The scope of this work is to determine if there is evidence of a possible additional events beyond the reaction mechanism traditionally held during the thermite reaction – i.e., simple oxygen exchange. Shortly after Cu formation, additional peaks appear above 600 °C (or scan number 25) suggesting the formation of another material. The presence of another material would suggest that traditional oxygen diffusion in a solid state ion transfer may not be the only mechanism at play; if the reaction was a true redox reaction, lacking any intermediate mechanisms, then Cu and Al would be the only present metallic peaks. The peaks of interest to this study occur in the range of 42°-44°, as peaks are present in the heating process that are later dissipated at high temperature. Despite needing further characterization to determine the exact identity of these peaks, several possibilities are inviting

Several peaks abruptly form and disappear throughout sample heating at different temperature ranges, as seen in Figure 2 and are likely amn indication of the presence of an intermetallic, as several eutectic points of Al-Cu intermetallic are within +/- 20 °C of 560 °C. The exact intermetallic formation may not be stoichiometrically balanced to a known intermetallic, seen experimentally in RNL systems. However, there are several probable identities, as seen below in Table 1.

Table 1: A sample of possible Al-Cu intermetallic formations.

Intermetallic	Cu % comp.	Primary reflection	Temperature onset [°C]	Temperature offset [°C]
$AlCu_4$	80%	43.32	300	360
Al_3Cu_2*	40%	43.67	560	960
$AlCu_3$	75%	43.97	567	1050
Al_4Cu_9	69%	42.21	300	870

The most probable intermetallic species that may be present are the intermetallics Al_3Cu_2 and $AlCu_3$. The peak present in the range of approximately 43.2° - 43.6° formed in the range of about 680 °C to 810 °C. This peak may be an impure phase similar to Al_3Cu_2 that formed during a Cu composition around 40% at the interface. The second peak of interes occurs in a range of approximately 43.6° - 43.8° at a temperature of about 600 °C to 810 °C, consistent with an impure phase similar to $AlCu_3$, with a Cu composition of 75%. However, it must be emphasized

that more studies are needed to determine the intermetallic formations at the interface. The formation of $CuAl_2$ And Cu_9Al_4 in the Al/CuO system has been cited in *in-situ* thermal analysis of nano-powders.

For the scope of this work, the existence of two peaks during the heating of the sample that are not present in the end result of the material is consistent with the idea of an alternative reaction mechanism. Formation of additional materials suggests that there is more than solid-state ion diffusion resulting in the terminal metal and metal oxide. More characterization is necessary to determine whether or not this is a secondary oxide phase, an intermetallic phase, or phase transformations of the materials present.

Exploring New Thermites Based on ZnO

An alternative initial oxide, zinc oxide, holds several benefits. Zinc oxide has a wide band gap, resulting in high electron mobility, and transparency at the morphology used in nano- thermite. The conductive nature of ZnO opens up sets of applications where conductivity of the thermite stack as a whole can be utilized. Zinc oxide can be deposited in a number of ways, via chemical vapor deposition, and physical vapor deposition processes. Specifically, PVD processes such as RF sputtering, DC sputtering, and DC reactive sputtering can be employed. In this work, zinc oxide is deposited via RF sputtering. However, the utilization of multiple sputtering methods is advantageous, as it is more easily accessible depending on power sources that are present. Zinc oxide grows in the (002) orientation at room temperature, making it an easily identifiable material on x-ray diffraction. In addition, ZnO is a relatively easy film to crystallize. Although a thermite stack itself cannot be heated to high temperatures, and low temperatures may introduce diffusion across the interface, it is possible that a ZnO thin film could be heated prior to deposition of the metal layer in a 1 BL sample.

Although CuO is a suitable oxidizer for shock studies, the opaque nature of the material after several hundreds of nanometers of material results in it acting as an optical density filter of the radiance of the material upon shock. Because of this, a clear thin film is advantageous in shock studies, as the signal is not dampened by the oxide transparency.

Finally, ZnO only has one stable valence state, making it much more tractable for computational approaches, there are a number of molecular dynamics potentials available for ZnO to facilitate large simulations, and one can make an epitaxial supercell between ZnO and Zr thus facilitating density functional theory approaches.

A 1-5 bilayers series of ZnO|Zr multilayers was deposited on silicon. The substrates were rinsed in acetone, isopropyl alcohol, methanol, and then placed in a UVO bath for 10 minutes.

Deposition rates were determined via XRR. Zirconium was deposited via DC sputtering at 40 W in 20.2 sccm Ar under 2 mTorr at 7.3 nm/min. Zinc oxide was deposited via RF sputtering of a 0.25” 2” ZnO target at 215 W by Kurt J. Lesker at 10.3 nm/min.

Post deposition, to facitate oxygen exchange reactions, the samples were then heated in an N_2 atmosphere at 250 °C, 350 °C, 450 °C, and 550 °C. The onset of reaction was characterized by the formation of metallic Zn in the sample, as seen in x- ray diffraction patterns.

Prior to the heating of the samples, significant peak shift of the (002) ZnO reflection was observed in the 1-5 BL stacks, suggesting that the deposition process of ZnO may be changing the thin film structure from sample to sample. Although more data must be collected to fully characterize the deposition of ZnO via RF sputtering for RNLs, plausible explanations are based upon intrinsic stress during deposition. Despite the irregularities of the ZnO thin film, preliminary studies have shown that the Zr/ZnO system undergoes a reaction, as evident by the formation of Zn as the system is heated.

Like the Zr/CuO and Al/CuO samples, the progress of the reaction can be characterized by the formation of the terminal metal. Thus, following the formation of Zn peaks in x-ray diffraction after heating was used to characterize if the reaction began. Upon heating of 1-5 bilayers of the Zr/ZnO system at 150 °C, 250 °C, 350 °C, 450 °C, and 550°C, reaction was evident in all five of the samples. Below, in Figure 3, the formation of Zn can be seen at 350 °C in the five bilayer Zr/ZnO sample. Zn appeared in the x-ray diffraction pattern for 2-5 bilayers at 350 °C. However, for the 1 bilayer sample, Zn peaks did not begin to appear until 550 °C.

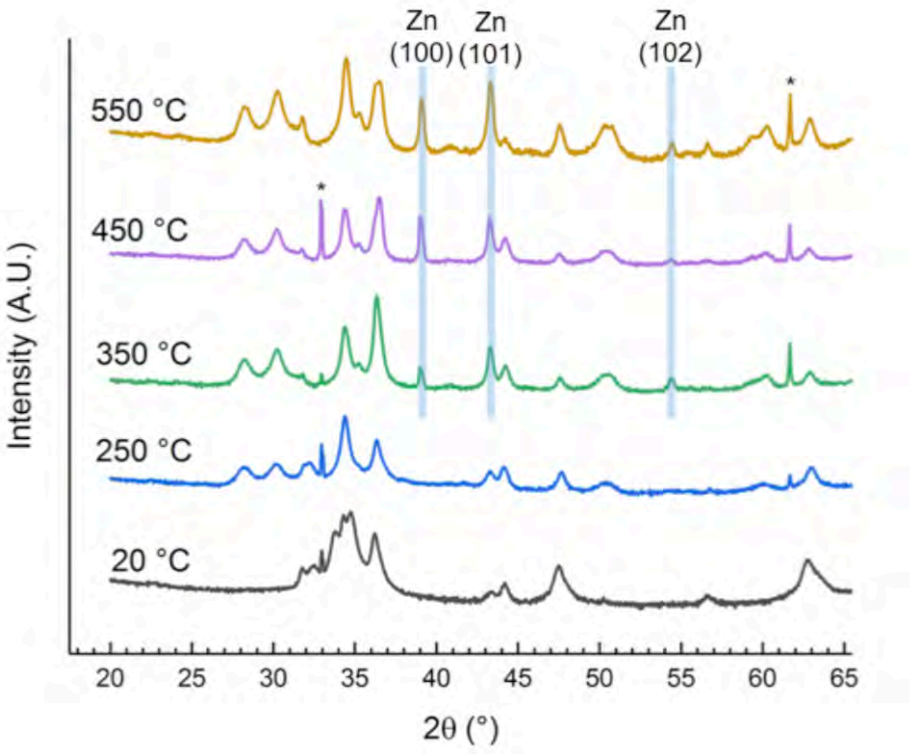

Figure 3: X-Ray Diffraction pattern of heating series of a 5 bilayer Zr/ZnO RNL sample. Evidence of reaction is seen at 350 °C by the formation of Zn. * denotes substrate peaks.

Further investigation of the deposition process utilized for ZnO revealed that rates were not steady, when compared to CuO. The deposition rate of ZnO begins rather elevated, and as time progresses, reaches a steady deposition time. In addition, if sputtering of Zr preceded ZnO deposition; the ZnO deposition rate was elevated again. Although more studies need to be done, we speculate that this could be due to the nature of ZnO as a wide band gap semiconductor, specifically the insulating nature of ZnO.

During sputtering, the sample on the stage and the vacuum chamber itself acts as an anode, and the sputtering target a cathode. This electric potential allows for free electrons to be repelled from the target source, and then collide with the carrier gas, producing positively charged ions that bombard with the target source. This electrical differential is important in sputtering, as it promotes the positive ionization of the carrier gas. Because of the insulating nature of ZnO, the issue of the “disappearing anode” is introduced. With conductive materials, such as metals and conductive oxides, the electric potential between the cathode and anode is uninterrupted, as the anode is coated with conductive material. However, because ZnO is a wide band-gap semiconductor, it is possible the ZnO is not reaching a conductive level, and is acting as an insulator. As the deposition progresses, insulating material is deposited on the anode, “masking” the charge differential between the cathode and anode. This results in a “floating” electrical potential during the deposition process. This has a cascading effect: as the electrical differential between the cathode and anode disappears, free electrons are not accelerated as much

The dropping deposition rate with time leads to samples that are not stoichiometric, and are not equal in the off balance of stoichiometry across varying number of bilayers. A 1-bilayer sample is only subjected to the increased deposition rate once, and then is deposited at a lower deposition rate than calculated. However, a 5-bilayer sample is subjected to the elevated deposition rate five times, and then a lower deposition rate than accounted for. In order to account for this, further studies must be done to model the deposition rate, or a form of biasing must be applied to the sample stage. Alternatively, a doped ZnO source material should be used to avoid the disappearing anode issue

ABSTRACT

ROUTH, EVYN LEE. Engineering Reactivity in Thermite Reactive Nano-Laminates (Under the direction of Dr. Jon-Paul Maria.)

Thermite Reactive Nano-Laminates (RNLs) are a member of a broader class of materials called Metastable Intermolecular Composites (MICs). MICs are traditional energetic materials on the nano-scale, such as nano-thermite. Compared to conventional thermite, nano-thermite exhibits an increase of reactivity. RNLs are nano-thermite in thin-film morphology. The resulting geometry allows for a precise and reproducible system that allows for a clearer avenue of understanding for the fundamentals of the thermite reaction. Throughout this work, the reactivity of RNLs is explored via altering the geometry of the system, as well as the constituents present.

Changing the geometry of RNLs can alter the reactivity of the system. The effect on reactivity by increasing the number of bilayers, and consequentially, increased interfacial density, present in a nano-laminate of overall stack thickness can be characterized via laser driven flyer plate impact studies. Upon mechanical shock, Zr/CuO RNLs showed an increase in radiance as a function of bilayers present. Peak total radiance was observed at a slower velocity in the 3 bilayer system, when compared to the 2 and 1 bilayer Zr/CuO system, suggesting the onset of reactivity is decreased in higher bilayer samples.

An increase of interfacial density results in more reactive RNL systems, but at the expense of heat transport across the additional interfaces. Using TDTR, the thermal conductivity as a function of increasing number of bilayers was studied. A slight downward trend of thermal conductivity of a 1-6 bilayer Al/CuO system was found as a function of increasing interfacial density. The modest decrease in thermal conductivity suggests that the increasing number of interfaces present does not hold significant impact on the reactivity of the system.

Reactivity can also be altered via the reactants in a thermite system. The Zr/ZnO system is a less energetically dense system when compared to Zr/CuO. Preliminary work done with the Zr/ZnO RNL system has shown that the reaction proceeds to completion, and displays reaction onset comparable to the Zr/CuO RNL system. The Zr/ZnO system holds promise for a clear avenue of the fundamentals of the thermite reaction, as well as chemical composition flexibility of thermite.

In order to fully understand the reactivity of thermite, the fundamental reaction mechanism must be studied. *In situ* heating XRD was performed on a 20 bilayer Al/CuO RNL, allowing for further exploration of the thermite reaction mechanism on the nano-scale, providing insight on the possibility of intermediate reaction mechanisms.

The reactivity of thermite on the nano-scale shows to have a dependence on the geometry of the system, as well as the reactants present. Throughout this work, the flexibility of reactivity via geometry and chemical composition of thermite RNLs is highlighted, holding promise for applications in which tunable power densities can be employed.

Engineering Reactivity in Thermite Reactive Nano-Laminates

by
Evyn Lee Routh

A thesis submitted to the Graduate Faculty of
North Carolina State University
in partial fulfillment of the
requirements for the degree of
Master of Science

Materials Science and Engineering

Raleigh, North Carolina

2018

APPROVED BY:

_____	_____
Dr. Michael Dickey	Dr. Donald Brenner

_____
Dr. Jon-Paul Maria
Committee Chair

DEDICATION

For Eli

BIOGRAPHY

Evyn grew up 25 minutes outside of NC State University, in Cary, North Carolina. She attended Appalachian State University, obtaining a Bachelor of Science in Applied Physics, and a minor in chemistry in December 2015. After a semester of graduate studies at Appalachian State, Evyn transferred to NC State University and joined Dr. Jon-Paul Maria's group in June of 2016. A few of Evyn's favorite things include, but are not limited to: tacos, good beer, dogs, the outdoors, spending time with friends and family, corny science jokes, and oxford commas.

ACKNOWLEDGMENTS

I'd like to acknowledge Dr. Jon-Paul Maria for his immense support throughout my graduate education. Dr. Maria saw something in me that I did not see in myself, and helped me develop into the scientist I am today. Without his support, none of this would have been possible.

I'd like to thank my group members, past and present: Dr. Kyle Kelley, Kevin Ferri, George Ktsonis, Trent Borman, Delower Houssain, Richard Floyd Jr., Dr. Xiaoyu Kang, Dr. Christina Rost, Sarah Lowum, Dr. Evan Runnerstrom, Dr. Christopher Shelton, Dr. Edward Sachet, Dr. Petra Hanusova, and Fermi Maria. Thanks for answering questions, helping with designs and brainstorming, and grabbing after lab brews with me. Special thanks for helping me conduct research a couple hundred miles apart.

Science is always a collaborative effort. Thank you to Dr. Patrick Hopkins and Dr. Christina Rost of the Department of Mechanical and Aerospace Engineering at the University of Virigina for your work on the thermal conductivity of nano-thermite. Thank you to Dr. Sergey Matveev and Dr. Dana Dlott in the Department of Chemical Sciences at the University of Illinois at Urbana-Champaign for your work on shock studies of nano-thermite. Thank you to Dr. Everett Grimley, Rachel Jackson, and Dr. James LeBeau in the Department of Materials Science & Engineering at NC State University for imaging of thermite nano-laminates.

Thank you to my mentors and professors at Appalachian State University for taking the time to listen and discuss my career goals, as well as encouraging me to pursue graduate education. More importantly, thank you for creating an environment where I could fall in love with science.

Thank you to my parents, Heidi and Conal Veazey, who listened and guided me during tough decisions about my graduate education, and career goals. Thank you for the hours of

listening to my worries and frustrations, and following with reassurance. Thank you to all of my friends and family for always encouraging me and believing in me, and listening to me get excited about science. Thank you to Daisy Dog for always being excited to see me when I came home from lab.

Finally, I'd like to acknowledge my husband, Eli, for his unwavering support of me throughout my graduate education. Thank you for supporting me, encouraging me, and believing that I could do this.

TABLE OF CONTENTS

LIST OF TABLES

LIST OF FIGURES

CHAPTER 1. INTRODUCTION TO NANO-THERMITE

1.1 Development of Explosive Material

Fire has been apart of the history of humanity for hundreds of thousands of years, and central to the development of humanity. Charles Darwin asserted in his book, *The Descent of Man*, "This discovery of fire, probably the greatest ever made by man, excepting language, dates from before the dawn of history." [1] The successful utilization and control of fire allowed for humanity make large advances, including but not limited to: obtaining warmth and protection, advancement of diets via cooking, and utilization of time after the sun had set [2,3]. The utilization of fire to cook meat contributed an increase in caloric intake and ease of digestion for early humans [4]. Later in history, fire would be used to clear areas for human development, and create fertile areas for farming [2,3]. Despite the idea of building a fire for survival may seem trivial to modern civilization today, the control and utilization of fire and it's applications has been intermixed into the development of human kind [5].

1.1.1 Gunpowder

Although humanity had been utilizing the control of fire for hundreds of thousands of years, it was not until recent human history in which fire was used for explosive and energetic applications. As civilizations developed, conflict between neighboring civilizations arose, and the need for defense grew. In fact, the development and utilization of gunpowder in the world, is deemed the "Gunpowder Age" [6]. Evidence of the discovery of gunpowder can be traced to the Tang Dynasty in the 9^{th} century, when a 6:6:1 mixture of sulfur, potassium nitrate, and birthwort herb were mixed [7]. Following a systematic process, Alchemists would mix various compounds and study their applications. Upon the mixing of a nitrate, sulfur, and charcoal at the correct

proportions, and the proper activation energy added, the energetic reaction of gunpowder was discovered [6].

The scientific development of gunpowder was then explored in the 11th century in the Song Dynasty of China [7]. The Song Dynasty can be attributed to much technological and scientific advancement in Chinese history, and is cited as one of the most advanced civilizations in the world during that time, according to some anthropologists [6,8]. During the later portion of the Song Dynasty, rising competition of neighboring states could be attributed to the military advancements during this time [7]. The first instances of Song gunpowder were unlike the later developed gunpowder mixtures, as they were developed as incendiaries. Later, gunpowder would be developed into an explosive material as the nitrate concentration was increased, which lead to the development of gunpowder weapons.

1.2 High Explosives

Gunpowder is classified as a low explosive, due to its deflagrating nature. Characteristics of low explosives will be discussed below, in Section 1.3. The development of additional low explosives was halted as the regime of chemical explosives, also called high explosives, was investigated with the discovery of nitroglycerin. Materials that are classified as high explosives are by definition, materials that undergo detonation [9]. Detonation is a form of combustion that occurs very rapidly, resulting in the production of a shock front that moves at supersonic speeds [10]. The propagation of the shock front through media can be further described by shock wave physics and condensed matter physics [11].

Because of this, the energetic release of high explosives is dominated by the shock wave that is produced via detonation. Although some high explosives materials do expel energy in the form of thermal energy, the vast majority of the energetics that are produced by high explosives

are in the form of a shock wave that creates a pressure front at speeds at or higher than the speed of sound [10]. Further discussion of shock waves can be seen Section 2.2.1: Shock Waves.

Explosive materials are characterized by their sensitivity to their surroundings, stability in their environments and over time, and reactivity [9]. The combinations of these characteristics in explosives of unique chemical composition result in materials that have unique applications and are utilized accordingly.

1.2.1 Nitroglycerin and Dynamite

For many years, gunpowder was the primary explosive material used. Gunpowder was utilized in many forms of weapons, due to its technological advancement for the time, and ease of utilization in other weapons.

However, the utilization of nitrogen in chemical explosives took off in 1847 when Italian chemist Ascanio Sobrero invented nitroglycerin upon the nitration of glycerin [9,12]. The medicinal applications and explosive nature of nitroglycerin was discovered when a small beaker Sobrero was holding exploded. Upon the explosion of the material, a small amount of the liquid landed in Sobrero's mouth, where he noticed the headache and numb limbs that followed his accidental tasting (a general note: tasting chemical mixtures today is considered terrible lab practice) [12]. Nitroglycerin was later developed into a medicinal treatment for angina pectoris.

Nitroglycerin, the leading precursor in later explosives that would be developed, is an oily, colorless liquid that is extremely sensitive, detonating at the slightest shock. Nitroglycerin opened the doors to the development of other chemical explosives, and the first detonating materials were developed. Unlike gunpowder, nitroglycerin, and its subsequent precursors, react at speeds greater than the speed of sound. Because of the reaction mechanisms of chemical explosives, like nitroglycerin, the length in which the reaction occurs is on the molecular scale,

which results in extremely sensitive material, that is prone to detonation upon the introduction of contact energy to the system. This unleashed a whole new level of explosive materials, dubbed high explosives.

The creation of nitroglycerin was one of many nitrogen based chemical explosives. The presence of C—N, O—N, and N—N bonds in materials results in a large amount of potential energy being stored in the bonds. Upon reaction, the nitrogen is released, allowing for the formation of the much more stable configuration of nitrogen, as N_2 gas.

Nitroglycerin was utilized for mining and blasting applications in construction across Europe, and later the United States, after the work Alfred Nobel did with developing it for industry use [12]. However, it was quickly discovered that liquid nitroglycerin was far too sensitive to be transported, following several accidents, including an accident in San Francisco in 1866 where one of the three crates intended to be used to blast through the Sierra Nevada Mountains for the construction of the Summit Tunnel caused the death of 15 people [13]. Due to improper technological abilities to transport the extremely volatile material, widespread miscommunication of the danger of the material, as well as the lack of safety protocols, a ban on transportation of nitroglycerin was later enacted [12].

Alfred Nobel held an interest in nitroglycerin, leading to the development alternative methods of nitroglycerin production, as well as the development of the blasting cap. However, the true dangers of liquid nitroglycerin were realized to Nobel after a fatal lab accident involving the material where his younger brother and four other people lost their lives. Alfred Nobel developed dynamite, by combining nitroglycerin with diatomaceous earth (also known as Kieselguhr), a naturally geologically occurring material consisting predominately of silica [12,14]. The combination of an inert solid with the extremely volatile liquid resulted in a

safer way to transport the explosive material. More manageable and more powerful than gunpowder, dynamite became the primary blasting material for mining applications, which is still used today.

It is important to note, that although not developed for military applications, nitroglycerin and dynamite have also been used extensively in military history. Consequentially, Albert Nobel made a substantial amount of money off of his invention of dynamite, holding 355 patents and creating 87 companies world-wide [14]. In his will, Alfred Nobel bequeathed his estate to the creation of annual prizes awarded to those who contributed greatly to mankind in the subjects of physics, chemistry, medicine, literature, and peace, later known as the Nobel Prizes [14].

1.2.2 Other High Explosives

Other common chemical and plastic explosives have been used throughout civilian, and military history. Along side the development of nitroglycerin based explosive material, trinitrotoluene (TNT) was developed in the late 1863 [12]. Like dynamite and nitroglycerin, the material derives its energetic nature from the chemical bonding of nitrogen, found in the C—N bond between the three nitro groups and the aromatic hydrocarbon ring, seen in Figure 1. However, due to its relatively stable nature under standard conditions, and TNT's ability to be handled roughly, the explosive nature of the material was not realize until approximately 20 years later until it was utilized with a detonator [12]. Unlike its nitroglycerin counterparts, TNT must be detonated via a primary detonation. The energy output of TNT is used as a comparison source for other materials, often referred to as "TNT equivalent" where "one [metric] ton of TNT" is equivalent to 4.184 gigajoules of energy [15]. Table 1.1 can be seen below with a comparison of energy densities, power densities, RE Factor, and reaction speesd of conventional energetic materials. The relative effectiveness factor (RE factor) is another metric used to

compare the explosive nature of an energetic material. The RE factor is compared to the energetic output of 1 kg of TNT, in the units of TNT equivalent/kg, with TNT having a RE factor of 1.0 [16].

During World War II, a more energetic explosive than TNT called “Research Department Explosive” (RDX) with the chemical name of cyclotrimethylenetrinitramine, was developed [12]. Previously, energetic materials such as nitroglycerin, TNT, and dynamite, used in military applications had also been used and developed for civilian applications, such as for mining, construction, and demolition. RDX, however, was developed primarily with military applications in mind. RDX is unique from TNT and nitroglycerin compounds due to the nitrogen-nitrogen bond present in the molecule. RDX was used as a precursor for plastic explosives. A common explosive that was created fro RDX was Composition C, later varied into C-4. C-4 is a composition of 91% RDX, with 9% of plasticizers and binders to create a malleable material [17].

Although still in its infancy, in the sense that it is has not yet left the research lab, Octanitrocubance (ONC) is one of the most effective and fastest chemical explosives known. Developed by and published about by Philip Eaton and Mao-Xi Zhang in 2002, ONC undergoes theoretical detonation at speeds upwards of 9,900-10,100 m s^{-1}, and boasts an RE factor of 2.38 [18–20]. The material derives its energetic output from the physical structure of cubane. With eight carbons in the corners of a cubic molecule, the material can be synthesized with eight nitro groups bonded to eight carbons. ONC opens the potential for chemical engineering of the cubane precursor, by altering the number of nitro groups bonded to the carbons present. However, only small amounts of ONC have been synthesized in the laboratory, due to the expensive production and inability to scale up the creation of the material, resulting in a lack of

larger detonation experiments of ONC [21]. Like TNT, ONC is insensitive to shock. Due to the expensive nature of ONC, it is still more cost effective to use more of a less energetic high explosive to achieve a desired energetic output. Although ONC is not a practical high explosive, it is an example of the theoretical capabilities of chemical explosives.

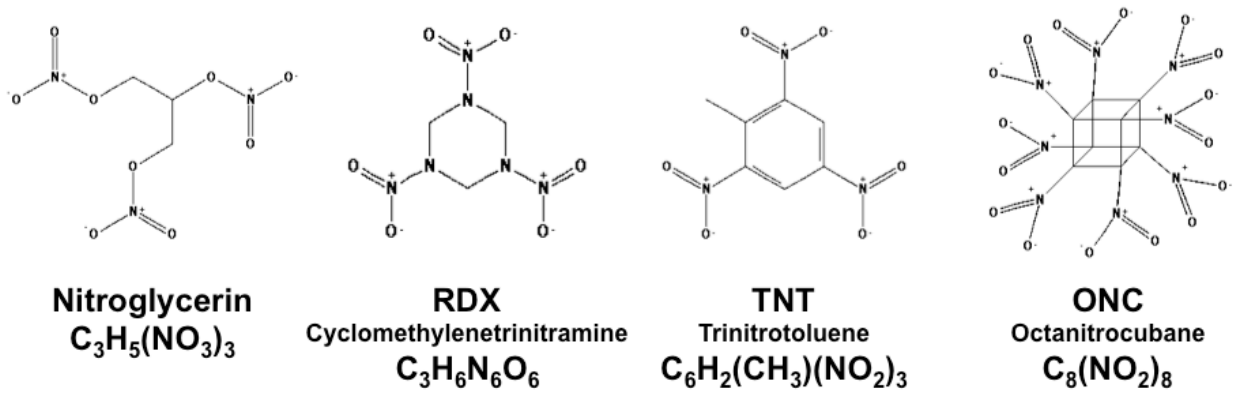

Figure 1.1. Chemical structures of nitroglycerin, RDX, TNT, and ONC. [22–25]

The explosives mentioned are just a few of the many high explosives that have been developed and utilized today and throughout history. For the scope of this work, the materials mentioned provide a brief overview of explosive chemical materials. In Table 1.1, seen below, a comparison of these energetic materials can be seen. These energetic materials also highlight a history of engineering materials for preferred energetic outcomes and characteristics. The development of dynamite to create a less sensitive material than that of nitroglycerin, the utilization of plasticizers in C-4 to create a more malleable RDX material, and the alteration of nitro groups on the cubane precursor are all examples of engineering energetic materials to obtain different levels of sensitivity, stability, and reactivity. Engineering of explosive materials can be applied to low explosive materials to change sensitivity, stability, and reactivity of the materials.

1.3 Low Explosives

Low explosives, as described previously by gunpowder, are materials that undergo combustion by a self-contained oxygen source [9]. Like wood and other common combustible materials, which undergo combustion upon the introduction of enough energy to ignite, combustion of low explosives is fueled by oxygen. However, low explosives are able to achieve self-propagation due to an internal oxygen source. Low explosives deflagrate, with rapid flame propagation once reaction takes place [26].

As previously mentioned, the main mechanism of reaction for high explosives is chemical mixing on the molecular scale; many instances of reactions occurring at once on the molecular scale over short distances leads to fast reaction rates, and sequentially, large energy outputs in the form of detonations. Low explosives, on the other hand, partake in different reaction processes. Low explosives, due to macromolecular mixing of the precursors that must occur, result in slower reaction kinetics, and consequentially, in deflagration, instead of detonation. It is important to note the difference of deflagration and detonation between low explosives and high explosives, as low explosives are characterized by their sub-sonic pressure wave propagation.

At first glance, it would seem that deflagrating materials are inferior to high explosives, due to their slower reactions. However, low explosives hold many benefits for civilian and defense applications [27,28]. The utilization of materials that do not detonate can be advantageous in other applications, as well as complimentary materials to detonating systems. Instances where a blast front would not be advantageous have proven to benefit from low burning materials and deflagrating materials. In addition, because of the high volatility of detonating materials, there is not much room for engineering the reaction outcomes of the

material. The combination of low explosives/propellants and high explosives have been developed and utilized extensively in military applications [9].

1.4 Thermite

Aside from gunpowder, thermite is an example of a common low explosive material. In 1898, Hans Goldschmidt utilized the stability of alumina and the quality of aluminum as a reducing agent as a method to produce pure metals from metal oxides, as discussed in his paper titled, “Aluminum as a heating and reducing agent” [29]. Originally cited as a process to produce pure metals from their metal oxide sources, such as pure, carbon free chromium. In his paper, Goldschmidt states that the estimated temperature of the reaction is at least 3,000 °C. Realizing the application of the high temperature output of the reaction, Goldschmidt patented “thermic welding” in 1897 in United States [30]. This process was first used to weld tram tracks in Essen, and railroad tracks in the United States in the 1930’s [31]. Thermite welding proves to be a very sturdy welding process, due to the creation of pure iron with low carbon content, as previously cited by Goldschmidt.

The Goldschmidt reaction/thermite reaction is a reduction-oxidation reaction between a metal and a metal oxide, resulting in a large exothermic heat output:

$$\boldsymbol{M + AO \rightarrow MO + A + \Delta H}$$

where *M* is the initial metal, *AO* the initial oxide, and *MO* and *A* being the terminal oxide and terminal metal, respectively. This reaction is driven by the large difference in enthalpy of formation between the initial metal oxide and the terminal oxide [32]. The large enthalpy of formation difference drives the reaction to the terminal materials, resulting in a large exothermic heat output in the form of heat and light.

Thermite is a low explosive, meaning it undergoes little gas production and deflagrates, as previously mentioned in Section 1.2. In order for the reaction to occur, the activation energy of the system must be met to promote mass transport between the initial metal and metal oxide. In addition, sufficient energy must be provided to the system to achieve self-propagation, to sustain the continued mass transport. Once self-propagation is achieved, the reaction can proceed to completion, resulting in the formation of the terminal metal and metal oxide.

1.5 Metastable Intermolecular Composites

In Goldschmidt's original 1898 paper where the capabilities of thermite are first discussed, Goldschmidt states, "we find that in nearly every case the aluminum must be in a powdered or granulated condition, and intimately mixed with the finely crushed oxide or sulfide to be reduced." [29] Although these powders were on the micro-scale, Goldschmidt recognized that creating a material with smaller morphology resulted in a reaction output, which had been reported before as nonexistent in studies of using aluminum as a reducing agent for manganese oxide [29]. Nearly a century later, the idea of decreasing the morphology of aluminum particles on the nano-scale was utilized [33]. It was reported that by reducing the size of the aluminum powders, when compared to flat surfaces, the activation energy threshold was lowered, citing an increase of surface area as the leading factor in activation energy threshold reduction [33]. Materials that utilized this smaller morphology where dubbed Metastable Intermolecular Composites. Metastable Intermolecular Composites (MICs) are a class of low explosive, energetic material in which an oxide and metal fuel are combined, with morphologies on the nano-scale.

Thermite began to be combined on the nano-scale, in the form of nano-powders with one or two of the reactant constituents on the nano-scale [34–37]. Various reactants from the

traditional Al/Fe_2O_3 mixture began to be utilized, such as Al/CuO [38], and other metal/metal oxide formations [32,39,40,28,41,42].

The reduction of the morphology characteristics of MICs results in an increase of surface area in which the material can interact. For example, once a particle is reduced to the size of a nanometer, approximately 10% of the atoms present in the material are located on the surface [43]. As a result, nanoparticles see a reduction in activation energy, as there are more atoms present on the surface compared to the volume of atoms present, ready to partake in reaction. Melting temperatures of metallic nanoparticles can be depressed up to 300 K [43,44]. In addition, MICs also benefit from a more intimate and homogenous mixture of the components of the reaction on the nano-scale vs. the micro-scale [43]. This results in reduction of the distance that must be travelled in order to achieve mass transport. Because MICs are a low explosive, the macromolecular mixing involved is directly dependent on the reduction of the material morphology to the micro- and nano-scale has proven to open new doors for a wide range of applications [33–37]. High explosive materials, such as dynamite, reach reactions speeds of several thousands of m/s, resulting in detonation. The power density of these materials is dependent on the reaction speed. Thermite has a relatively high energy density, at 18 kJ/cm^3, but low reaction speeds [45]. However, it has been observed that a reduction of the size of the constituents of thermite, such as in MICs, has resulted in an increase in reaction speed [46–48]. Because power densities are time dependent, and therefore dependent on the reaction speed of the material, thermite can provide an avenue to tunable power densities by altering the morphology of the material. As seen in Table 1.1, the reaction velocities of MICs can push the deflagration threshold of reaction fronts for low explosives, at 1,000 m/s reported [41,46–49],

which increases the reaction front of conventional bulk thermite by a factor of 100. As a result, power densities of nano-thermite has the potential for a large range of tunable power densities.

Discussed in Chapter 3, the energy density of thermite can be utilized to create different power densities, as well. By altering the reactants present in the thermite mixture, the specific energy, and consequentially, the energy density can be altered. By combining a tunable energy density and reaction velocity, a wide range of power densities can be achieved.

Table 1.1. Comparison of conventional high energetic material to thermite.

	Reaction velocity [m/s]	**RE Factor [TNTe/kg]**	**Energy Density [kJ/cm^3]**	**Power Density [MW/cm^3]**
ONC	9,900-10,100	2.38	21	207-211
RDX	8,350	1.6	12	100
Nitroglycerin	7,700	1.5	10	77
TNT	6,900	1	7	48
Dynamite (Nobel)	6,100	0.92	4.8	29
Thermite, bulk	10	N/A	18.3	0.18
MICs	1000	N/A	18.3	18

*Energy density and power densities calculated using RE factor and reaction velocities [50], as well as the energy equivalence of 1 metric ton of TNT [15]. ONC is calculated via theoretical values [18,19,21]. For thermite, Al/Fe_2O_3 thermite was used. [22,45,51].

1.5.1 Thermite Reactive Nano-Laminates

As mentioned, the reaction outputs of MICs and nano-thermite have proven to have a dependency on the morphology of the system. Recently, another geometry of MICs has been explored in the form of thermite Reactive Nano-Laminates (RNLs). RNLs are MICs that are in the thin-film morphology, with their thicknesses on the nano-scale. An example of a 7 bilayer Al/CuO RNL can be seen in Figure 1.2 (imaging courtesy of Dr. Everett Grimley, Dr. Jim LaBeau, and Rachel Jackson of AIF, 2017).

RNLs are composed of altering layers of a metal and metal oxide, where a layer of the two is deemed a “bilayer” (BL) throughout this work. RNLs are deposited via physical vapor

deposition (PVD), as discussed in Section 1.4.1. The geometry of RNLs still achieves the same results as nano-powders: a decrease in the distance mass transport must traverse and an increase in surface area results in a decrease in effective activation threshold. However, the addition of constant contact between the metal and oxidant also results in an interface in which the reaction can readily proceed. Throughout this work, the effects of altering the interfacial density and constituents present in the RNL stack is investigated.

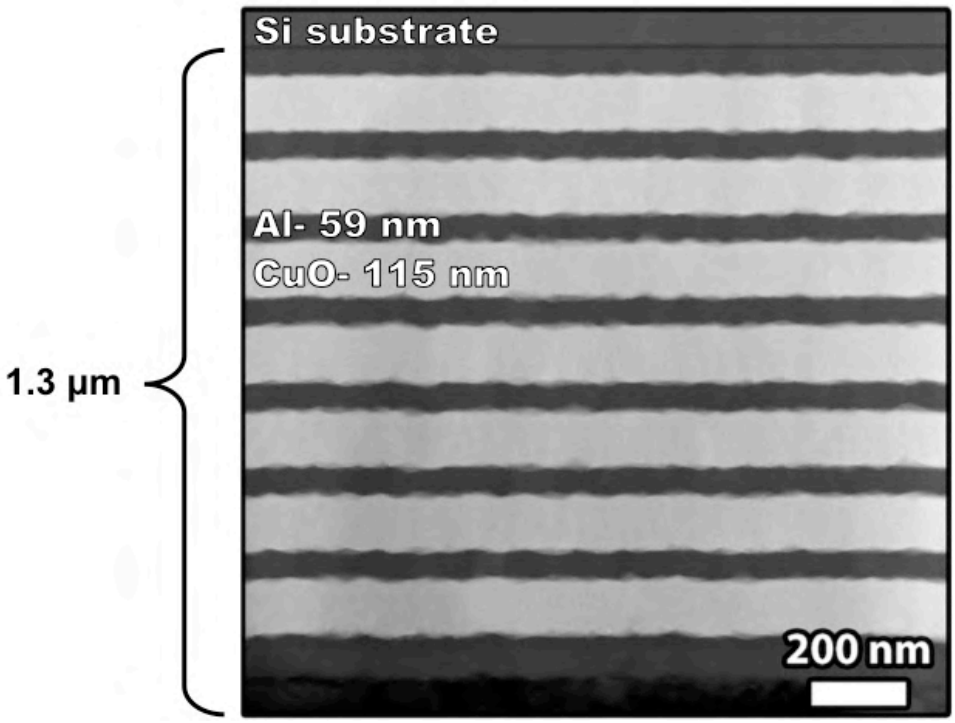

Figure 1.2. Thermite Reactive Nano-Laminate (RNL) consisting of 7 bilayers of Al/CuO on a silicon substrate with an 80 nm capping layer of Al.

As seen in Figure 1.2, the thin film morphology is reproducible throughout the sample deposition process, as well as across multiple samples. The deposition conditions used to create the samples throughout this work are optimized to have surface roughness of less than 5 nm rms of a sample approximately 80-100 nm thick. Thus, the roughness is not propagated substantially

throughout the multilayers through the deposition process, as seen in Figure 1.2. For details of the thin films of the material used throughout this work, refer to Appendix A.

Creation of nano-thermite in this geometry holds several advantages. Thermite nano-powders provide a challenge to create regular and simple model morphology. The utilization of thin-film geometry allows for a more accessible avenue to fundamental reaction mechanics, which are precise and reproducible.

1.6 Nano-Thermite Production

There are several different methods in which thermite has been created on the nano- and micro- scale [28,33–36,39,40,48,52–54]. Upon the discovery of thermite, as previously mentioned, aluminum and iron powders were mixed to create thermite for welding applications on railroads [31,55,56]. Unbeknownst early on, the mixing of these powders was taking advantage of the very property we take advantage of today with nano-thermite: by decreasing the overall features of the reactants, the surface area is increased for the reaction to take place, resulting in a more reactive system.

1.6.1 Nano-Powder Mixing

Nano-powder mixing is a relatively straightforward method to combine materials on the nano-scale. Powders with dimensions of approximately 1-100 nm enter a new regime, with new characteristics of the material, due to the surface to volume ratio enhancement; more area readily participating in the reaction, and the smaller distance the material must traverse in order to interact [36,37,48]. Dry mixing of nanoparticles can be achieved by mixing pre-determined sized particles by weighing out the stoichiometric equivalences of the material. In addition, the materials may be mixed via the assistance of a volatile organic solvent and then sonicated to

achieve homogeneous mixing. The solvent can then be evaporated out of the mixture, resulting in an evenly mixed material [57].

1.6.2 Arrested Reactive Milling (ARM)

Following similar basis as thin film nano-laminates, samples prepared by Arrested Reactive Milling (ARM) achieve similar results in the decrease of length that mass transport must occur. Unlike nano-powder mixing, ARM methods start with ball-milling micron sized particles of a metal and metal oxide. Because of the size of the materials, mechanical ignition of the thermite mixtures can be reached via ball milling. In ARM, the material is ball milled until just before self-propagation of the reaction is reached. This process leads to dense, lamellar micron sized particles with nano-sized morphology [58,59].

1.6.3 Physical Vapor Deposition

Laminate structures can also be achieved in thin-film morphology. Physical vapor deposition (PVD) is another method in which nano-sized components can be achieved. Physical vapor deposition is a relatively popular form of deposition used to create thin films that is used extensively in semiconductor applications. Forms of PVD include electron beam deposition, molecular beam epitaxy (MBE), Pulsed laser deposition (PLD), and sputtering deposition. Of these PVD methods, sputtering is the chosen method of choice on throughout this work, due to its reproducibility of deposition parameters, ease of calibration, and cost of equipment.

The sputtering process is a technique in which source material is deposited onto a substrate on the atomic scale. This process is done under high vacuum environments. An inert gas is introduced into the chamber from the range of 1-100 mTorr. The source material, attached to the sputter gun, is subjected to a negative bias. The negative bias results in free electron bombardment with the inert gas, creating positively ionized gas molecules, resulting in the

formation of a plasma. These plasmas, referred to as glow discharge, emit light due to recombination and relaxation events [60]. In the case of magnetron sputtering (the sputtering employed in this work), an electric field is produced by a magnetic field imposed on the gun. The resulting electric field can accelerate the ionized gas molecules at a faster rate towards the negatively biased target. The ionized gas then has sufficient energy, on the order of 1 KeV, results in a cascade when a balance of secondary electron generation and recombination in the glow discharge is met, and a plasma is sustained [60]. Generally, argon is the chosen inert gas, as it is a heavier inert gas, allowing for easier ionization. Below 1 mTorr, there is not enough gas to sustain a cascade event, and above 100 mTorr, there is too much scattering of the material, and the discharge becomes unstable. Once the energy of the ionized gas species is high enough, the bombardment of the cascade results in collisions with the target material, and atoms from the target material are ejected [61]. The resulted atoms are sputtered onto the substrate.

Throughout this work, two methods of magnetron sputtering are utilized: Direct current (DC) and radio frequency (RF) magnetron sputtering. DC sputtering is utilized for metal materials. However, materials that act as insulators, such as metal oxides, require RF sputtering, as the DC bias cannot be sustained on the insulator due to charge build up on the target surface. RF sputtering utilizes AC in order to circumvent the charge buildup on the insulator surface. Once the polarity of the current is reversed, built up charge and atoms are then ejected from the target. RF power supplies require impedance matching, and thus can prove to be more costly. In addition, RF sputtering is traditionally slower than DC sputtering, but must be utilized for insulating materials.

Although, metal oxide sputtering is not limited to RF sputtering; metal oxides can be reactively sputtered. In this method, a reactive gas is introduced into the chamber, in addition to

the inert gas. The resulting glow discharge from the inert gas subsequently ionizes the reactive gas. The reactive gas then reacts with the target material, and is then sputtered off. This process requires more calibration due to the dependency of the stoichiometry on the flow rate of the reactive gas.

Sputtering can be utilized in nano-thermite applications by creating laminates of the constituents, *AO* and *M,* in altering layers. Sputtering of thermite into thin film morphology is advantageous for a number of reasons. Although ARM does result in nano-scale features across a micron of material, similar to that of thin-film thermite, there is large size and shape variation from particle to particle, proving to be hard to reproduce and isolate exact experiments. Thin films, on the other hand, have the advantage in that simple and regular morphology that is easily reproducible. Sputtering allows for relatively smooth interfaces and surfaces, as well as consistent reactant density throughout the process. The interfaces, layer thickness, and density of material are easily controllable via sputtering of a thin film, and can be reproduced for further studies.

In the case of RNLs, they are deposited in a vacuum chamber with a base pressure in the 10^{-8} Torr range. The vacuum chamber used throughout this work is dedicated to the creation of thermite samples, and thus is free of contamination. Two variations of the chamber were used throughout this work: Thermite I Chamber and Thermite II Chamber. Thermite II was a rebuild to compensate for additional source material, as well as an attempt to keep cross contamination of sputters guns minimized. A schematic of the chamber can be seen below, in Figure 1.3. Thermite II geometry is similar to Thermite I, with an additional sputter gun added, resulting in the guns being 120° from each other, as opposed to 180° in Thermite I. This orientation allowed for less direct deposition on the opposing guns/shields. The sputter guns of Thermite II were

equipped with sputter shields to eliminate material contamination. Throughout this work, the depositions specific to the experiment are described in detail. Additional information about the calibration of the depositions can be found in Appendix A.

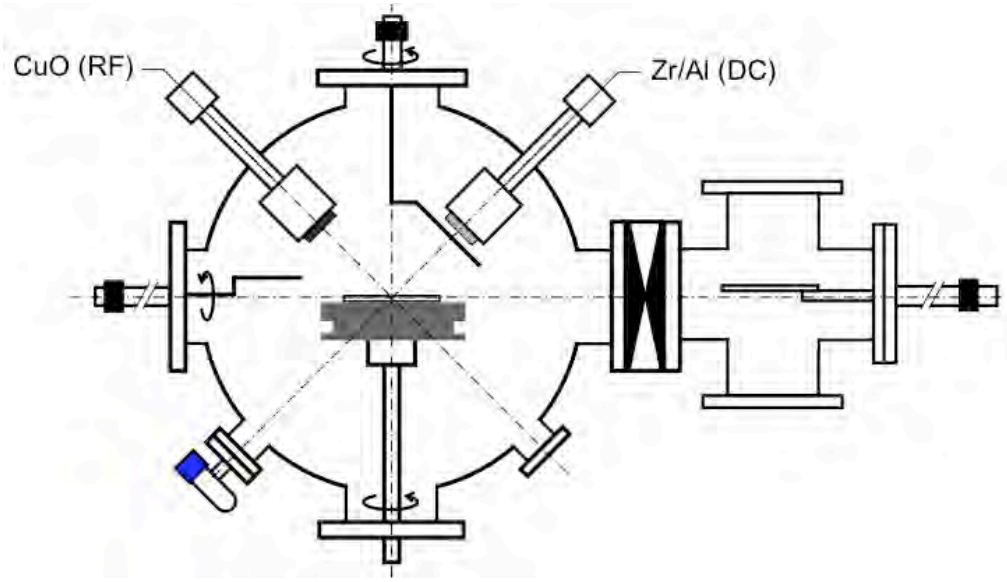

Figure 1.3. Schematic of Thermite I Chamber. Thermite II Chamber follows similar build, but with an additional gun and individual gun shields.

CHAPTER 2. GEOMETRY: STRUCTURAL ENGINEERING OF NANO-THERMITE

2.1 Introduction

Thermite has drastically slower reaction speeds than organic energetic materials and high explosives, comparatively. As highlighted in Chapter 1, organic energetics and high explosives benefit from the advantage of fast kinetics, which are responsible for detonation. The reaction kinetics of these materials benefit from monomolecular mixing, resulting in short distances required for the material to react. The smaller distance scale allows for comparatively small activation needed, to produce large mechanical work output.

Thermite, on the other hand, requires mass transport. The reaction of thermite is facilitated by the mass transport between the metal *M* and the oxide, *AO*. The distance between the two constituents serves as a rate limiter. This results in slower reaction kinetics than other organic energetics, as seen in Table 1.1. However, due to the large enthalpy of formation of the terminal oxide, thermite benefits from large energy densities, as discussed in Section 1.5.1.

Because the reaction kinetics are dependent on the mass transport of the material, engineering a system that allows for faster and more efficient mass transport should help us obtain higher power densities and faster kinetics, without altering energy density or density of the system. In addition, flexible power densities obtained by engineered nano-thermite allows for a wide breadth of applications of the material, depending on the energy needs.

One of the primary tools utilized is the quantitative control of the diffusion length in which the mass transport is occurring. By keeping the overall volume of material the same across a micron thick stack, but varying the number of layers present, we observe two effects:

1. Decreasing the distance for mass transport to occur results in a faster reaction.

2. By fitting more layers into the same volume, we acquire more interfaces, resulting in more surface area for reactions to occur simultaneously.

Together, these two effects work together to contribute to a lower activation threshold needed to begin the reaction, and reach a self-sustaining reaction that goes to completion.

Previously, we have seen that exothermic peak temperature is dependent on the bilayer thickness [49], as seen in Figure 2.1. In Figure 2.1, calorimetric data is shown for the Al/CuO system under slow heating, where the exothermic temperature was monitored as a function of number of bilayers present. From this, we can conclude that reactivity of the material is higher with the more bilayers present, due to an increased amount of exothermic activity and propagation of the reaction to completion.

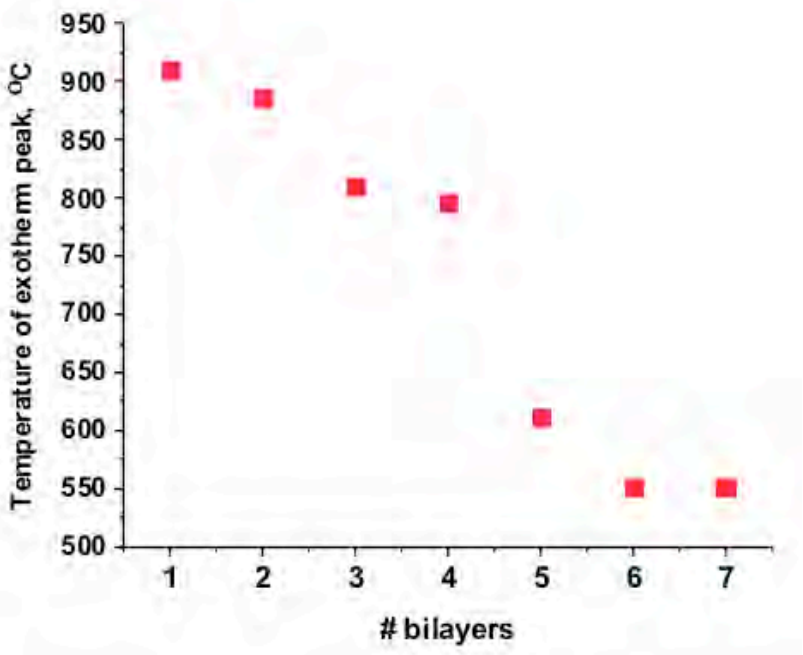

Figure 2.1 Temperature of peak of exothermic activity as a function of number of bilayers present in the Al/CuO system obtained via DSC.

2.2 Shock Studies

The reactivity of nano-thermite can further be characterized when subjected to mechanical shock. Previous work with flyer plate studies have shown us that thermite does respond to mechanical shock, and that flyer plate studies have shown to be a great tool for analysis of reaction outputs of nano-thermite [62–65].

2.2.1 Shock Waves

A shock wave is the result of a pressure front produced when it is propagated through a medium at supersonic speeds. The drastic increase in pressure is followed by an abrupt drop in pressure, creating a pressure differential. In a gaseous medium, pressure differentials are propagated at specific speeds and temperatures, depending on the source of the disturbance. On the fundamental scale, a pressure wave can be visualized as the collisions of gas molecules, resulting in a compressed medium with a sudden increase of density. In a gaseous system, a compression wave introduced results in the movement of the gas molecules, resulting in collisions and closer proximity of the gas molecules. As the compression propagates through the system, the sequential release of the pressure differential results in a relaxation of the gas molecules, returning the previously compressed molecules back to their original states. [11] This movement allows for a compression front to move through the material, similarly as a stone thrown into a pond creates ripples through water. At speeds below the speed of sound, these waves are able to propagate throughout the material, undisturbed. [66,67]

At speeds at or above the supersonic barrier, a shock wave propagates faster than the speed of sound, resulting in a large build up at the reaction front. In instances of detonation, as seen in high explosives discussed in Section 1.2, the shock wave is produced by a large release of chemical potential energy in a short period of time. The result of the chemical reaction in

situations of detonation creates pressurized gas, which expands quickly. The air that is pushed from this expansion creates a shock wave [66]. Although low explosives also result in large chemical potential energy release, the wave propagation does not reach supersonic speeds.

In instances where shock waves are created by a projectile, the projectile breaks the sound barrier. At low speeds, a projectile is able to "cut through" the atmosphere. When a projectile breaks the sound barrier, such as a bullet does, the air in front of the projectile is subjected to a large pressure differential, resulting in the formation of a shock wave front that precedes it.

Similarly, shock waves can be propagated to condensed matter upon impact with a solid. The compression of the material can result in phase changes or chemical reactions.

2.2.2 Laser Driven Flyer Plates

Laser-driven flyer plates have been utilized in several applications to study shock compression physics and response to mechanical shock in various materials. For thermite RNL's, laser-driven flyer plate studies have been utilized the ignition of thermite composites when subjected to shock waves, as previously mentioned [65]. Previously, through continuous collaboration with the University of Illinois at Urbana-Champaign, the sensitivity of the Al/CuO, Mg/CuO, and Zr/CuO systems when subjected to shock has been studied, as well as the increased reactivity of the number of bilayers present [49].

A Nd:YAG laser (Spectra-Physics Quanta-Ray Pro 350-10, 2.5 J, 1064 nm, 10 ns) is first stretched to a 20 ns pulse, described elsewhere and then focused onto a 50 μm thick aluminum sheet, attached to a glass substrate via an epoxy [68]. The pulse then heats up the epoxy, and the rapid expansion results in the expulsion of a 0.5 mm diameter cut out, called a flyer plate, as seen in Figure 2.2.

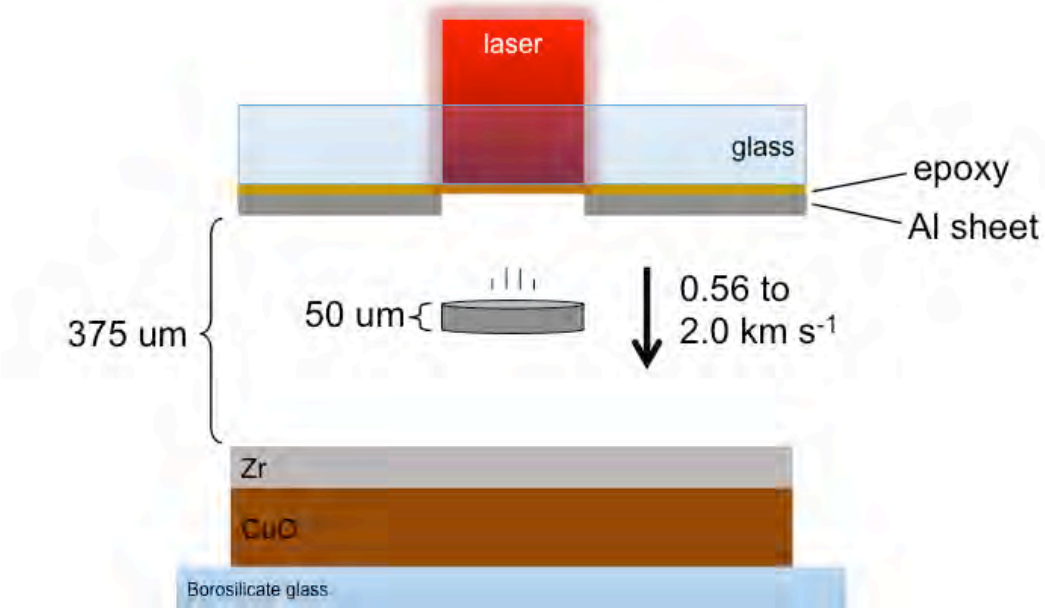

Figure 2.2. A schematic diagram of flyer plate ignition of thermite RNLs.

The flyer plate travels in vacuum at 140 mTorr across a 375 µm distance, where speeds of 0.5 – 2.0 km s^{-1} are reached, in the scope of this study. Velocities of the flyer plates are measured via photon Doppler velocitry (PDV) [62,69]. The resulting shock wave that precedes the flyer plate produces a one-dimensional planar shock wave that travels at supersonic speeds, in which the thermite thin films are subjected to, prior to flyer plate impact [62,68]. The resulting shock compression ignites the thermite, resulting in optical radiance that is measured by an emission spectrometer. The temporal resolution of the resulting emission is approximately 1 ns, and the range is 1 ns to 1 ms [68].

2.2.3 Shock Ignition

The introduction of a shock wave to a condensed material provides information on the system's response to high strain rates. A shock wave allows for the system to undergo compression, without subjection to violent damage, as it would be from physical mechanical compression. Although with the utilization of flyer plates, plastic deformation does result from

the impact of the flyer plate, the shock wave that interacts with the material prior to this can be studied.

2.2.4 Experimental

Zr/CuO thermite samples were deposited on 2”x2”x¼” borosilicate glass windows. Due to the velocity of the flyer plates, the thicker windows have proved to be advantageous; previously, a high velocity flyer plate could result in a crack in the glass window, rendering the whole window useless. The windows were rinsed with isopropanol, acetone, and methanol, dried, and then placed in a UVO bath for 10 minutes. Custom made shadow masks were used to create 2 mm diameter spot sizes of thermite for shock, as seen in Figure 2.3. The size and number of wells on the mask allowed for the maximum amount of testing sites, without compromising the deposition of the material. In order to minimize shadow effects from deposition, wells were taped over to ensure there was minimal bowing in the mask.

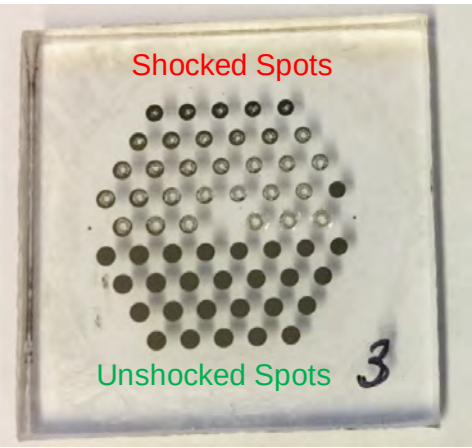

Figure 2.3. 2”x2”x¼” borosilicate glass window with 2 mm Zr/CuO spots. The 2 mm spots are achieved by depositing over a custom-made shadow mask adhered to the glass. Spots subjected to flyer plates can be seen on the top of the image, and pre-shocked spots below. [68]

The window was then adhered to a 3” diameter stage using Arctic Silver 5 thermal paste to lower the heating of the sample during deposition. Due to the thermal heat produced from a long sputtering process, the steel shadow masks, and subsequently the glass windows, heat up. The thermal paste allows for heat transfer between the window and the large stage that serves as a heat sink. This was done in an effort to combat premature ignition in the chamber. CuO was deposited via RF sputtering of a 2” 99.7% CuO target by Kurt J. Lesker at 200 W, in 2 mTorr of Ar at a stage height of 3.45”. These parameters resulted in a deposition rate of approximately 15.3 nm/min, as determined via XRR. Zr was deposited via DC sputtering of a 2” Grade 702 Zr target by Kurt J. Lesket at 40 W in 2 mTorr of Ar at a stage height of 3.45”, resulting in a deposition rate of 10.5 nm/min, determined via XRR.

XRR data of thin films of CuO and Zr deposited under these conditions can be seen in Appendix A. The total thickness of the 1 to 3 bilayer (BL) samples can be seen in Table 2.1. Due to the sensitivity of the Zr/CuO system, the samples were rested for one hour between each layer deposition. The samples were then rested overnight after the completion of the deposition. Prior to the longer rest periods, higher BL stacks (3 to 4) displayed an increased sensitivity to external stimuli, leading to premature ignition in the chamber, or upon removal from the chamber. Increased rest periods allowed for a reduction of the chance of premature ignition, and a decreased amount of pre-reacted material at the interface.

Table 2.1. Target thicknesses of 1-3 BL Zr/CuO samples used for flyer plate studies.

	1 BL	**2 BL**	**3BL**
CuO thickness	700 nm	350 nm	233 nm
Zr thickness	390 nm	195 nm	130 nm
Bilayer thickness	1090 nm	545 nm	363 nm
Total thickness	1090 nm	1090 nm	1090 nm

Samples were measured via high throughput shock studies by Dr. Sergey Matveev and Dr. Dana Dlott in the Department of Chemical Sciences at the University of Illinois in Urbana-Champaign.

2.2.5 Varied Interfacial Density

As previously mentioned, by maintaining the overall stoichiometric balance between the metal and metal oxide, as well as the overall volumetric material present to participate in the reaction, but varying the number of bilayer present in the stack, we can create a system with higher interfacial density. The higher interfacial density results in more stages in which the reaction may take place. This results in a more exothermic reaction output, and decreased reaction threshold needed to achieve ignition, as well as self propagation.

Zr/CuO samples with a total of one-micron stack thickness, but ranging from 1 bilayer to 3 bilayers were subjected to flyer plates ranging from speeds of 0.56 km s^{-1} to 2.0 km s^{-1}.

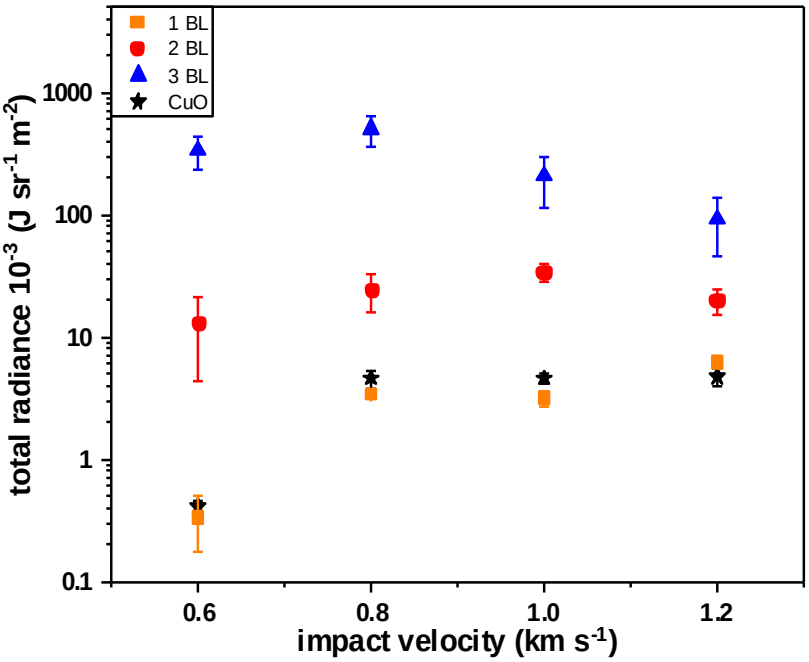

Figure 2.4. Total radiance as a function of impact velocity of the 1,2, and 3 BL Zr/CuO samples, as well as a CuO standard.

As seen in Figure 2.4, there is a clear trend of increased total radiance at each velocity, as a function of the number of bilayers present. Total radiance, being defined as the integral of the radiance vs. time curve at a specific velocity, provides the total emission output of the shock event. From this data, we can draw several interesting observations. One, being that the 1 BL sample, is not very reactive, comparatively to the CuO standard. Second, the optimal impact velocity between the 2 BL and 3 BL samples varies, as they are 1.0 km s^{-1} and 0.8 km s^{-1}, respectively. Less impact is needed for the sample containing less distance for mass transport to occur, as well as more interfaces for the reaction to take place, to achieve the maximum amount of total radiance. This suggests that at these impact velocities, the samples are reaching a self-propagating state, and thus going to completion. At higher velocities, however, the structural integrity of the samples begins to fail, as the sample is unable to recover from the mechanical load from the flyer plate. As seen in Figure 2.4, the total radiance of the 3 BL sample decreases at 1.0 km s^{-1}, compared to the 0.8 km s^{-1}, as the sample is now fighting the destructive counter effect of the high energy mechanical shock. Despite the 2 BL sample exhibiting more total radiance at the 1.0 km s^{-1} impact velocity, it may be dampened due to the destruction of the thermite nano-laminates.

The propagation of the reaction front can be seen in the post-mortem photographs of the thermite spots. As seen in Figure 2.5, the impact velocity of 2.0 km s^{-1} results in destruction of the nano-laminate. However, at 0.7 km s^{-1}, it is clear that there is a difference of reaction propagation between the 1 BL, 2 BL, and 3 BL sample. In the 1 BL sample, the reaction barely goes past the flyer plate impact point. In the 2 BL sample, the reaction begins, and propagates, but does not reach completion. In the 3 BL sample, the reaction is propagated across the sample completely. This also brings up another important finding, that the directionality of thermite in

nano-laminate formation is not unilateral. As material diffuses across the interfacial barrier and achieves mass transport, the material propagates across the plane of the interface, as well, despite being subjected to one-dimensional shock.

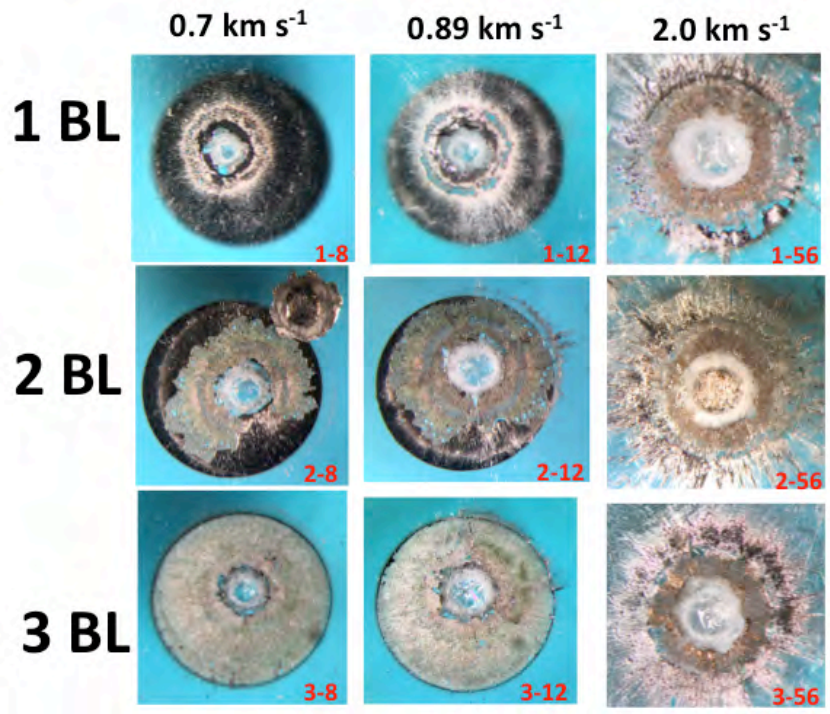

Figure 2.5 Photographs of 1-3 BL Zr/CuO after subjection to 0.7, 0.89, and 2.0 km s^{-1} flyer plate velocities.

2.2.6 Varied Stack Thickness

As previously mentioned, by keeping the overall stack thickness the same, and varying the number of bilayers present, we see the two contributing affects of increased interfacial density, allowing for more points of reaction, as well as decreased mass transport distances needed. In order to explore the affects of bilayer thickness without the contribution of added interfacial density, the number of bilayers present was kept constant, with an overall stack thickness increased, as seen in Table 2.1. The stoichiometric balance was kept the same.

The thinnest sample showed to have elevated total radiance at 0.67 km s^{-1}, whereas the first instance of elevated total radiance for the middle and thickest samples were seen at 0.87 km s^{-1}. This shows that the thinnest thermite sample required less of a shock front to initiate the reaction than its thicker counter parts. However, the thickest sample showed the highest total radiance of the three samples, as there was more material to participate in the reaction.

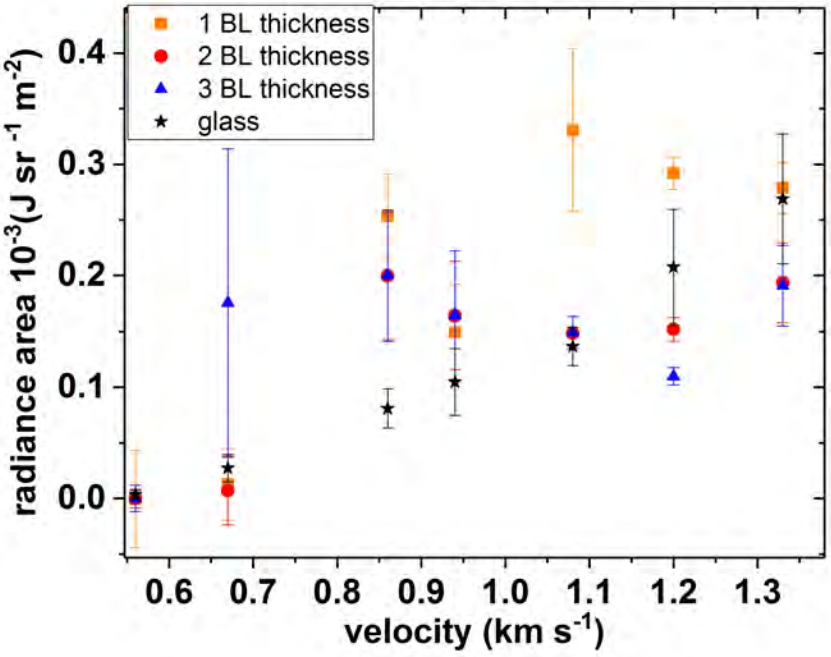

Figure 2.6. Total radiance vs. velocity of a 1 Zr/CuO bilayer samples with thicknesses equivalent to the 1, 2, and 3 BL Zr/CuO samples.

The thinnest thermite sample also shows the longest temporal activity at its respective lowest velocity of ignition, as seen in Figure 2.3. However, at 0.87 km s^{-1}, the thicker samples do not exhibit the same behavior. At the 0.67 km s^{-1}, the thinnest sample undergoes a much larger reaction, and perhaps reaches completion. However, at 0.87 km s^{-1}, the 2 and 3 BL thicknesses seem to peak in total radiance. The 1 BL thick sample peaks in radiance at 1.08 km s^{-1}.

It is important to note that the total radiance of the samples are obtained via an average of three shots at each velocity for thre1 and 2 BL thick samples, and 4-5 shots at each velocity for

the 3 BL thick samples, resulting in a larger margin of error when the data is analyzed. The glass standard had undergone 5 shots at each velocity. In order to obtain an average with smaller error, more shots need to be obtained. Although not conclusive, this data further supports the mass transport model of thermite, and that the decreased thickness results in less distance the material must traverse prior to the reaction beginning.

2.3 Time-Domain Thermoreflectance

Time-domain Thermoreflectance (TDTR) is an optical pump-probe technique that can be utilized to obtain thermal properties of materials, and is particularly beneficial for measuring thin films [70,71]. Thermoreflectance is defined as the derivative of optical reflectivity with respect to temperature [72]. The change of optical reflectivity can be attributed to the localized heating of a material due the thermal stress induced on the sample. Thus, by using an optical pump probe, a modulated heating event can be created at a localized heating event on the sample. Measuring the change of reflectivity and the delay time of the probe and then fitting a thermal model provides acoustic properties, thermal properties, and information on electron-phonon interaction [70,73].

2.3.1 Thermal Conductivity and Nano-Thermite

Previous work has shown information about heat generation of nano-thermite. Previously, we have seen that the temperature where peak of exothermic activity occurs is dependent on bilayer thickness in samples of varied interfacial density. From this study, we can see the onset of reaction occurs at earlier temperatures when the interfacial density is increased. From this information, we can deduce that the threshold of reactivity can be lowered with increasing number of bilayers present in the stack

However, as interfacial density is increased in the stack, so are the areas where heat dissipation may occur, as well as a potential resistance to heat flow in the stack. Interfaces may play a role in heat flow and overall heat propagation of thermite. Thermal conductivity in thin films on the nano- and micro-scale are subjected to imperfections in the system, interfacial barriers, and the microstructure itself [70]. It is of particular interest to study the thermal conductivity properties of thermite nano-laminates, as a function of bilayers present in a stack. Although by increasing the number of interfaces present results in a decrease in threshold of reaction onset, the cost of the increased interfaces may play a role in the thermal conductivity of the stack.

2.3.2 Thermal conductivity of Varied Interfacial Density

For TDTR experiments, the Al/CuO system was selected as a prime candidate. Compared to the Zr/CuO counterpart, the Al/CuO system results in a slower reaction rate and passive oxide formation, the Al/CuO system allows for a wider range of bilayer thicknesses to be studied across the same stack thickness.

The samples were prepared in a chamber with a base pressure of 1.8×10^{-7} Torr. 1-7 bilayer samples totaling a stack thickness of 1070 nm were deposited on ½ of a 2” silicon wafer. The silicon wafer was rinsed with acetone, isopropanol, and methanol, and then placed in a UVO bath for 10 minutes. The substrate was adhered to the stage with Arctic Silver 5 thermal CPU paste.

CuO was deposited via RF sputtering of a 2” 99.7% CuO target by Kurt J. Lesker at 200 W, in 2 mTorr of Ar at a stage height of 3.45”. Al was deposited via DC sputtering of a 2” 99.99% Al target by Kurt J. Lesker at 30 W and 5 mTorr of Ar, at a stage height of 3.45”. The sample was rested for 15 minutes in between each deposition, to limit the amount of pre-reacted

material at the interface. CuO and Al were deposited at 12.4 nm/min and 8.57 nm/min, respectively, as determined by XRR. Each sample began with Al on the bottom of the sample (Al-Si interface) to allow for each sample to be capped with an 80 nm transducer layer on top, for TDTR measurements.

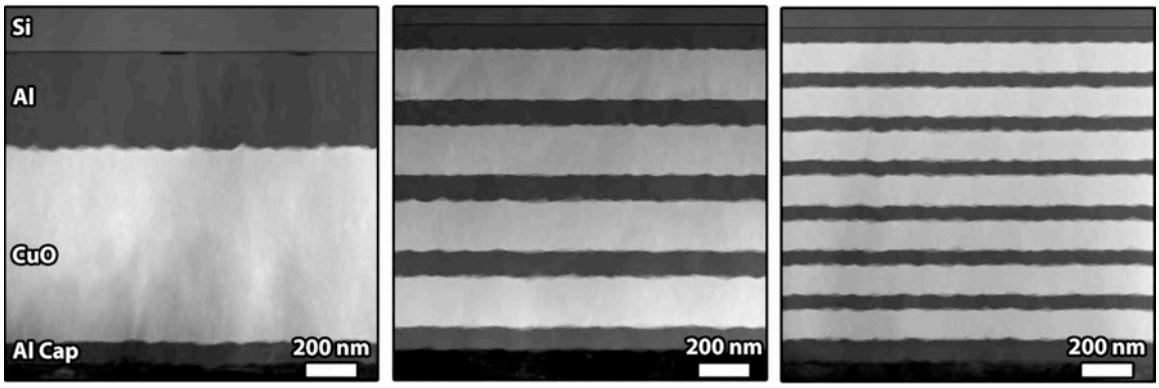

Figure 2.7. STEM Image of a 1,4, and 7 bilayer 1 micron Al/CuO TDTR sample with an Al transducer layer.

The thickness of the bilayers were measured by Dr. Everett Grimley, Rachel Jackson, and Dr. James LeBeau via STEM in the Department of Materials Science and Engineering at NC State University. In Table B.1 in Appendix B, The thickness of each individual layer can be seen, as well as additional images of the Al/CuO stacks. The layer thicknesses were measured via integrated line profiles.

The samples were then measured via TDTR and modeled by Dr. Christina Rost and Dr. Patrick Hopkins in the department of Mechanical and Aerospace Engineering at the University of Viriginia. The samples were measured at 1.15, 4.15, 7.15, and 10.15 MHz. Details of the TDTR system are described in detail elsewhere [73].

2.3.3 Results: Thermal Conductivity

For each sample, the thermal conductivity of the stack as a whole was solved for, k2. In addition, the interfacial conductivity between the Al transducer layer and the top CuO layer, G1 was also measured for each sample.

For the value of k2, the stack was treated as one collective layer, with an overall thermal conductance. From the model of k2, we can see that there is approximately a 20% reduction of thermal conductivity as the number of bilayers present is increased, as seen in Figure 2.8a.

Roughness of a thin film can propagate upwards as the deposition progresses. In order to test if the decrease of thermal conductivity of the samples when the interfacial density is increased was not due to the increasing roughness of the stack, the thermal conductivity of the interface between the transducer and the top of the sample was measured. The resulting values taken from the model, G1, were relatively constant, as seen in Figure 2.8b. Despite the accumulation of surface roughness with increasing bilayers present, the interfacial conductance of the top layer is relatively constant.

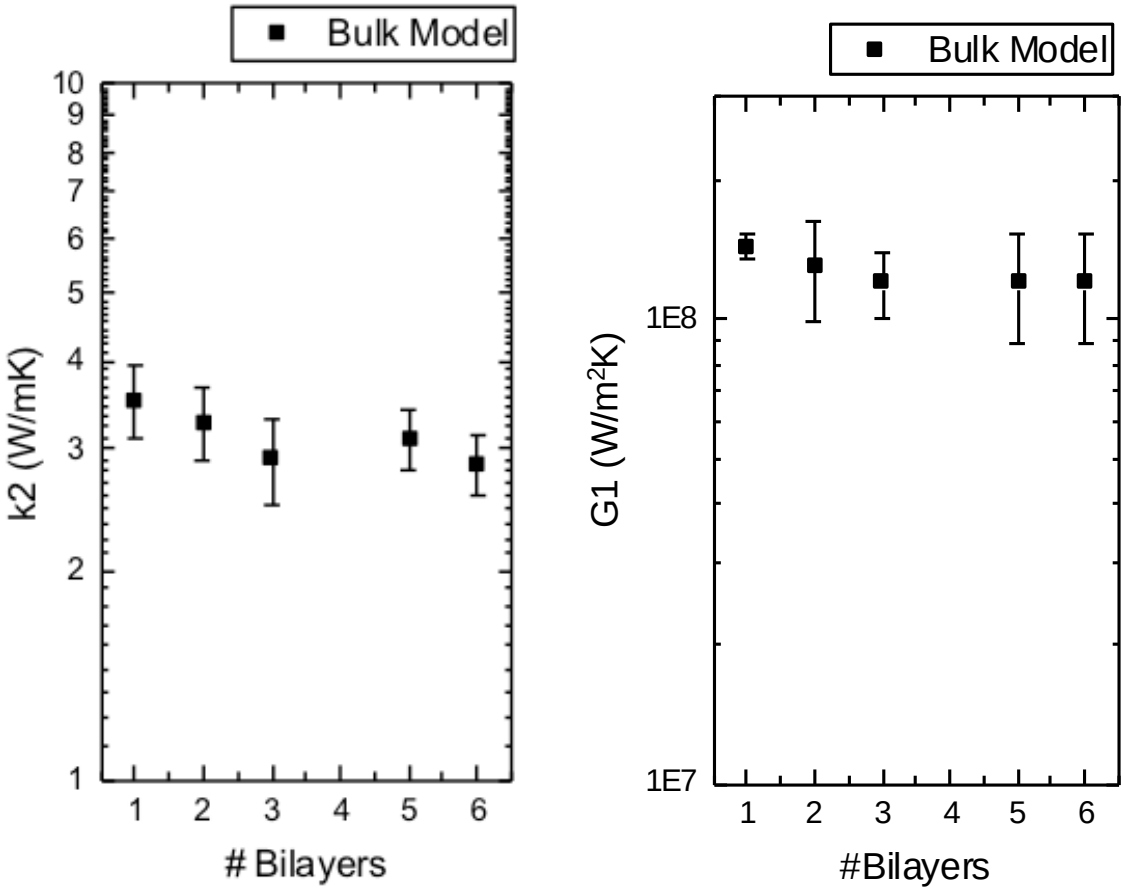

Figure 2.8. a) (left) Thermal conductivity of the Al/CuO stack. **b)** (right) interfacial conductivity between the Al transducer and the top CuO layer.

However, the extent of interface contribution is still not decoupled from the contribution of the CuO layers. The presence of the CuO in the stack contributes heavily to the thermal resistance of the samples. However, since the overall volume of CuO in the system is relatively constant across samples, we can deduce that the interfaces do play a role in thermal conductivity. However, the extent when compared to the contributions of CuO in the stack is still unknown.

Although we can deduce that the interfaces are playing a role in the thermal conductivity, we cannot further characterize the role it plays until the stoichiometry and interfacial thickness is

addressed. We are unsure of the nature or stoichiometry of the interface that forms during deposition, and if the bilayer thickness affects this. The interface appears to be on the order of 10s of nanometers, and it is possible it contributes its own unique thermal profile to the stack.

CHAPTER 3. REACTANTS OF NANO-THERMITE

3.1 Introduction

Traditionally, the thermite reactants were aluminum and iron oxide, forming aluminum oxide and iron, as mentioned in Chapter 1. However, the reaction requires fundamentally, a metal fuel source, and a metal oxide, and a terminal oxide formation with a higher enthalpy of formation to drive the reaction. Therefore, a number of combinations of metal and metal oxide can be possible for nano-thermite applications. The exploration of differing types of metal and oxide combinations yields the potential of a tunable energy density of MICs. As mentioned in Section 1.5, power density is dependent on the reaction velocity of the reaction and energy density of the material. By being able to alter the reaction velocity via geometry, and the energy density via constituents, a more flexible power density can be achieved. In addition, in situations where a specific geometry is preferred, such as a specific thickness of a RNL, or a specific size of nano-particles of other MICs, flexibility of the material is preferable. Table 3.1 [74] shows the theoretical energy densities of various combinations of thermite reactants.

Table 3.1. Comparison of specific energies and energy densities of thermite systems with different reactants.

Thermite System	**Specific Energy [-kJ/g]**	**Energy Density [-kJ/cm^3]**
2Be + PbO_2	3.16	26.7
2Al + 3PdO	3.67	23.0
2Al + 3CuO	4.08	20.8
Zr + 2CuO	3.15	20.2
Hf + 2CuO	2.38	19.8
Mg + CuO	4.61	18.2
2Al + Fe_2O_3	3.96	16.5
Zr + 2ZnO	1.56	9.16

*ZnO system calculated.

Energy densities are directly dependent on the specific energy and the density of the reactants. Therefore, engineering systems with a high specific energy and high density will result

in a high energy density. Because power densities are dependent on energy densities, this results in a large range of power densities that can be achieved. By altering the morphology and geometry of MICs, varied reaction velocity can be achieved. By altering the reactants present in the thermite system, a range of energy densities can be obtained. Thus, combining the effects of geometry and constituents present, thermite systems power densities ranging over two orders of magnitude can be developed. For example, a Zr/ZnO system with thick morphology that results in a reaction speed of 10 m s^{-1} has a theoretical power density of 0.09 MW cm^{-3}, whereas a Be/PbO_2 system with thin morphology could reach theoretical a power density of 26.7 MW cm^{-3}.

Flexibility of materials also provides an avenue in which MICs can be tuned for sensitivity, reactivity, and stability. A full understanding of different nano-systems with different reactants provides an avenue for engineering energetic thermite materials to meet the specifications of the environment in which they will be utilized.

3.2 Varied Metal

Several different combinations of metal and metal oxide pairs have been studied [32,39,28,41,27]. As seen previously, varying the metal fuel source of thermite results in different degrees of reactivity of nano-thermite. *Ex-situ* studies of annealing of the Al/CuO, Mg/CuO, and Zr/CuO nano-laminates have shown to have onset of copper formation at 800 °C, 500 °C, and 300 °C, respectively [32]. Due to this, the Al/CuO system throughout this work is treated as the more stable, less reactive counterpart, and Zr/CuO as the more reactive species. Discussed below, the sensitivity of Zr/CuO is much higher than it's Al/CuO counterpart, which is preferable or not, depending on the situation in which the material is being utilized in. As seen in Table 3.2 the TMD and theoretical maximum temperatures can be seen for each system.

Table 3.2 Comparison of theoretical density and adiabatic reaction temperature of Al/CuO, Zr/CuO, and Mg/CuO.

	Theoretical Maximum Density (TMD) [g/cm^3]	**Theoretical Maximum adiabatic reaction temperature [K]**
Al/CuO	5.109	5718
Zr/CuO	6.400	6103
Mg/CuO	3.934	4502

The less sensitive thermite, such as Al/CuO provides a system where a wide range of geometries can be explored. In addition, the stability at ambient conditions allows for safe storage, easy transport, and long-term studies of the material. Whereas, the Zr/CuO system is more beneficial for situations such as shock studies, as it is easily ignited with shock and mechanical work. In addition, the Zr/CuO system is more reactive, thus the characterization of the system by the radiance of the resulting reaction can be seen at a higher level than the Al/CuO counterpart. However, due to the reactive nature of the Zr/CuO system, the number bilayers present in the stack is limited, as the system is prone to ignition inside the chamber at higher numbers of bilayer present.

3.2.1 Al/CuO RNLs

The melting point of Aluminum is 660 °C, making it a prime candidate for the thermite reaction, making it so that the metal will not vaporize prior to the completion of the reaction. Theoretically, the Al/CuO system can reach a reaction temperature of 5718 K [74].

Using aluminum as an initial metal results in the refractory oxide formation, alumina. However, one major draw back of alumina as the terminal oxide is the formation of a passivation layer at the interface of the Al/CuO system. Because alumina is refractory, the formation of a passivation layer at the interface may hinder the oxidation of the aluminum. This could result in an increase of reactivity threshold, or a decrease in propagation to completion. As seen

previously in Section 2.3, there is a balance between the reaction output of an increased amount of interfaces present, vs. the hindrance that an increased number of passivation layers may play. As the thickness of the layers is decreased in a thermite stack, the number of passivation layers increases. Thus, the passivation layer present in RNLs with higher interface density becomes more important, as the thickness of the passivation layers to thickness of the bilayer ratio is increased. In a 10 bilayer Al/CuO sample with an overall stack thickness, a theoretical 5 nm passivation layer is 15% the thickness of the target thickness of a 33 nm aluminum layer. Not only does this hinder potential diffusion, but also alters the stoichiometry of the overall system, which plays a larger role in the higher bilayer samples.

The enthalpy of formation for alumina is -1675.69 kJ/mol, resulting in a large exothermic heat output, meaning that once the initial energy for the threshold of reactivity is met, the ending products is a much more stable configuration.

From an experimental perspective, the progress of the Al/CuO reaction can be monitored by XRD, as the formation of copper can be traced, due to the ease of the crystal formation at the elevated temperatures the reaction occurs at.

3.2.2 Zr/CuO RNLs

The replacement of zirconium with aluminum in copper oxide nano-thermite systems results in a much more reactive system, comparatively. As previously seen in Chapter 2, the utilization of zirconium results in the ability of the material to undergo shock ignition relatively simply. Previously, we have seen that although the Al/CuO can undergo shock ignition when the flyer plate reaches speeds of 0.92 km s^{-1}, it does not readily react as easily as the Zr/CuO system does, and results in significantly less radiance emission [49]. In addition, when comparing the

x-ray diffraction data of Al/CuO vs Zr/CuO, we see the formation of C at 300 °C, as opposed to 800 °C for Al/CuO [32].

The source of the reactive nature of the Zr/CuO system compared to the Al/CuO system could be attributed to the resulting oxide formed after the completion of the reaction. Oxygen transport plays a vital role in the reaction of nano-thermite. Zirconia, when compared to alumina, has a much lower thermal conductivity. The order of magnitude lower thermal conductivity of the terminal oxide layer readily promotes thermal transport throughout the thermite stack. In addition, the slightly conductive nature of zirconia allows for ionic diffusion to occur more readily [32]. Thus, when utilizing a metal that forms a less passive terminal oxide, less thermal activation is needed.

The comparative work between Al/CuO and Zr/CuO has been studied extensively elsewhere [32,49,48]. In the scope of this work, the findings discussed were utilized for engineering applications for further studies of *in situ* reaction mechanics, and engineering new systems. In addition, these systems were used as baselines for studying a new thermite reactants combination.

3.3 Varied Oxidizer

Several characteristics of a metal oxide must be considered prior to the oxide being selected. CuO, cupric oxide, is a relatively stable oxide, and does not typically decompose into Cu_2O, cuprous oxide, in ambient conditions as the stability of Cu(II) ion at standard conditions [75]. However, the decomposition of CuO to Cu_2O upon heating releases free oxygen anions, available for diffusion into the metal layer, which may play a role in the intermediate mechanism of the Al/CuO reaction. Cupric oxide when deposited exhibits a monoclinic

structure, as opposed to the cubic form of Cu. At elevated temperatures, cubic CuO does form, upon the transformation from cupric oxide to cuprous oxide, which is cubic.

Despite CuO being an ideal candidate due to the diffusive nature of the oxide, from the perspective of understanding the reaction mechanisms, the phase change of cuprous oxide to cupric oxide convolutes the overall reaction mechanism. As discussed in Chapter 4, the formation of an intermetallic or intermetallic oxide may contribute in the Al/CuO system at temperatures prior to the onset of the thermite reaction [76].

3.3.1 Zr/ZnO RNLs

An alternative initial oxide, zinc oxide, holds several benefits. Zinc oxide has a wide band gap, resulting in high electron mobility, and transparency at the morphology used in nano-thermite [77,78]. The conductive nature of ZnO opens up sets of applications where conductivity of the thermite stack as a whole can be utilized. Zinc oxide can be deposited in a number of ways, via chemical vapor deposition, and physical vapor deposition processes. Specifically, PVD processes such as RF sputtering, DC sputtering, and DC reactive sputtering, as previously mentioned in Chapter 1, as film properties can be finely controlled with the deposition parameters. In this work, zinc oxide is deposited via RF sputtering. However, the utilization of multiple sputtering methods is advantageous, as it is more easily accessible depending on power sources that are present. Zinc oxide grows in the (002) orientation at room temperature, making it an easily identifiable material on x-ray diffraction [77]. In addition, ZnO is a relatively easy film to crystallize. Although a thermite stack itself cannot be heated to high temperatures, and low temperatures may introduce diffusion across the interface, it is possible that a ZnO thin film could be heated prior to deposition of the metal layer in a 1 BL sample. This allows for a better

match between computational models and experimental samples, if the ZnO is able to reach a crystalline state. In addition, this also introduces a new parameter of the reaction.

Due to the transparency of zinc oxide thin films, it is also a prime candidate for shock studies. Although CuO is a suitable oxidizer for shock studies, the opaque nature of the material after several hundreds of nanometers of material results in it acting as an optical density filter of the radiance of the material upon shock. Because of this, a clear thin film is advantageous in shock studies, as the signal is not dampened by the oxide transparency.

3.3.2 Experimental

A 1-5 bilayers series was deposited on silicon. The samples were rinsed in acetone, isopropyl alcohol, methanol, and then placed in a UVO bath for 10 minutes.

Deposition rates were determined via XRR, further discussed in Appendix A. Zirconium was deposited via DC sputtering at 40 W in 20.2 sccm Ar under 2 mTorr at 7.3 nm/min. Zinc oxide was deposited via RF sputtering of a 0.25” 2” ZnO target at 215 W by Kurt J. Lesker at 10.3 nm/min.

The samples were then heated in an N_2 atmosphere at 250 °C, 350 °C, 450 °C, and 550 °C. The onset of reaction was characterized by the formation of Zn in the sample, as seen in x-ray diffraction.

3.3.3 Results

Prior to the heating of the samples, it was observed that there is a significant peak shift of the (002) ZnO peak of the 1-5 BL stacks, suggesting that the deposition process of ZnO may be changing the thin film from sample to sample. Although more data must be collected to fully characterize the deposition of ZnO via RF sputtering for RNLs, plausible explanations are proposed in Section 3.35 for the extent of this work via the preliminary data obtained. One

possible explanation is that ZnO is prone to intrinsic stress during deposition. Another possible explanation is the behavior of the ZnO target as a wide band-gap semiconductor during the RF sputtering process.

However, despite the irregularities of the ZnO thin film, preliminary studies have shown that the Zr/ZnO system undergoes a reaction, as evident by the formation of Zn as the system is heated.

3.3.4 Zr/ZnO *ex situ* Heating

Like the Zr/CuO and Al/CuO samples, the progress of the reaction can be characterized by the formation of the terminal metal. Thus, following the formation of Zn peaks in x-ray diffraction after heating was used to characterize if the reaction began. Upon heating of 1-5 bilayers of the Zr/ZnO system at 150 °C, 250 °C, 350 °C, 450 °C, and 550°C, reaction was evident in all five of the samples. Below, in Figure 3.1, the formation of Zn can be seen at 350 °C in the five bilayer Zr/ZnO sample. Zn appeared in the x-ray diffraction pattern for 2-5 bilayers at 350 °C. However, for the 1 bilayer sample, Zn peaks did not begin to appear until 550 °C.

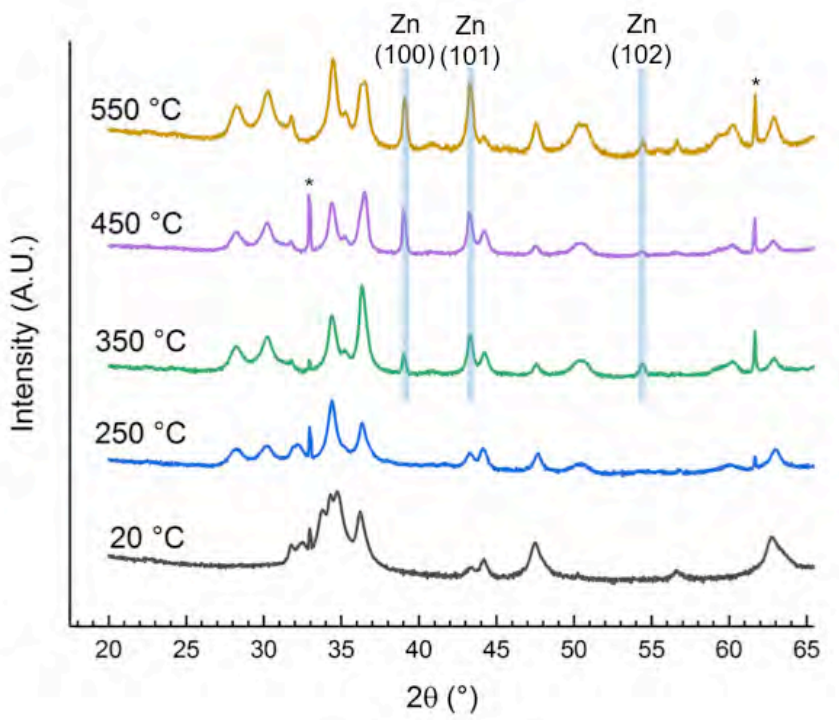

Figure 3.1 X-Ray Diffraction pattern of heating series of a 5 bilayer Zr/ZnO RNL sample. Evidence of reaction is seen at 350 °C by the formation of Zn. * denotes substrate peaks.

Additional x-ray diffraction data for 1-4 bilayers can be seen in Appendix C. The 150 °C x-ray data showed no change from the room temperature data, and therefore was omitted for simplicity purposes. The formation of Zn at 550 °C in the 1 bilayer sample as compared to the multi-bilayer samples follows the same trend as decreased temperature of onset of reaction with increasing number of bilayers, as discussed in Section 2.1 However, it would be beneficial to reproduce the data with a smaller step size of heating, or upon heating in an *in-situ* environment, to determine if the 2-5 bilayer samples follow a trend of differing onset of reaction between temperatures above 250 °C and below 350 °C.

The formation of Zn at 350 °C is on par with onset of reaction with the Zr/CuO system at 300 °C [32]. In the same vacuum chamber, the Zr/CuO system undergoes ignition at 4 bilayer

thicknesses during deposition, and cannot be transferred out of vacuum without reaction. The Zr/ZnO system has reached interfacial density of 5 BL thus far, suggesting that the Zr/ZnO system is a much less sensitive system, comparatively. The preliminary results of Zr/ZnO onset of reaction shows the potential of creating an RNL system that is a less sensitive alternative to Zr/CuO, but still holds a similar lower reaction threshold as compared to the Al/CuO system.

3.3.5 Intrinsic Film Strain in ZnO

As previously mentioned, a discrepancy between the peak positions of the ZnO (002) peak exists across the deposition of 1-5 bilayers of Zr/ZnO. Although more studies must be done to determine the exact nature of the discrepancy and root of the shifts, the scope of this work identifies the speculations of the origin of the shifts.

Zinc oxide exhibits a wurtzite crystal structure, preferring the (002) orientation during deposition. As deposited, ZnO thin films exhibit shifts that could be due to tensile strain, as evident in the shift in the (002) peak [77], which is evident in the x-ray diffraction data, seen below in Table 3.3.

Table 3.3 2Theta, FWHM and d spacing for the (002) ZnO peak in 1-5 BL Zr/ZnO stacks, as well as a ZnO thin film.

	2Theta [°]	**FWHM**	**d spacing [Å]**
(002) Theoretical	34.441	-------	2.602
Thin film	33.973	0.504	2.757
1 BL	34.008	0.278	2.754
2 BL	33.670	0.399	2.779
3 BL	34.214	0.242	2.740
4 BL	34.184	0.202	2.742
5 BL, 1	33.781	0.236	2.770
5 BL, 2	34.298	0.203	2.734

During thin film deposition, there are several stresses that may occur. Thin films are confined to the substrates they are grown on, and are subjected to lattice mismatch, and differing

coefficients of expansion. In the beginning of thin film growth, the material is subjected to compressive stresses due to surface stresses; this results in very thin films being subjected to surfaces stresses at a greater level than thicker samples, comparatively. Because of this, very thin films present in higher bilayers samples are subjected to surface stresses during the rest time in deposition. This results in a compressive stresses becoming evident in very thin films [79]. Because the surface of a thin film contains fewer bonds than the interior of a thin film, the spacing of the atoms at the surface differs from the interior atoms. The larger interatomic spacing of the surface atoms results in a pressure being placed onto the inner atoms, called the Laplace pressure [79]. Although the films throughout this work are typically thicker than the thin films that are subjected to compressive strain due to surface stress, the multilayers are still subjected to surface-surface stresses at the interface. In samples with a higher interfacial density, the interface stresses have a larger effect on the intrinsic stresses of the stack as a whole.

In 1-bilayer samples, ZnO is subjected to lattice mismatch between the Si substrate. As the film grows, this effect is minimized. However, the mismatch between the coefficients of thermal expansion can still play a large role. During deposition, as the sample is heated due to energy transfer during sputtering, the substrate begins to heat, resulting in a thermal stress on the film. Because the film has become confined to the substrate and the mismatch between thermal expansion coefficients, a strain is introduced to the film. In higher number of bilayer samples, the oxide is also subjected to lattice mismatch between the metal, as well as the metal's coefficient of thermal expansion.

In thicker thin films, as deposition continues, the film is subjected to tensile stress, as a result of island coalescence [77,79]. As islands grow, and begin to coalesce, cohesion occurs

between the islands. As the islands reach a critical size, the lattice parameters are propagated throughout the growth.

In the 1-5 BL Zr/ZnO, there appears to be significant variation of the (002) ZnO peak, when compared to ZnO powder diffraction. In addition, the (002) ZnO peak varies between the 1-5 BL samples. The intrinsic stresses introduced to the ZnO layers in the stack undergo different stresses, depending on the thickess of the ZnO sample. In addition, in increased interfacial density samples, the ZnO layers each have individual stresses that differ. For example, the bottom ZnO layer of a 3 BL sample will be subjected to more compressive forces than the top ZnO layer.

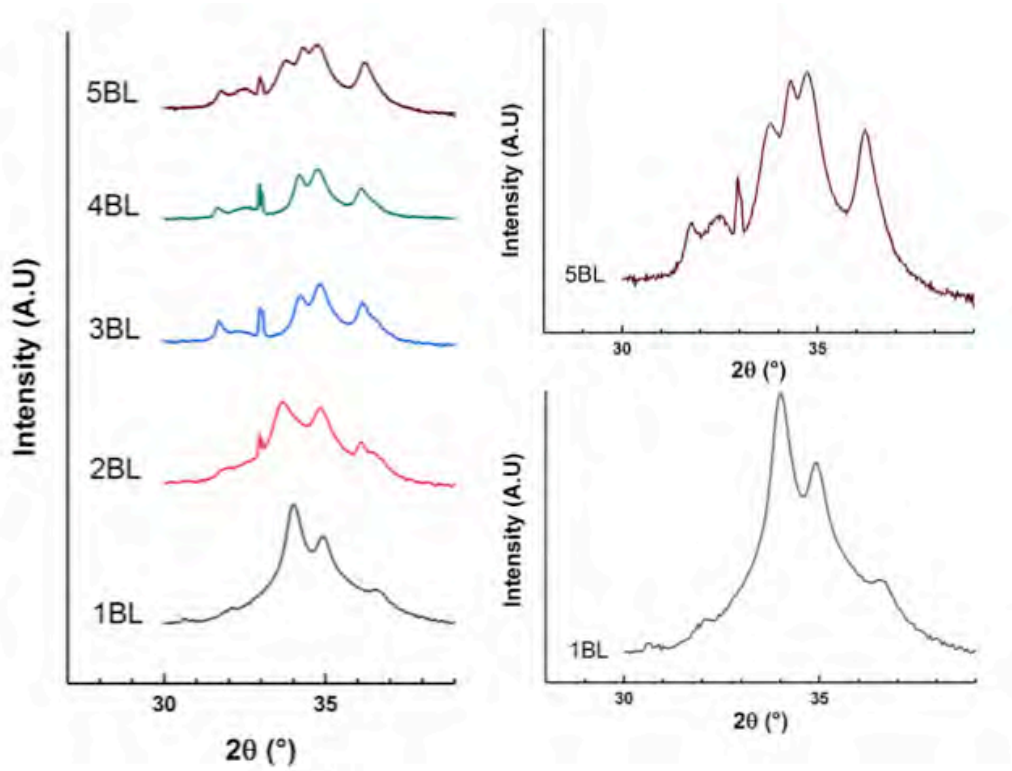

Figure 3.2 a) (left) Comparison of the ZnO/Zr peaks present in a 1-5 BL sample as deposited. **b)** (top) Zr/ZnO 5 BL as deposited. **c)** (bottom) Zr/ZnO 1 BL as deposited.

As seen above in Figure 3.2, there is significant variation of the 1-5 BL XRD pattern at room temperature. In the 5-bilayer sample, an additional peak appears. However, the (110) Zr

peak does not appear to shift, suggesting it is not as sensitive to the deposition process as ZnO, resulting in less intrinsic stresses being present in the film itself.

3.3.6 RF Sputtering of ZnO

Upon further investigation of the deposition process utilized for ZnO, it was found that the deposition rates were not steady, when compared to CuO. The deposition rate of ZnO begins rather elevated, and as time progresses, reaches a steady deposition time. In addition, if sputtering of Zr preceded ZnO deposition; the ZnO deposition rate was elevated again. Although more studies need to be done, the author speculates this could be due to the nature of ZnO as a wide band gap semiconductor, specifically the insulating nature of ZnO.

During sputtering, the sample on the stage and the vacuum chamber itself acts as an anode, and the sputtering target a cathode. This electric potential allows for free electrons to be repelled from the target source, and then collide with the carrier gas, producing positively charged ions that bombard with the target source. This electrical differential is important in sputtering, as it promotes the positive ionization of the carrier gas. Because of the insulating nature of ZnO, the issue of the “disappearing anode” is introduced. With conductive materials, such as metals and conductive oxides, the electric potential between the cathode and anode is uninterrupted, as the anode is coated with conductive material. However, because ZnO is a wide band-gap semiconductor, it is possible the ZnO is not reaching a conductive level, and is acting as an insulator. As the deposition progresses, insulating material is deposited on the anode, “masking” the charge differential between the cathode and anode. This results in a “floating” electrical potential during the deposition process. This has a cascading effect: as the electrical differential between the cathode and anode disappears, free electrons are not accelerated as much

towards the carrier gas, the carrier gas is less frequently ionized, resulting in less ejection of target material, and thus decreasing the deposition rate over time.

In the case of creating multilayers, ZnO deposition is followed by Zr deposition. Depositing the conductive material onto the anode allows for the electrical potential to be restored. Thus, when ZnO is deposited again, an increase in deposition rate is seen initially, and then decreases as the anode disappears. Because ZnO is RF sputtered, there is a cycle of positive and negative charge on the target. Traditionally, the negatively charged cycle results in the attraction of the ionized carrier gas, and the positively charged cycle results in the ejection of the target material and positively ionized carrier gas. If the ZnO deposition on the anode results in an insulating layer, the ejection of the positively ionized carrier gas during the positively charged cycle on the target may not be repelled by the anode, resulting in positive charge build up on the film, and consequentially, in the multilayers.

Despite the source of the deposition rate dropping over time, it consequentially has lead to samples that are not stoichiometric, and are not equal in the off balance of stoichiometry across varying number of bilayers. A 1-bilayer sample is only subjected to the increased deposition rate once, and then is deposited at a lower deposition rate than calculated. However, a 5-bilayer sample is subjected to the elevated deposition rate five times, and then a lower deposition rate than accounted for. In all five of the samples, after they were heated to 550 °C, the ZnO peaks were still seen, as seen in Figure 3.3, implying an excess of ZnO was present.

In order to account for this, further studies must be done to model the deposition rate, or a form of biasing must be applied to the sample stage. The results of the onset of Zn may change as a result of achieving a stoichiometric balance between the metal and metal oxide.

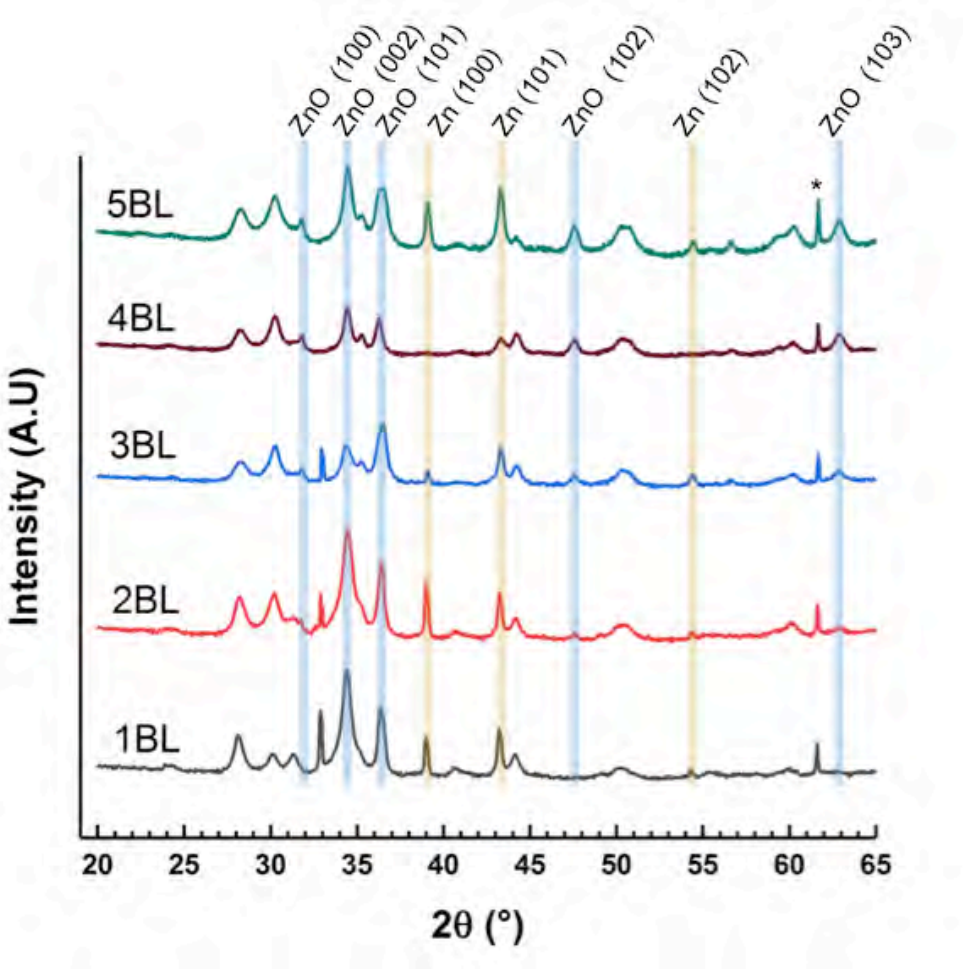

Figure 3.3 XRD data of 1-5 bilayer Zr/ZnO samples after heating to 550 °C, highlighting the excess ZnO present after reaction.

As seen in Figure 3.3, several ZnO peaks appear in the XRD pattern. Note: Zn does not appear in the 4-bilayer sample heated to 550 °C, but does appear in the 350 °C and 450 °C pattern. The 4-bilayer x-ray diffraction data can be seen in Appendix C.

The appearance of several Zn peaks along side the ZnO peaks shows that the samples underwent reaction, but that the reaction was limited by the amount of zirconium present. This can be seen in the x-ray diffraction data in Appendix C, where the presence of Zr disappears around 250 °C for most of the samples.

3.4 Concluding Remarks

The Zr/ZnO system is interesting due to its smaller energy density, compared to the Al/CuO and Zr/CuO system, as well as the transparent nature of ZnO. This opens up applications where transparent oxides could be utilized, as well as advantages for shock studies of the system. The Zr/ZnO system also provides a cohesive bridge between experimental and computational studies of the system. However, more studies must be conducted to determine the best mechanism of deposition for ZnO, as well as the behavior of the material as a whole.

Preliminary studies presented in this work show that the Zr/ZnO system is less sensitive than it's Zr/CuO counterpart, leading to the potential of thinner bilayers in the RNL stack. The formation of Zn in the x-ray diffraction data is evident, making tracing the reaction of relative ease. Because of this, *in-situ* XRD studies could be benefitial in determining a more precise onset of Zn formation, and reaction onset. DSC studies conducted on Zr/ZnO will also help understand the exothermic output and onset of reaction.

CHAPTER 4: INTERMETALLIC FORMATION IN NANO-THERMITE

4.1 Introduction

The thermite reaction is often described as a “simple” redox reaction between a metal, *M*, and a metal oxide, *AO*. As previously mentioned throughout this work, the end result of this reaction is a more energetically favored metal oxide formation, *MO* and left over metal constituent, *A*, driven by the enthalpy of formation of *MO*. In a perfect environment, and ideal situation, these two materials would mix perfectly, and oxygen would be swapped between the two metals via mass transport.

However, as the geometry of the system is decreased, it is possible that the traditional mechanism of the thermite reaction changes. This resulting mechanism change may result in intermediate material formation, such as an intermetallic or intermetallic oxide material at the interface.

From an engineering standpoint, the existence of an intermetallic intermediate mechanism opens up new methods in which the reaction output can be controlled. The promotion of the intermetallic formation could potentially enhance or dampen the resulting energetic output of a thermite nano-laminate. Furthermore, an understanding of the overall reaction mechanism allows for the utilization of developing a tunable energetic material.

4.2 Intermetallic formation in Al/CuO System

In the bulk system, the thermite reaction has been traditionally treated as a reduction-oxidation reaction between a metal and a metal oxide. In the nano-regime, this still holds true in the beginning and end of the reaction, but the question arises: what intermediate steps are occurring between the initiation and completion of the reaction? In the bulk reaction, intermediate or secondary reactions that occur on the nano-scale may be negligible. When the

morphology of the reaction is decreased to the nano-scale, these secondary reactions begin to play a larger role, and may alter the characteristics of the reaction entirely. Diffusion at the interface begins to govern the reaction.

Traditionally, the main mechanism for nano-scale thermite in the lower activation energy regime is considered to be solid-state ion transport [32,48,80]. In prior work, it has been observed that exothermic activity was seen below the melting point of aluminum, 660 °C [81]. DSC studies of CuO and passivized Al nano-particles has shown evidence of reaction occurring at 570 °C, with $CuAlO_2$ formation in a 2:1 ratio of Al:CuO at 1000 °C, as well as Cu_2O formation [76]. Al/CuO nano-composites reacted showed evidence of multiple intermetallic constituents forming [82]. The peak of exothermic behavior of materials with bilayer thickness of 400 nm and below occurs around the eutectic melting point of the intermetallic melting point of Al-Cu, as seen in prior work [49] , as seen in Fig. 4.1. The evidence of melting suggests that the reaction mechanism is shifting from a traditional solid-state ion transport to a different mechanism involving a molten state of the metals, as well as parallel reactions occurring.

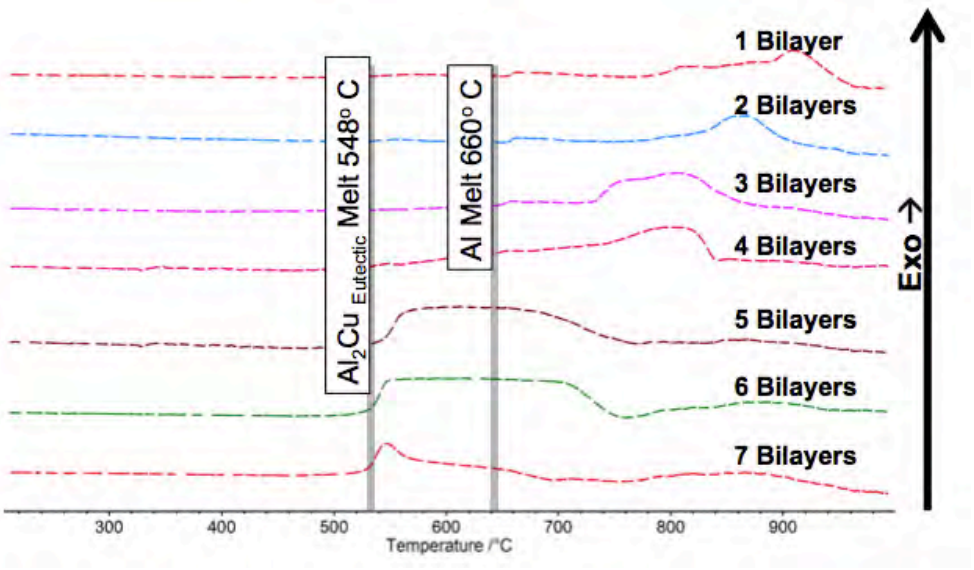

Figure 4.1. Exothermic activity in DSC measurements seen below the melting point of Al observed in thermite samples with bilayer thicknesses below 400 nm [49].

At the metal oxide *AO* and metal *M* barriers of the RNLs, intermixing occurs and is the area where the reaction begins, as seen in Figure 4.2a. Traditionally, it is believed that oxygen defused from the initial metal oxide *AO* through the forming terminal metal *A* and to forming terminal oxide *MOx*. While this is occurring, the initial metal *M* is also diffusing to the forming oxide layer. The combination of these two diffusions is suspected to be the main reaction pathways in the solid-state ion diffusion model, as seen in Figure 4.2b. The forming *MOx* in the solid-state diffusion mechanism poses an energetic barrier for the reaction to become self propagating; the oxygen must be able to diffuse through the stable configuration of the forming oxide layer to reach the diffusing *M* in order to go to completion, as seen in previous work, this energetic barrier is overcome via mechanical stress, thermal energy, and electrical ignition [48].

At thinner bilayer geometry, the author proposes the mechanism changes. The intermetallic or intermetallic oxide formed during deposition has a more prominent presence in

thinner bilayer geometry, as there is more interfacial density. This intermediate species A_xM_y (which may or may not be oxidized throughout this process) becomes a bridge for oxygen diffusion, as seen in Figure 4.2c. The presence of a Cu rich intermetallic may suggest that Al diffusion plays a larger role than previously anticipated.

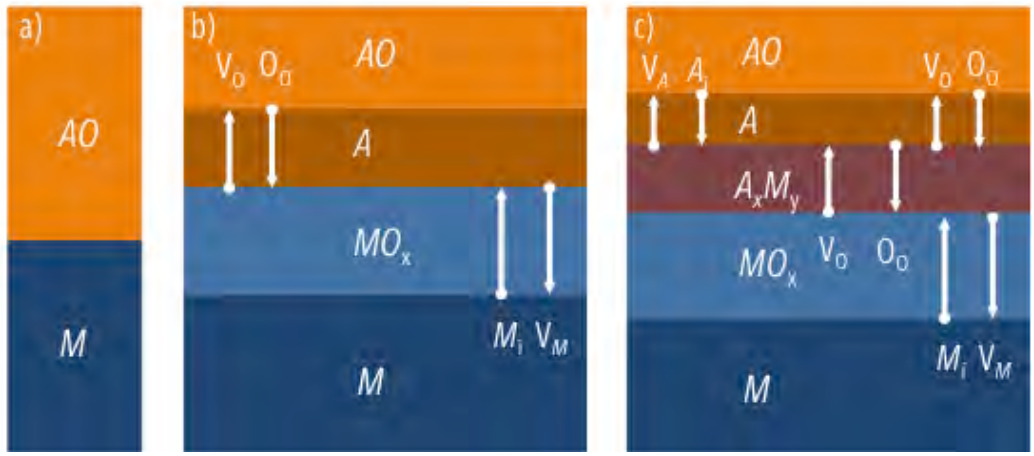

Figure 4.2. a) The initial geometry of an *AO* and *M* bilayer. **b)** The solid-state ion diffusion model showing movement of the oxygen from *AO* and the metal from *M* to form the final oxide MO_x. **c)** The proposed model with the formation of an intermetallic A_xM_y between the final constituents of the bilayer.

This work is focused on identifying the evidence of an intermetallic and intermetallic oxide layer present in the reaction mechanism of Al/CuO. Al/CuO is a relatively robust thermite system, compared to its other *M*/CuO counterparts studied previously [32,81] making the identification of an intermetallic phase more attainable. This work utilizes *in-situ* hot stage XRD analysis to determine the presence of the intermetallic. The presence of a eutectic melting point in thermite bilayers has the potential to provide a tunable ignition, as the exact temperature of the eutectic melting point may be used as the effective activation energy in future nano-thermite applications [28].

4.2.1 Experimental

A twenty-bilayer RNL sample was layered in an alternating geometry on a 2” diameter sapphire substrate via physical vapor deposition using dual beam magnetron sputtering. The total stack thickness was 2 micometers. The sample was allowed to rest for twenty minutes between depositions, and an hour every four bilayers. Deposition rates were determined via X-Ray reflectivity (XRR). Al was deposited at 11 nm/min using DC magnetron sputtering at 4 mTorr. CuO was deposited at 15 nm/min using RF magnetron sputtering at 2 mTorr. The resulting sample contained twenty bilayers of Al/CuO, comprised of 37 nm of Al and 67 nm of CuO, with an overall thickness of approximately 2 microns.

The samples were placed in an XRK 900 Reactor Chamber with an N_2 environment at a flow rate of 20 sccm. The sample was heated at 5 °C/min, and held at 900 °C for 30 minutes, and cooled at 5 °C/min. The sample was analyzed at a 2theta range of 30°- 60° with an omega offset of 2° to limit the presence of the substrate. The results were analyzed for the existence of the final constituents and the presence of possible intermetallic peaks.

4.2.2 Results

The resulting x-ray pattern shows ignition, as indicated by the presence of two prominent Cu peaks at 42.8° and 50° (indicated by the symbol ¢), seen below in Figure 4.3.

There are several areas of interest. Two prominent peaks appear at room temperature, consistent with the presence of monoclinic CuO (indicated by ✚), 35.38° and 38.56°. The as deposited CuO takes the form of monoclinic CuO, as seen in prior work [49]. A strain of the peaks is expected at low thin film thicknesses. At approximately 423 °C, the 35.38° peak begins to shift towards 36.53°, consistent with the formation of Cu_2O (indicated by ■). The most prominent Cu peak begins to appear around 42.48°.

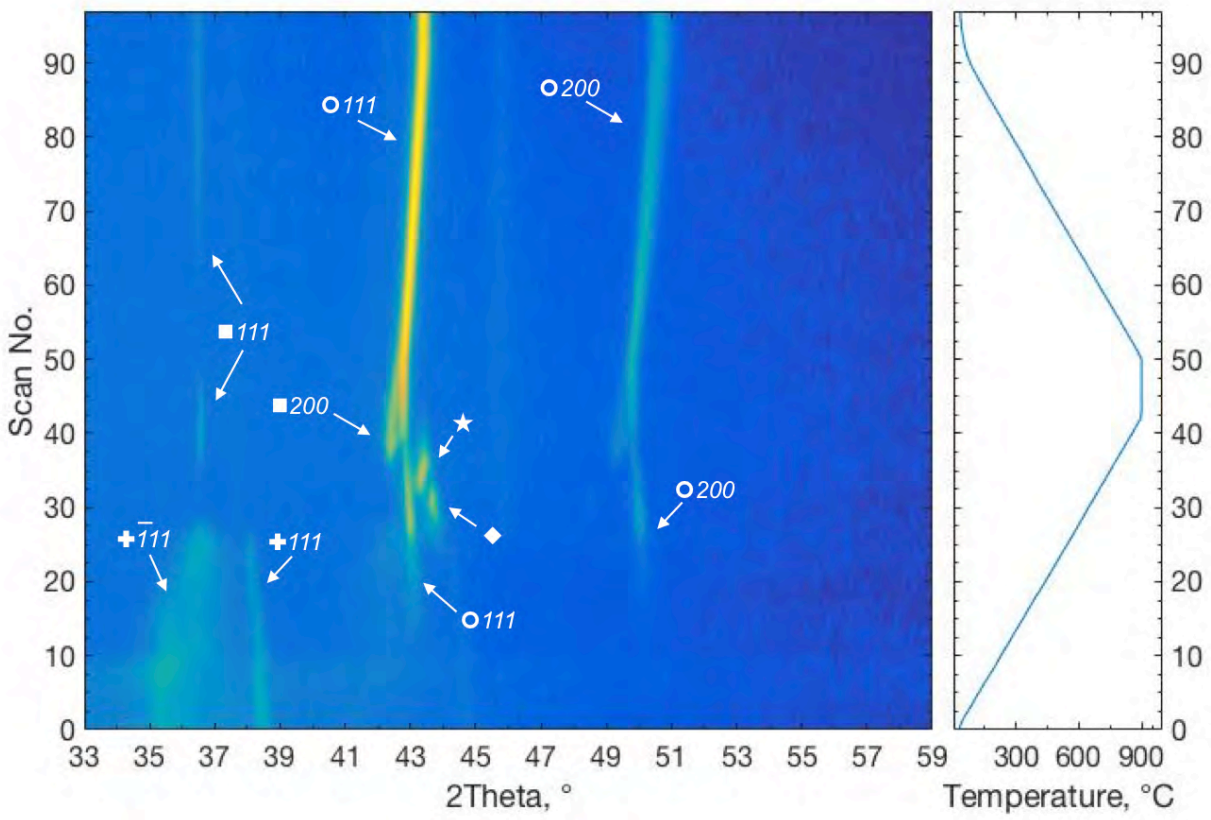

Figure 4.3: The resulting x-ray diffraction patterns of Al/CuO thermite obtained *in situ* at a heating rate of 5 °C/min that underwent ignition, seen by formation of Cu (O).

Due to the amorphous nature of sputtered Al, and the forming amorphous Al_2O_3 constituent, the reaction onset and completion is characterized by the formation of Cu. The resulting diffraction pattern shows an end result of ignition, with Cu peaks present at approximately 42.8° and 50°. The presence of Cu is seen as early as 300 °C, but reaches a prominent intensity around 550 °C, consistent with previous DSC studies, seen in Figure 4.1. The Cu peaks also undergo a shift during the heating and cooling of the sample, consistent with thermal expansion and relaxation. Through the heating process, Cu metal is observed at (111) and (200).

4.2.3 Discussion: Intermetallic Peak Formation

The scope of this work is to determine if there is evidence of a possible deviation from the reaction mechanism traditionally held during the thermite reaction. The formation of reversible peaks prompts additional studies to determine the identify of these peaks, as well as what prompts a deviation from the traditionally believed solid-state ion diffusion, and what conditions lead to it.

Shortly after Cu formation, additional peaks appear above 600 °C, suggesting the presence of the formation of another material. The presence of another material would suggest that traditional oxygen diffusion in a solid state ion transfer may not be the only mechanism at play; if the reaction was a true redox reaction, lacking any intermediate mechanisms, then Cu and Al would be the only present metallic peaks. The peaks of interest to this study occur in the range of 42°-44°, as peaks are present in the heating process that are later dissipated at high temperature. Despite needing further characterization to determine the exact identity of these peaks, several possibilities come to mind.

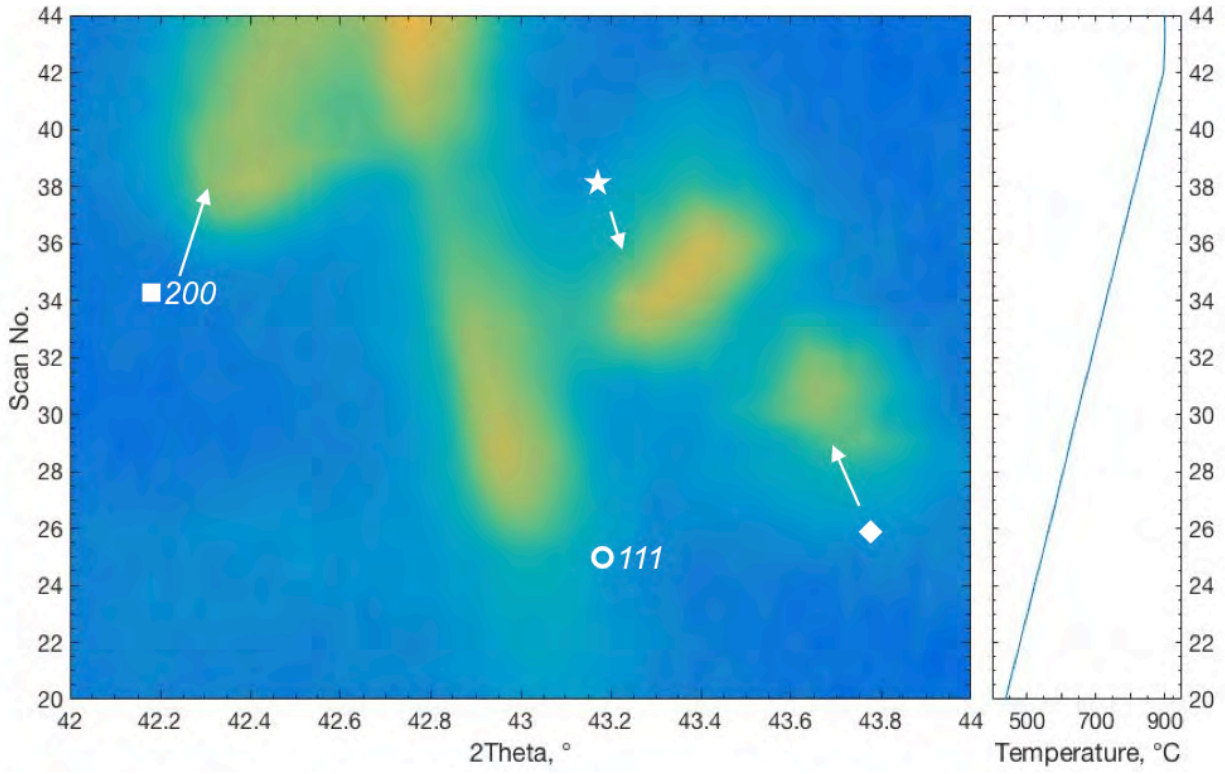

Figure 4.4. Two unknown peaks (indicated by ★ and ◆) in the temperature range of about 600 °C to 810 °C abruptly form and disappear throughout the reaction.

Several peaks abruptly form and disappear throughout sample heating at different temperature ranges, as seen in Figure 4.4. The abrupt intensity of these peaks may be an indication of the presence of an intermetallic, as several eutectic points of Al-Cu intermetallic are within +/- 20 °C of 560 °C, as seen in Figure D.1 in Appendix D. The exact intermetallic formation may not be stoichiometrically balanced to a known intermetallic, seen experimentally in RNL systems. However, there are several probable identities, as seen below in Table 4.1.

Table 4.1: A sample of possible Al-Cu intermetallic formations.

Intermetallic	Cu % comp.	Primary reflection	Temperature onset [°C]	Temperature offset [°C]
$AlCu_4$	80%	43.32	300	360
Al_3Cu_2*	40%	43.67	560	960
$AlCu_3$	75%	43.97	567	1050
Al_4Cu_9	69%	42.21	300	870

The most probable intermetallic species that may be present are similar to the intermetallics Al_3Cu_2 and $AlCu_3$. The peak present in the range of approximately 43.2° - 43.6° (indicated by ★ in Fig 4.) formed in the range of about 680 °C to 810 °C. This peak may be an impure phase similar to Al_3Cu_2 that formed during a Cu composition around 40% at the interface. The second unknown peak (indicated by ◆ in Fig 4.) occurs in a range of approximately 43.6° - 43.8° at a temperature of about 600 °C to 810 °C, consistent with an impure phase similar to $AlCu_3$, with a Cu composition of 75%. However, it must be emphasized that more studies are needed to determine the intermetallic formations at the interface. The formation of $CuAl_2$ And Cu_9Al_4 in the Al/CuO system has been cited in *in-situ* thermal analysis of nano-powders [82].

The intermetallic formation also may undergo a dynamic stoichiometric shift throughout the reaction, if the diffusion flux is time or temperature dependent. This would make the identification of the exact intermetallic present during the reaction difficult to identify in traditional x-ray diffraction, and may also be heat rate dependent. It is also important to note that the forming Al-Cu may be in a molten phase during the reaction. Further experiments are needed in order to determine the identity of the peaks present.

For the scope of this work, the existence of two peaks during the heating of the sample that are not present in the end result of the material is consistent with the idea of an alternative reaction mechanism. Formation of additional materials suggests that there is more than solid-

state ion diffusion resulting in the terminal metal and metal oxide. More characterization is necessary to determine whether or not this is a secondary oxide phase, an intermetallic phase, or phase transformations of the materials present.

4.3 Future Work: Engineering of Intermetallic formation in Al/CuO

The results of the *in-situ* heating of a twenty bilayer Al/CuO sample sparked a new question of engineering in thermites: can we facilitate the formation of an intermetallic intermediate material in thermite reactive nano-laminates? And if so, does this enhance or dampen the reaction?

The formation of an intermetallic species could potentially be stimulated by the presence of a metal-metal contact at each interface of the Al/CuO system. By depositing a very thin layer of the terminal metal at each interface of the thermite nano-laminate, the formation of an intermetallic species could potentially be engineered into the system. The added third species may play a role in hindering or enhancing the reaction. In the case of hindrance, the extra species may block the vital oxygen diffusion necessary for the reaction to proceed. However, the added metal may act as a reactive alloy, resulting in added energy needed to promote the reaction to self-propagation.

Introducing a thin terminal metal layer at each interface of traditional bilayer geometry Al/CuO system could hinder, or enhance the reaction. The terminal metal, in the case of the Al/CuO system is Cu, must be thin enough to not drastically alter the integrity of the thermite system, but also be thick enough to play a role in the reaction mechanism itself. Because the interfacial material that forms is predicted to be on the order of 1-10 nm, a 5 nm thick Cu layer deposited at each Al-CuO interface was chosen. It can be hypothesized that depositing a thin

layer of Cu would limit the formation of the passivation terminal oxide layer during deposition, thus facilitating mass transport across a very thin metal barrier.

CHAPTER 5: CONCLUDING REMARKS

5.1 Future Work

5.1.1 Engineered Power Densities of RNLs

From an engineering standpoint, the versatility of thermite as an energetic material allows for engineered characteristics in regards to stability, sensitivity, and reactivity. Particularly, on the nano-scale, MICs can be utilized to create materials that respond to specific external stimuli, and produce specific desired energetic outputs. The focus on tunable power densities can be achieved via multiple approaches. As seen in Figure 5.1, the engineering of tunable power densities in thermite follow two approaches:

1. Increasing the reaction velocity of the reaction increases the power density
2. Increasing the energy density and/or density of the material increases the power density

Looking at Option 1, this can be achieved as the morphology of RNLs continues to be studied. We have seen that the decrease in the distance in which mass transport must occur across results in an increase in reactivity. When compared to bulk thermite, we have observed that RNLs exhibit faster reaction velocities [48,83].

An increase in reaction velocity may also be achieved as mass transport is facilitated via increased diffusion rates of the terminal oxides present in the RNL stack. This can be achieved by using metals with terminal oxides of high diffusion coefficients, such as Al_2O_3. In 1 BL RNL samples, annealing the initial oxide layer to achieve a crystalline structure prior to the deposition of the initial metal may also promote mass transport across the barrier. Whether or not the facilitation of mass transport contributes more to the reactivity of the material in the sense that the threshold of reaction onset is lowered, or if the velocity at which the reaction occurs must

still be studied. Similar to how high explosives benefit from molecular mixing via short distances, and short time scales, the decrease in distance of mass transport, and the increase of diffusion rate could achieve higher reaction velocities.

Following Option 2, engineering materials with increased power densities via intrinsic energetic and physical characteristics holds an advantage in creating tunable power densities of MICs. So long as the reaction remains exothermic, and the terminal oxide has a lower energy of formation than the initial oxide, many combinations of metal and metal oxides can be attempted in thermite MICs, contributing to an increase in energy density. By creating a system with a large specific energy, the energy density can be increased, thus increasing the power density.

Exploring the idea of binary or ternary initial metals opens up the realm of metal alloys being utilized in thermite RNLs. Alloying the initial metal species of thermite can achieve a more dense material, resulting an increase in power density. In addition, alloying the metallic species of thermite is approachable via PVD techniques, as the metal constituents of the alloy can be co-sputtered in the same chamber.

5.2 Broader Impact and Scientific Merit

Thermite and nano-thermite hold many potential applications, both military and civilian. Due to the stability of thermite and the temperature of the reaction, thermite has been utilized in military anti-munitions applications, such as melting through engine blocks or steel apparatuses. RNLs can be extended to anti-munitions applications of advanced weapons; integrating RNLs into microchips can provide method of remote disarmament. The combustive nature of thermite holds promise as incendiary devices. Outside of military applicants, nano-thermite holds promise in transportation, medicine, energy storage, and microbial defenses. The utilization of MICs as fuel additives provides more energetic output from fuel sources for advanced propellants.

Thermite in small quantities on the nano-scale can be utilized in medical applications as micro-cautery implants. The large energy storage of nano-thermite could be utilized as one-time energy storage reservoirs. The high temperature of reaction of MICs can be employed as anti-microbial defenses.

The morphology of thermite RNLs provides an avenue in which the fundamental materials science, physics, and chemistry of the system can be studied in a controlled environment. Grasping the fundamentals of the thermite reaction presents the opportunity for advancement in a number of technological areas. The results of studying thermite provides us with a more fundamental understand of energy release, where solid-state systems and other nano-laminate systems can be developed. Further studies of mechanisms of transport on the atomic scale of reduction-oxidation reactions in the solid-state and their relationship to properties, structure, and boundary conditions further contributes to the fundamental understanding of this system.

5.3 Conclusion

Throughout this work, the idea of engineering thermite reactive nano-laminates has been presented. By studying the fundamentals of the thermite reaction, and applying that knowledge to systems, we can obtain thermite systems where we have engineered desired energetic outputs and behaviors of the system. Revisiting the three main defining features of energetic systems: sensitivity, stability, and reactivity, we can see that thermite can be engineered to alter any of these three features.

By altering the number of bilayers present in a thermite RNL system, we have seen that the sensitivity can be increased, as the onset of reactivity threshold is lowered. Increasing the bilayers in a system has also shown to increase the reactivity of the system, as seen in the shock

studies of Zr/CuO. Altering the geometry of thermite RNLs allows for structural engineering on the nano-scale of an energetic system, by decreasing the amount of distance mass transport must occur, and increasing the surfaces in which the reaction can occur, we see an increase in sensitivity, and an increase in reactivity.

Following the basic formula of combining a metal and a metal oxide that follows a redox reaction that results in a terminal oxide with a lower enthalpy of formation than the initial terminal oxide, a large set of thermite systems can be studied and utilized. In this work, the beginning investigations of the Zr/ZnO system were presented. From this, we see that by using materials with different standard energies of reaction, and differing density, we can engineer the energetic output of the system. In addition, by combining the unique compositions of thermite systems with the structural engineering of RNL morphology, we can fine tune power densities of thermite systems.

Finally, the idea of enhancing the thermite reaction by introducing a third reactant into the system investigates the idea of ternary thermite systems. Whether or not these enhance or suppress the thermite reaction must continue to be investigated. However, ternary systems that enhance or dampen the reaction results in another avenue in which thermite can be engineered.

The engineering of thermite on the nano-scale results in a wide range of energetic materials applications and holds promise for the implementation of energetic materials into multiple fields.

REFERENCES

[1] Charles Darwin, *The Descent of Man*, 1st ed. (London, 1871).

[2] J. A. J. Gowlett, Philos. Trans. R. Soc. Lond. B. Biol. Sci. **371**, (2016).

[3] A. Y. Glikson and C. Groves, *Climate, Fire and Human Evolution*, 10th ed. (Springer, 2016).

[4] R. Wrangham and R. Carmody, Evol. Anthropol. **19**, 187 (2010).

[5] J. Liu, S. Chen, and T. Liu, *Smart Energy: From Fire Making to the Post-Carbon World* (CRC Press, 2017).

[6] T. Andrade, *The Gunpowder Age : China, Military Innovation, and the Rise of the West in World History* (Princeton University Press, 2016).

[7] P. A. Lorge, *The Asian Military Revolution: From Gunpowder to the Bomb* (Cambridge University Press, Cambridge, 2008).

[8] J. R. Partington, *A History of Greek Fire and Gunpowder* (John Hopkins University Press, 1999).

[9] T. L. Davis, *The Chemistry of Powder and Explosives* (1941).

[10] W. Fickett and W. C. Davis, *Detonation: Theory and Experiment* (Toronto, 1979).

[11] J. W. Forbes, *Shock Wave Compression of Condensed Matter* (Springer-Verlag, 2012).

[12] G. I. Brown, *The Big Bang: History of Explosives* (Sutton, 1998).

[13] Placer Her. (1866).

[14] A. W. Levinovitz and N. Ringertz, *The Nobel Prize: The First 100 Years* (Imperial College Press, World Scientific Publishing Co. Pte. Ltd, London, Singapore, 2001).

[15] A. Thompson and B. Taylor, *Guide for the Use of the International System of Units (SI) SE - Special Publication* (2008).

[16] Department of the Army, *Field Manual 5-25: Explosives and Demolitions* (1967).

[17] J. J. Brady, B. L. Argirakis, A. D. Gordon, R. T. Lareau, and B. T. Smith, (n.d.).

[18] M.-X. Zhang, P. E. Eaton, and R. Gilardi, Angew. Chemie Int. Ed. **39**, 401 (2000).

[19] P. E. Eaton, M.-X. Zhang, R. Gilardi, N. Gelber, S. Iyer, and R. Surapaneni, Propellants, Explos. Pyrotech. **27**, 1 (2002).

[20] J. ying Zhang and X. dong Gong, Struct. Chem. **28**, 645 (2017).

[21] A. M. Astakhov, R. S. Stepanov, and A. Yu Babushkin, Fiz. Goreniya I Vzryva **34**, 93 (1998).

[22] PubChem Open Chemistry Database, *CID=4510* (National Center for Biotechnology Information, 2018).

[23] PubChem Open Chemistry Database, *ONC-201* (National Center for Biotechnology Information, 2018).

[24] PubChem Open Chemistry Database, *CID=8490* (National Center for Biotechnology Information, 2018).

[25] PubChem Open Chemistry Database, *CID=8376* (National Center for Biotechnology Information, 2018).

[26] J. Akhavan, *Chemistry of Explosives* (Royal Society of Chemistry, Cambridge, 2004).

[27] X. Sundaramd, X. Yangd, X. Xrichard, and A. Yetterd, Prog. Energy Combust. Sci. **61**, 293 (2017).

[28] L. L. Wang, Z. A. Munir, and Y. M. Maximov, J. Mater. Sci. **28**, 3693 (1993).

[29] H. Goldschmidt and C. Vautin, J. Soc. Chem. Ind. 543 (1898).

[30] H. Goldschmidt, (16 March 1897).

[31] C. P. Lonsdale, in (American Railway Engineering and Maintenance-of-way Association,

1999), pp. 1–5.

[32] E. J. J. Mily, A. Oni, J. M. M. LeBeau, Y. Liu, H. J. J. Brown-Shaklee, J. F. F. Ihlefeld, and J.-P. Maria, Thin Solid Films **562**, 405 (2014).

[33] C. E. Aumann, G. L. Skofronick, and J. A. Martin, J. Vac. Sci. Technol. B Microelectron. Nanom. Struct. Process. Meas. Phenom. J. Appl. Phys. J. Appl. Phys. Appl. Phys. Lett. J. Chem. Phys. J. Appl. Phys. **13**, 1178 (1995).

[34] B. W. W. Asay, S. F. F. Son, J. R. R. Busse, and D. M. M. Oschwald, Propellants, Explos. Pyrotech. **29**, 216 (2004).

[35] W. L. Perry, B. L. Smith, C. J. Bulian, J. R. Busse, C. S. Macomber, R. C. Dye, and S. F. Son, Propellants, Explos. Pyrotech. **29**, 99 (2004).

[36] J. Y. Ahn, W. D. Kim, K. Cho, D. Lee, and S. H. Kim, Powder Technol. **211**, 65 (2011).

[37] Y. Tao, J. Zhang, Y. Yang, H. Wu, L. Hu, X. Dong, J. Lu, and S. Guo, RSC Adv. **7**, 1718 (2017).

[38] Kaili Zhang, C. Rossi, M. Petrantoni, and N. Mauran, J. Microelectromechanical Syst. **17**, 832 (2008).

[39] T. Liu, X. Chen, H. Xu, A. Han, M. Ye, and G. Pan, Propellants, Explos. Pyrotech. **40**, 873 (2015).

[40] M. Petrantoni, C. Rossi, V. Conédéra, D. Bourrier, P. Alphonse, and C. Tenailleau, J. Phys. Chem. Solids **71**, 80 (2010).

[41] S. F. Son, B. W. Asay, T. J. Foley, R. A. Yetter, M. H. Wu, and G. A. Risha, J. Propuls. Power **23**, 715 (2007).

[42] C. Florinpetre, D. Chamberland, T. Ringuette, S. Ringuette, S. Paradis, and R. Stowe, Int. J. Energ. Mater. Chem. Propuls. **13**, 479 (2014).

[43] M. L. Pantoya and J. J. Granier, in *Propellants, Explos. Pyrotech.* (2005), pp. 53–62.

[44] T. X. Phuoc and R.-H. Chen, Combust. Flame **159**, 416 (2012).

[45] M. W. . J. Chase, J. Phys. Chem. Ref. Data, Monogr. 9 1 (1998).

[46] N. W. Piekiel, L. Zhou, K. T. Sullivan, S. Chowdhury, G. C. Egan, and M. R. Zachariah, Combust. Sci. Technol. **186**, 1209 (2014).

[47] G. M. Dutro, R. A. Yetter, G. A. Risha, and S. F. Son, Proc. Combust. Inst. **32**, 1921 (2009).

[48] G. C. Egan, E. J. Mily, J.-P. Maria, and M. R. Zachariah, J. Phys. Chem. C **119**, 20401 (2015).

[49] E. J. Mily, Thermite at the Nano-Scale, NC State University, 2015.

[50] USArmy, *US Army FM 3-34.214: Explosives and Demolition* (Washington ,D.C., 2007).

[51] M. Hoffman, *Density Distributions of Cyclotrimethylenetrinitramines (RDX)* (Livermore, CA, n.d.).

[52] L. Marín, B. Warot-Fonrose, A. Estève, Y. J. Chabal, L. Alfredo Rodriguez, and C. Rossi, ACS Appl. Mater. Interfaces **8**, 13104 (2016).

[53] J. Kwon, J. M. Ducéré, P. Alphonse, M. Bahrami, M. Petrantoni, J. F. Veyan, C. Tenailleau, A. Estève, C. Rossi, and Y. J. Chabal, ACS Appl. Mater. Interfaces **5**, 605 (2013).

[54] and Y. J. C. M. Petrantoni, C. Rossi, L. Salvagnac, V. Conédéra, A. Estève, C. Tenailleau, P. Alphonse, J. Appl. Phys. **108**, (2010).

[55] F. Merritt, M. K. Loftin, and J. T. Ricketts, *Standard Handbook for Civil Engineers* (2004).

[56] Y. Chen, F. V Lawrence, C. P. L. Barkan, and J. A. Dantzig, Proc. Inst. Mech. Eng. Part F

J. Rail Rapid Transit **220**, 207 (2006).

[57] D. Wei, R. Dave, and R. Pfeffer, J. Nanoparticle Res. **4**, 21 (2002).

[58] E. L. Dreizin, Prog. Energy Combust. Sci. **35**, 141 (2009).

[59] S. M. Umbrajkar, S. Seshadri, M. Schoenitz, V. K. Hoffmann, and E. L. Dreizin, J. Propuls. Power **24**, 192 (2008).

[60] B. N. Chapman, *Glow Discharge Processes : Sputtering and Plasma Etching* (Wiley, New York , 1980).

[61] K. Wasa, *Handbook of Sputter Deposition Technology : Fundamentals and Applications for Functional Thin Films, Nano-Materials and MEMS* (Elsevier Science, 2014).

[62] A. D. Curtis, A. A. Banishev, W. L. Shaw, and D. D. Dlott, Rev. Sci. Instrum. **85**, 103901 (2014).

[63] A. A. Banishev, W. L. Shaw, W. P. Bassett, and D. D. Dlott, J. Dyn. Behav. Mater. **2**, 194 (2016).

[64] T. Hongo, A. Matsuda, K.-I. Kondo, P. Ya-Jing, Z. Shu-Ping, W. Ying-Hui, W. L. Shaw, R. A. Williams, E. L. Dreizin, and D. D. Dlott, J. Phys. Conf. Ser **500**, (n.d.).

[65] W. L. Shaw, D. D. Dlott, R. A. Williams, and E. L. Dreizin, Propellants, Explos. Pyrotech. **39**, 444 (2014).

[66] R. Courant and K. O. Friedrichs, *Supersonic Flow and Shock Waves.* (Springer-Verlag, 1976).

[67] L. G. Bolkhovitinov and S. S. Batsanov, Combust. Explos. Shock Waves **43**, 219 (2007).

[68] S. Matveev, W. Basset, D. Dlott, E. Lee, and J.-P. Maria, APS Shock Compression Condens. Matter Meet. Avstracts B2.005 (2017).

[69] K. E. Brown, W. L. Shaw, X. Zheng, and D. D. Dlott, Rev. Sci. Instrum. **83**, 103901

(2012).

[70] D. G. Cahill, K. Goodson, and A. Majumdar, J. Heat Transfer **124**, 223 (2002).

[71] D. G. Cahill, Cit. Rev. Sci. Instruments Nanoscale Therm. Transp. J. Appl. Phys. Rev. Sci. Instruments Appl. Phys. Rev. **75**, 94901 (2004).

[72] Y. Wang, J. Y. Park, Y. K. Koh, and D. G. Cahill, J. Appl. Phys. **108**, 43507 (2010).

[73] C. M. Rost, J. Braun, K. Ferri, L. Backman, A. Giri, E. J. Opila, J.-P. Maria, and P. E. Hopkins, Appl. Phys. Lett. **111**, 151902 (2017).

[74] S. H. Fischer and M. C. Grubelich, *Theoretical Energy Release of Thermites, Intermetallics, and Combustible Metals* (1998).

[75] Q. Zhang, K. Zhang, D. Xu, G. Yang, H. Huang, F. Nie, C. Liu, and S. Yang, Prog. Mater. Sci. **60**, 208 (2014).

[76] J. Wang, A. Hu, J. Persic, J. Z. Wen, and Y. Norman Zhou, J. Phys. Chem. Solids **72**, 620 (2011).

[77] A. Ismail and M. J. Abdullah, J. King Saud Univ. - Sci. **25**, 209 (2013).

[78] N. B. Khelladi and N. E. C. Sari, Adv. Mater. Sci. **13**, (2013).

[79] R. C. Cammarata, T. M. Trimble, and D. J. Srolovitz, J. Mater. Res. **15**, 2468 (2000).

[80] S. Banerjee and P. Mukhopadyay, *Phase Transformaton: Examples from Titanium and Zirconium Alloys* (Pergamon Press, Oxford, 2007).

[81] *ASM Phase Diagram Database. Al-Cu Diagram No. 9006* (n.d.).

[82] S. M. Umbrajkar, M. Schoenitz, and E. L. Dreizin, Thermochim. Acta **451**, 34 (2006).

[83] M. Bahrami, G. Taton, V. Conédéra, L. Salvagnac, C. Tenailleau, P. Alphonse, and C. Rossi, Propellants, Explos. Pyrotech. **39**, 365 (2014).

[84] P. D. Desai, H. M. James, and C. Y. Ho, *Electrical Resistivity of Vanadium and Zirconium*

(Washington, D.C., 1982).

[85] C. Y. Ho, K. Y. Ackerman, T. N. Wu, R. H. Havill, R. . Bogaard, S. . Matula, and H. N. Oh, J. Phys. Chem. Ref. Data **12**, 197 (1983).

APPENDICES

APPENDIX A: DEPOSITION PARAMETERS

A.1 Calibration of Deposition Parameters

The deposition rates utilized for the creation of the thin films created in this work were optimized by measuring the density, surface roughness, and resistivity of the films by altering various parameters of the deposition process. The deposition rates yield different results with the thin films. For example, a deposition rate that is too fast may create a rough sample, whereas a deposition that is too low does not prove to be experimentally ideal, due to the length of time needed to create the samples.

One major challenge throughout deposition of thermite nano-laminates is keeping the sample from heating up too much. Due to the smaller features of the nano-laminates, premature ignition proved to be a challenge in thinner, more reactive samples. In addition, heating of the sample during the deposition process may lead to increased thickness of the interfacial layer. Theoretically, it is impossible to achieve an interface where the reaction does not occur at the interface. In the most ideal situation, only one monolayer of the reactants would mix to create the interfacial layer. However, experimentally, we observe an interface. In an effort to minimize the thickness of this interface, several steps were taken to decrease the overall temperature of the sample during the deposition process.

In order to promote heat transfer from the thermal energy created during the deposition process, a thicker puck for the sample stage was used. Creating a 3” diameter steel puck that was approximately 1” thick allowed for heat transfer from the plasma. Consequentially, the larger puck also allowed for larger samples to be created. In addition, Arctic Silver 5 thermal CPU paste was used to adhere the substrates onto the stage. This promoted heat transfer from the substrate to the puck.

During the deposition, rest times were introduced to minimize the amount of interfacial material formed during deposition. For Al/CuO samples, a rest time of 15 minutes was utilized. For many bilayer Al/CuO systems, the sample as rested an hour periodically throughout the deposition. Because the Zr/CuO system was much more reactive, it was rested for an hour in between individual layers, and then rested overnight upon completion of the deposition.

The overall pressure of the chamber was allowed to reach $1.0x10^{-7}$ Torr after the chamber was opened, to remove water vapor from the walls of the chamber. A pressure below 10 mTorr in Ar was utilized throughout this work in order to achieve smooth films.

A.2 XRR Data of Reactants

X-ray reflectivity (XRR) was utilized for calibration of deposition rates, and characterizing the thin films. In addition, resistivity was measured on metal thin films via resistivity. An example of XRR data for each reactant used throughout this work can be seen below in Figure A.1. Generally, the RMS roughness of the films is approximately 5% of the total thickness. The resistivity of Zr and Al are $1.7x10^{-4}$ and $6.8x10^{-6}$ Ω m, respectively. The bulk resistivity of Zr at 298 K is $4.21x10^{-7}$ Ω m [84], which is approximately 4 times that of a standard thin film used in this work. The bulk resistivity of Al is $2.65x10^{-6}$ Ω m [85], which is approximately 2.5 times the resistivity of the Al thin film.

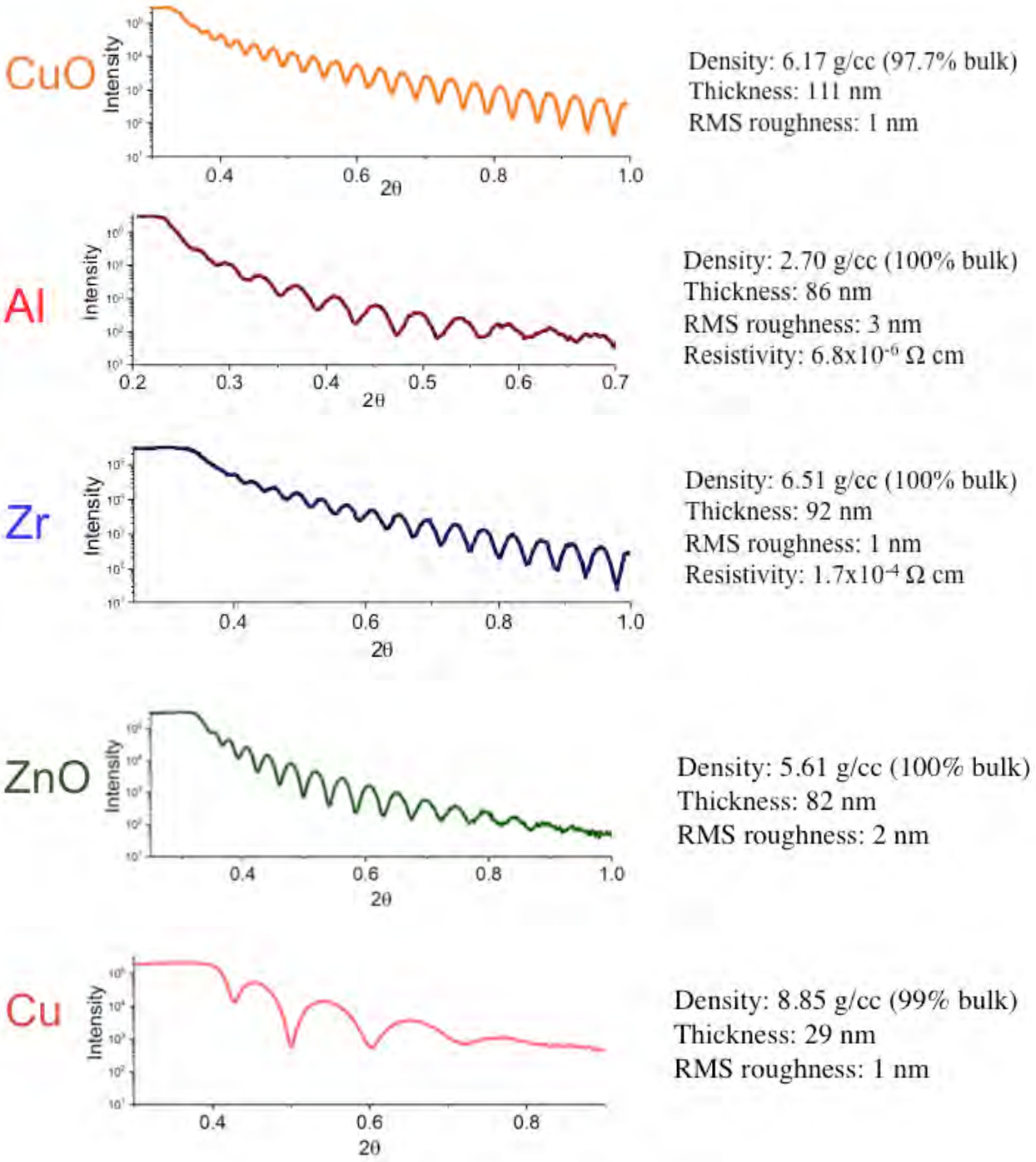

Figure A.1 XRR Data of CuO, Al, Zr, ZnO, and Cu showing the density, thickness, RMS roughness, and resistivity of a standard thin film used throughout this work.

APPENDIX B: STEM IMAGING OF Al/CuO BILAYERS

Table B.1. Measurements of layers in Al/CuO stacks, obtained via integrated line profiles. All values are the mean of two separate 1.3 micron regions, with the exception of the 1 BL measurements.

Layer	**1 BL [nm]**	**2 BL [nm]**	**3 BL [nm]**	**4 BL [nm]**	**5 BL [nm]**	**6 BL [nm]**	**7 BL [nm]**
Stack thickness	**1141**	**1208**	**1135**	**1193**	**1205**	**1192**	**1227**
Al 1	375	198	131	96	76	63	55
CuO 1	766	403	270	198	163	135	116
Al 2		201	133	102	79	67	59
CuO 2		406	269	196	163	136	116
Al 3			134	103	80	64	58
CuO 3			272	197	162	137	115
Al 4				103	81	64	59
CuO 4				198	160	140	121
Al 5					82	67	60
CuO 5					159	144	116
Al 6						63	59
CuO 6						142	116
Al 7							59
CuO 7							118
Al cap	87	88	86	90	87	85	89

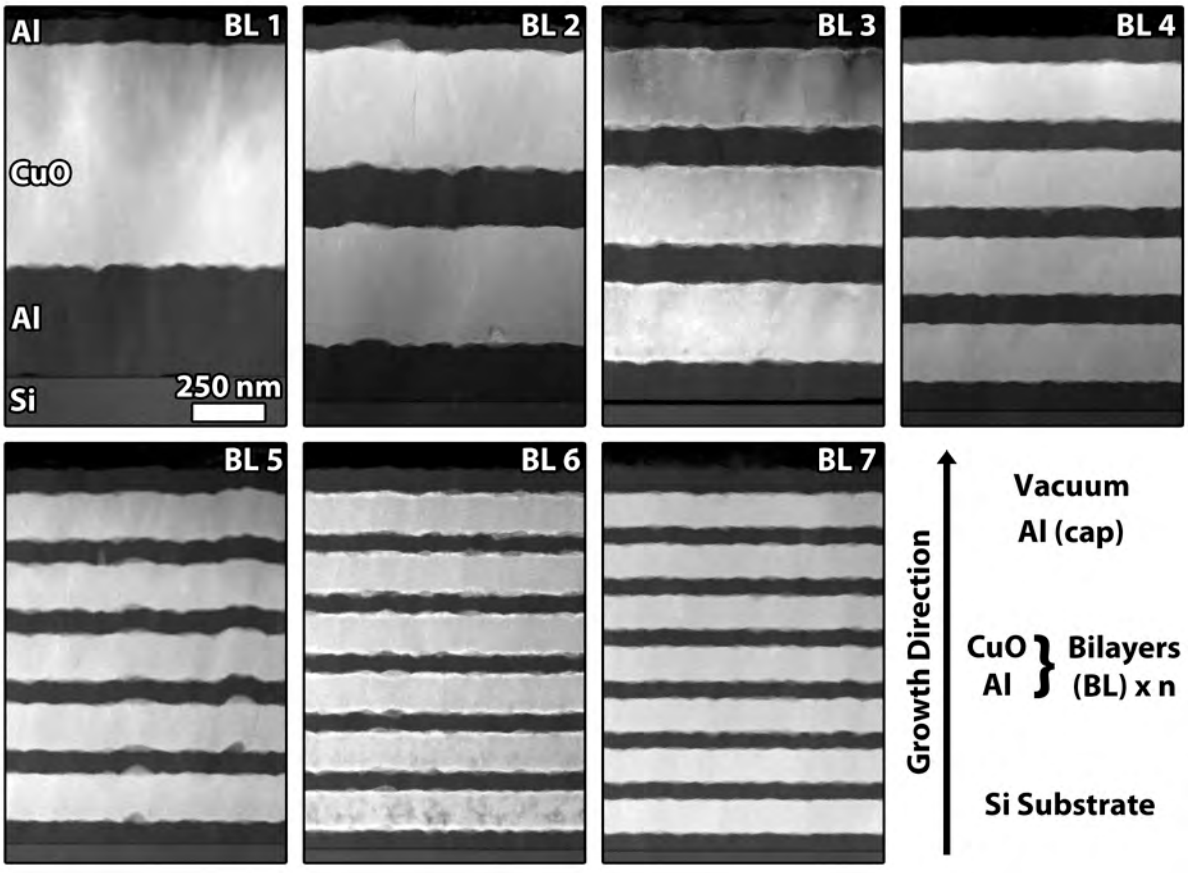

Figure B.1. STEM imaging and measurements of 1-7 bilayer Al/CuO stacks used for TDTR studies.

The STEM imaging and thickness measurements were conducted by Dr. Everett Grimley, Rachel Jackson, and Dr. James LeBeau of the department of Materials Science & Engineering at NC State University.

APPENDIX C: XRD OF Zr/ZnO BILAYERS

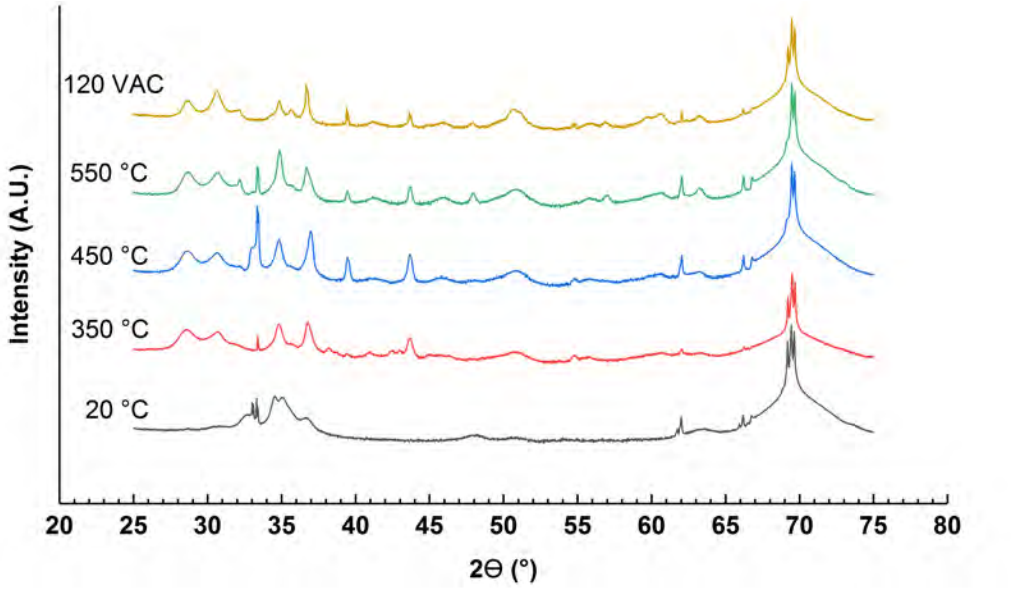

Figure C.1. *Ex situ* heating series of Zr/ZnO 3 bilayer sample prepared via DC reactive sputtering of Zn in an oxygen rich environment. For comparison purposes, the sample was also subjected to 120 V AC.

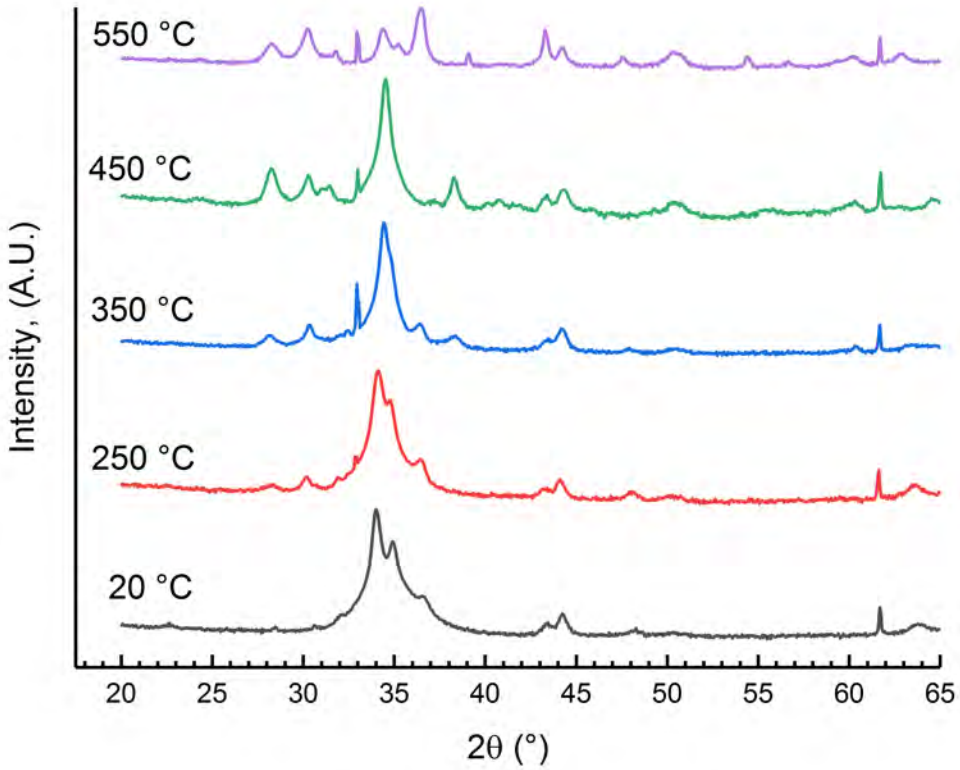

Figure C.2. *Ex situ* heating series of Zr/ZnO 1 bilayer sample.

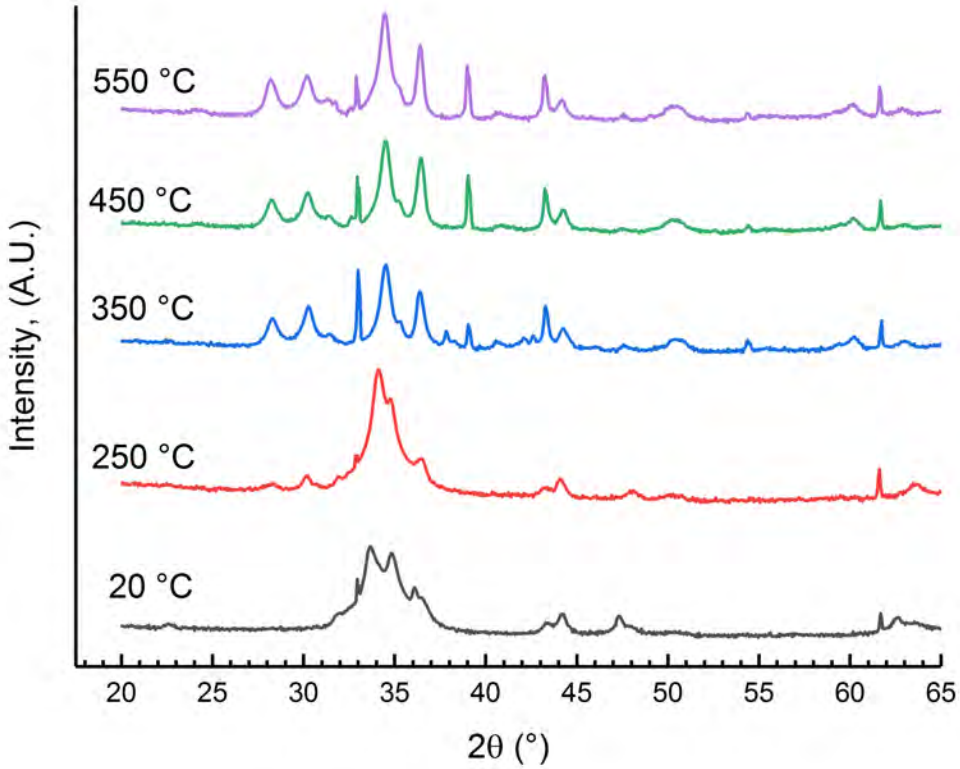

Figure C.3. *Ex situ* heating series of Zr/ZnO 2 bilayer sample.

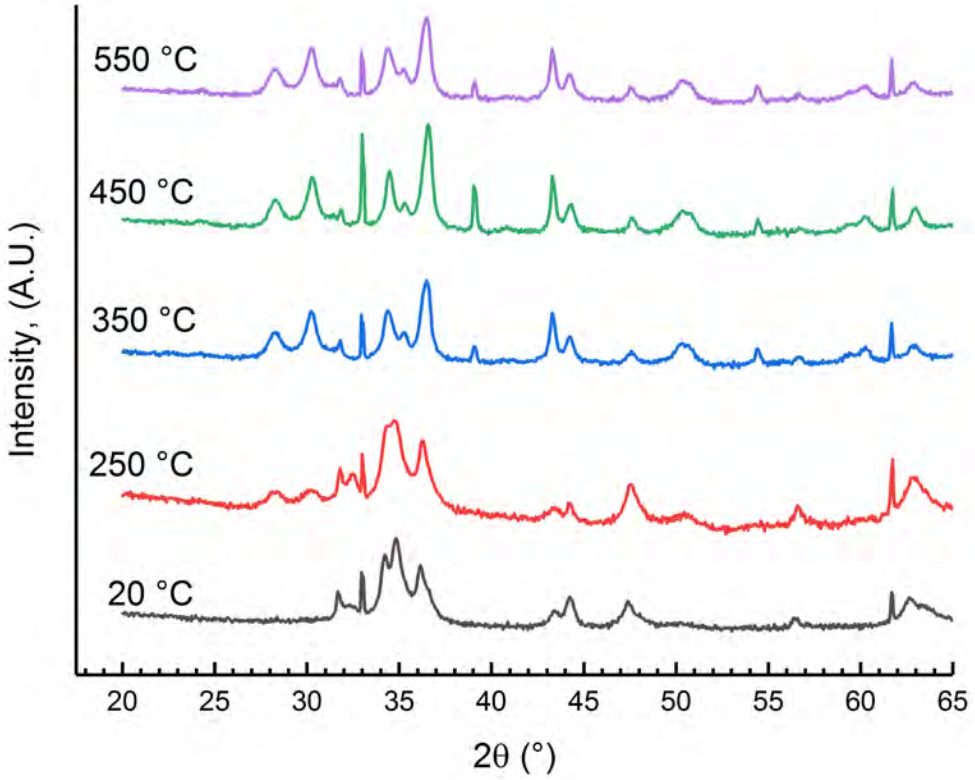

Figure C.4. *Ex-situ* heating of Zr/ZnO 3 bilayer sample.

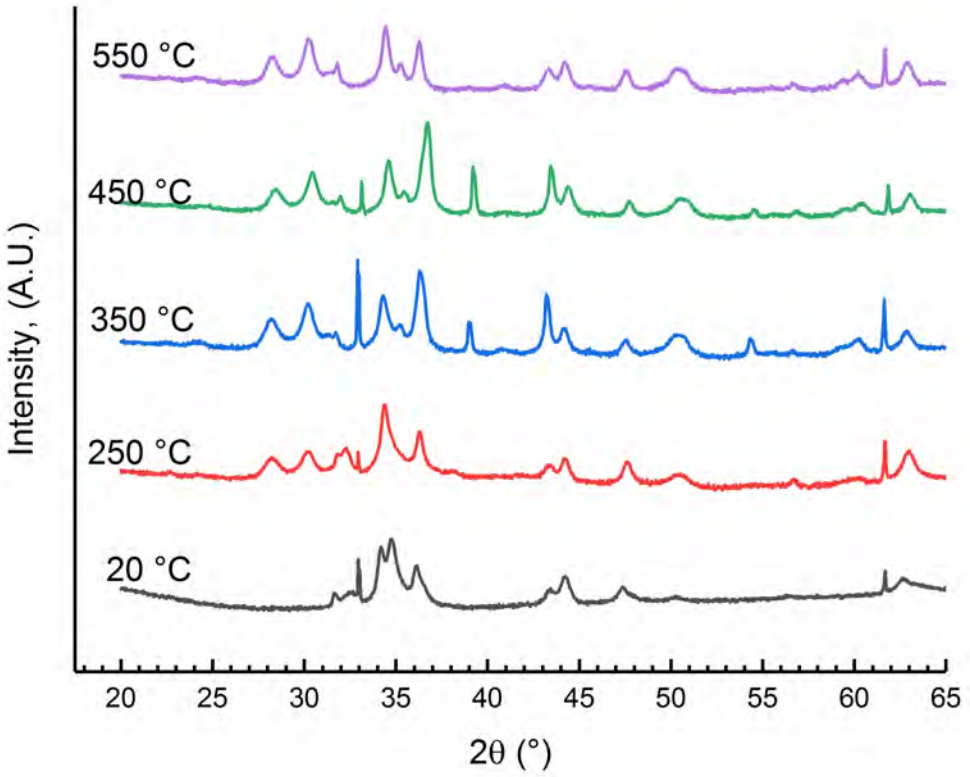

Figure C.5 *Ex-situ* heating of Zr/ZnO 4 bilayer sample.

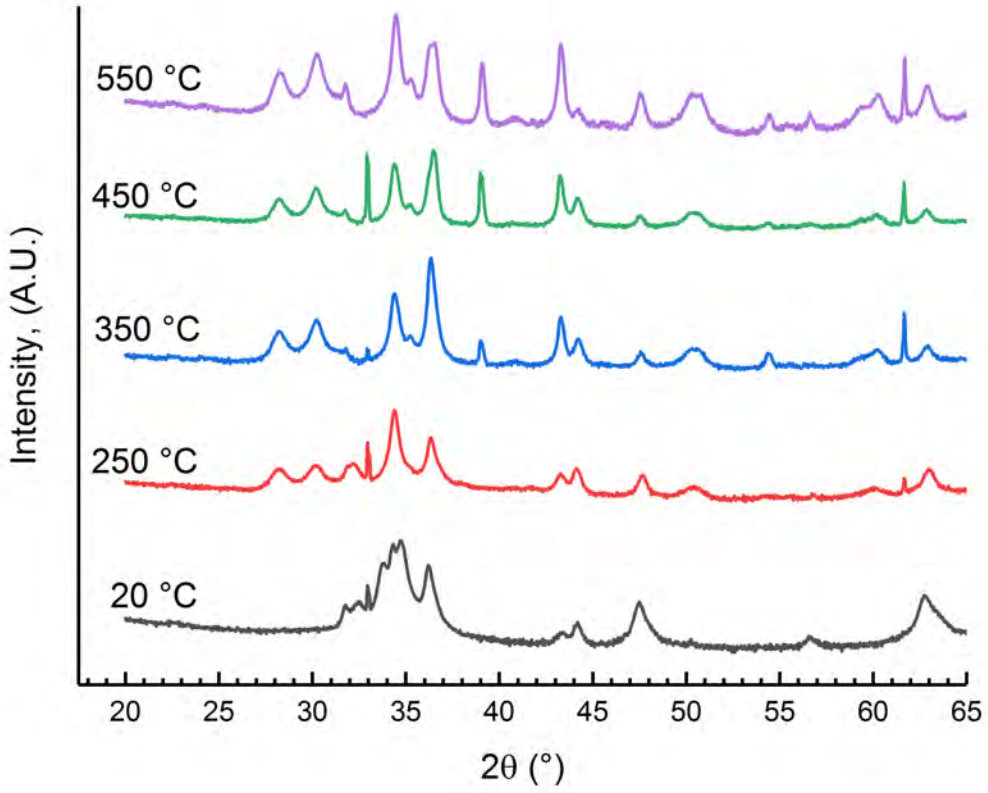

Figure C.6. *Ex-situ* heating of Zr/ZnO 5 bilayer sample.

APPENDIX D: Al/Cu PHASE DIAGRAM

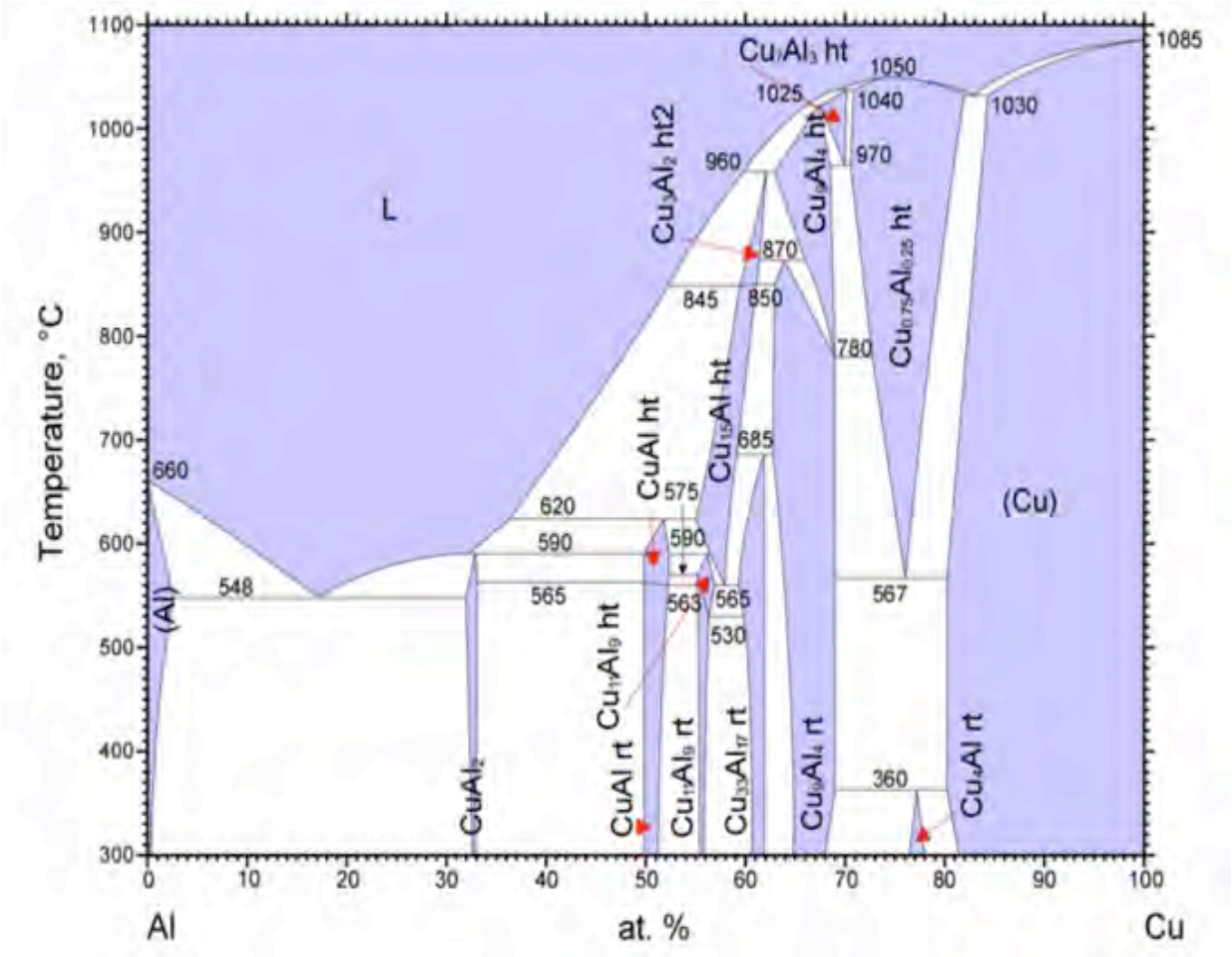

Figure D.1. Phase diagram of Al-Cu. [81]

Engineering Reactivity in Thermite Reactive Nano-Laminates

Evyn Lee Routh

Thesis Defense

May 17, 2018

Outline

I. Introduction & Motivation

II. Intermetallic Formation in Nano-Thermite

I. Geometry of Thermite RNLs

I. Reactants of Thermite RNLs

I. Concluding Remarks

"The discovery of fire, probably the greatest ever made by man, excepting language, dates from before the dawn of history."

–Charles Darwin,

The Descent of Man

Historic Overview

Hans Goldschmidt, “Aluminum as a reducing agent”

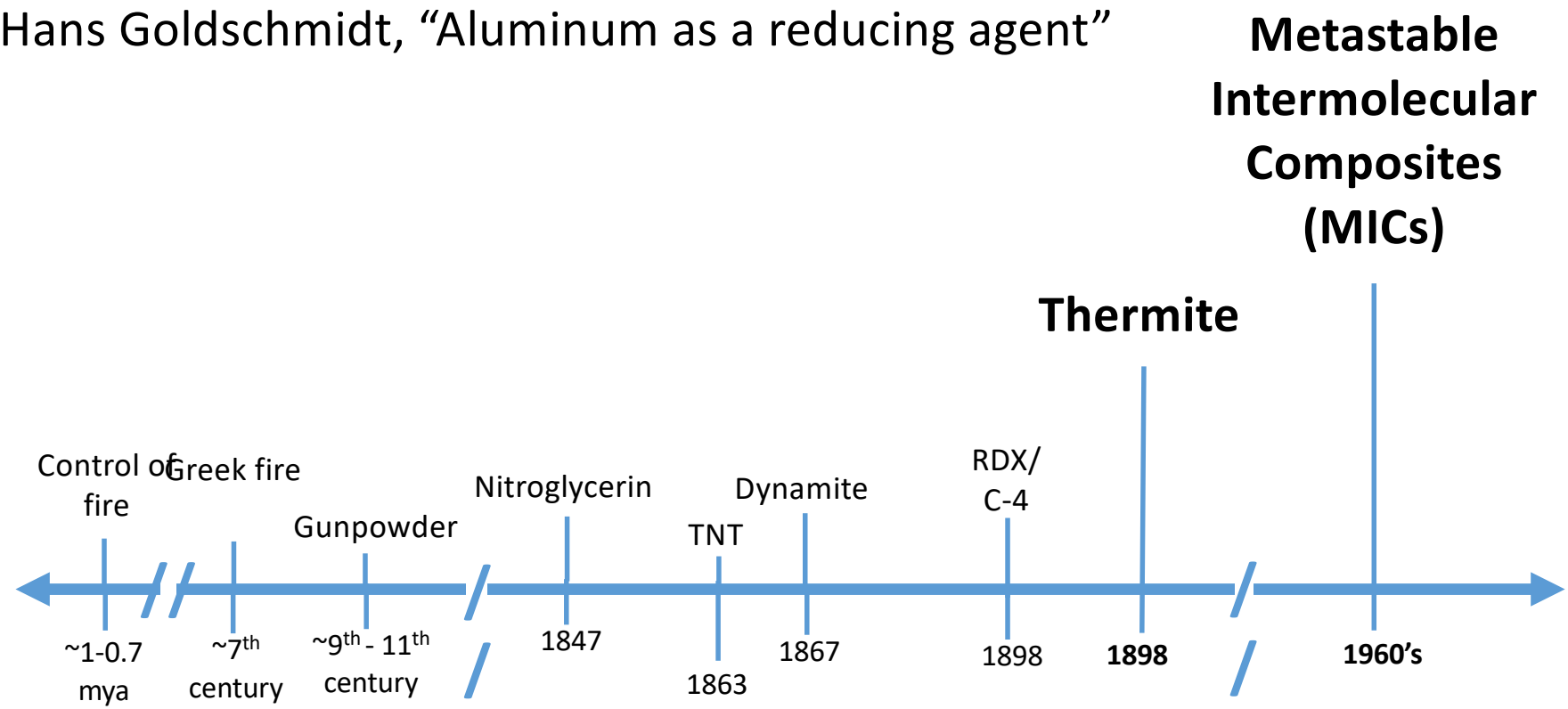

Thermite

$$M + AO \rightarrow MO_x + A + \underline{\Delta H}$$

- mass transport between metal *M* and oxide *AO.*
- **Driving force:** enthalpy of formation of terminal oxide.
- **Large exothermic energy output**

Nano-Thermite (MICs)

- **Metastable Intermolecular Composites (MICs)**: traditional energetic materials (thermite) combined on the nano-scale
  - Nano-particles
  - Motivation: decrease morphology to increase reactivity
    - Surface area
    - Better mixing
  - Disadvantages:
    - Inconsistent particle size
    - Reproducibility
    - Inconsistent reactivity

Definition of Reactivity

Reactivity can refer to:

- Rate of reaction
- Intensity of reaction output **(power density)**
- How easily the reaction occurs
  - Sensitivity
- The response to environment, short term and long term
  - Stability

Research Question: How can we engineer reactivity in thermite?

Hypothesis: If the reactivity of thermite depends on the fuel-oxidizer interface, then controlling morphology and reactants will allow tunable reactivity.

Method: Growth and characterization of thermite reactive nano-laminate thin films

How can we engineer reactivity?

- From the perspective of power density…

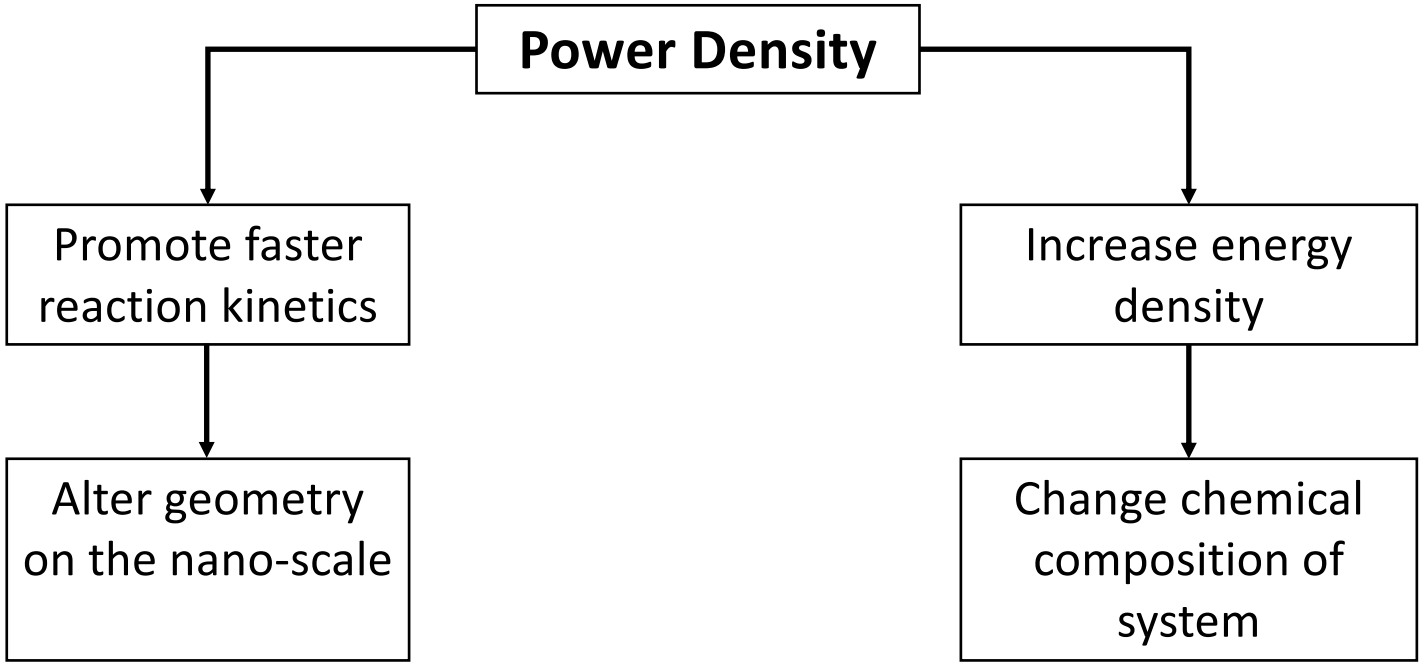

Thermite Reactive Nano-Laminate (RNL)

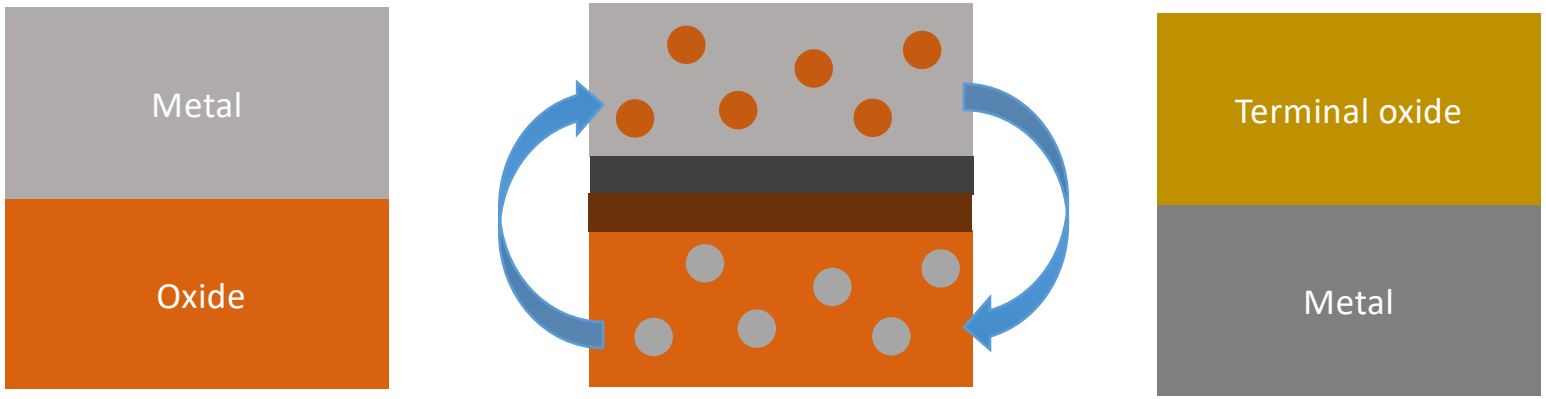

- RNL advantage:
  - Reproducible conditions and samples
  - Precise thin film morphology
    - Fundamental information of thermite reaction

Sputtering RNL thin films

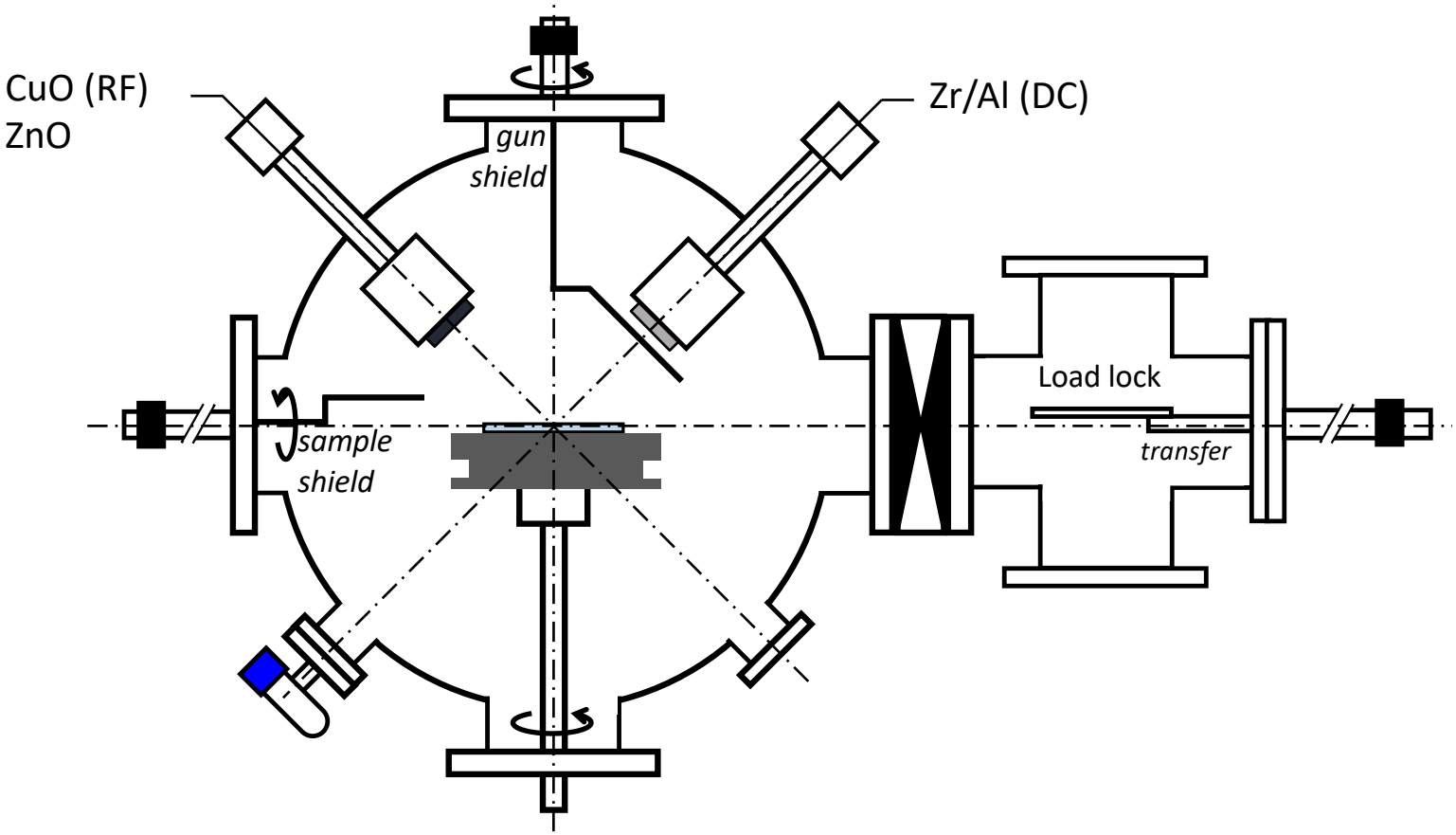

PVD Advantages

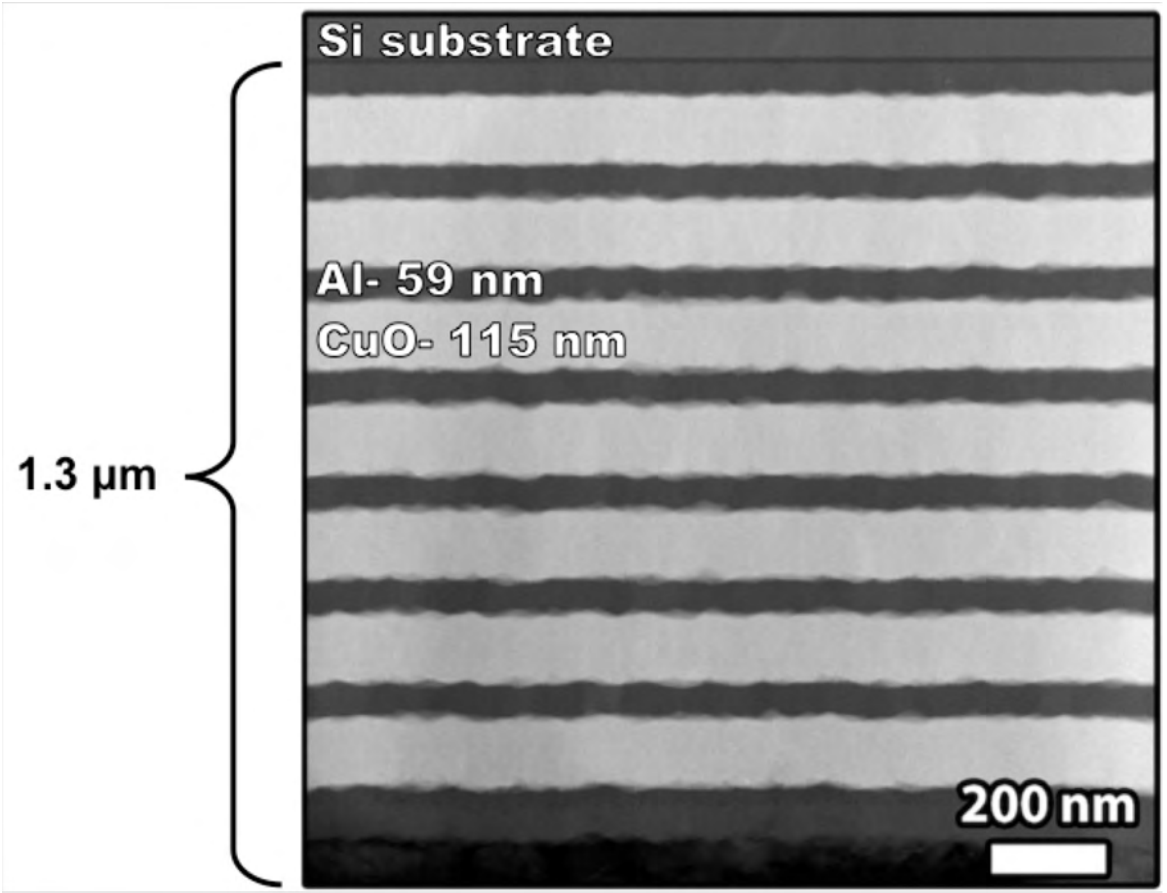

Micrograph courtesy E. Grimley
R. Jackson, J. LaBeau, NCSU
MSE 2017

PVD Advantages

CuO

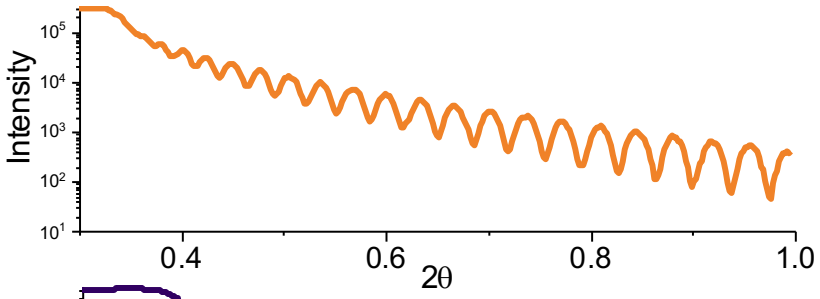

Density: 6.17 g/cc (97.7% bulk)
Thickness: 111 nm
RMS roughness: 1 nm

Zr

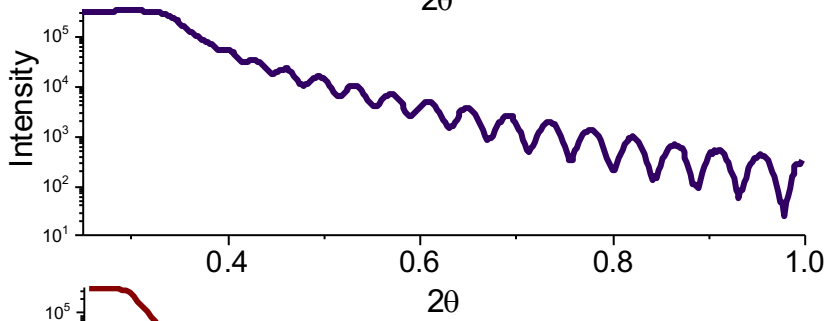

Density: 6.51 g/cc (100% bulk)
Thickness: 92 nm
RMS roughness: 1 nm
Resistivity: 1.7×10^{-4} Ω cm

Al

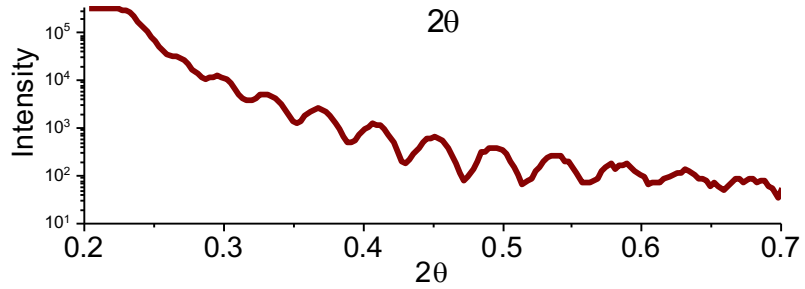

Density: 2.70 g/cc (100% bulk)
Thickness: 86 nm
RMS roughness: 3 nm
Resistivity: 6.8×10^{-6} Ω cm

Outline

I. Introduction & Motivation

II. Intermetallic Formation in Nano-Thermite

I. Geometry of Thermite RNLs

I. Reactants of Thermite RNLs

I. Concluding Remarks

Reaction mechanism of thermite

On the bulk scale, “simple” redox reaction:

- **$M + AO \rightarrow MO_x + A + \underline{\Delta H}$**

- Is there an intermediate reaction mechanism occurring?

Previous DSC studies of Al/CuO

- When Al/CuO is reduced to 5-7 BL, activity is seen around the eutectic melt for Al_2Cu
- How does the reaction mechanism change in thinner layered samples?
- Is there an intermediate material forming?

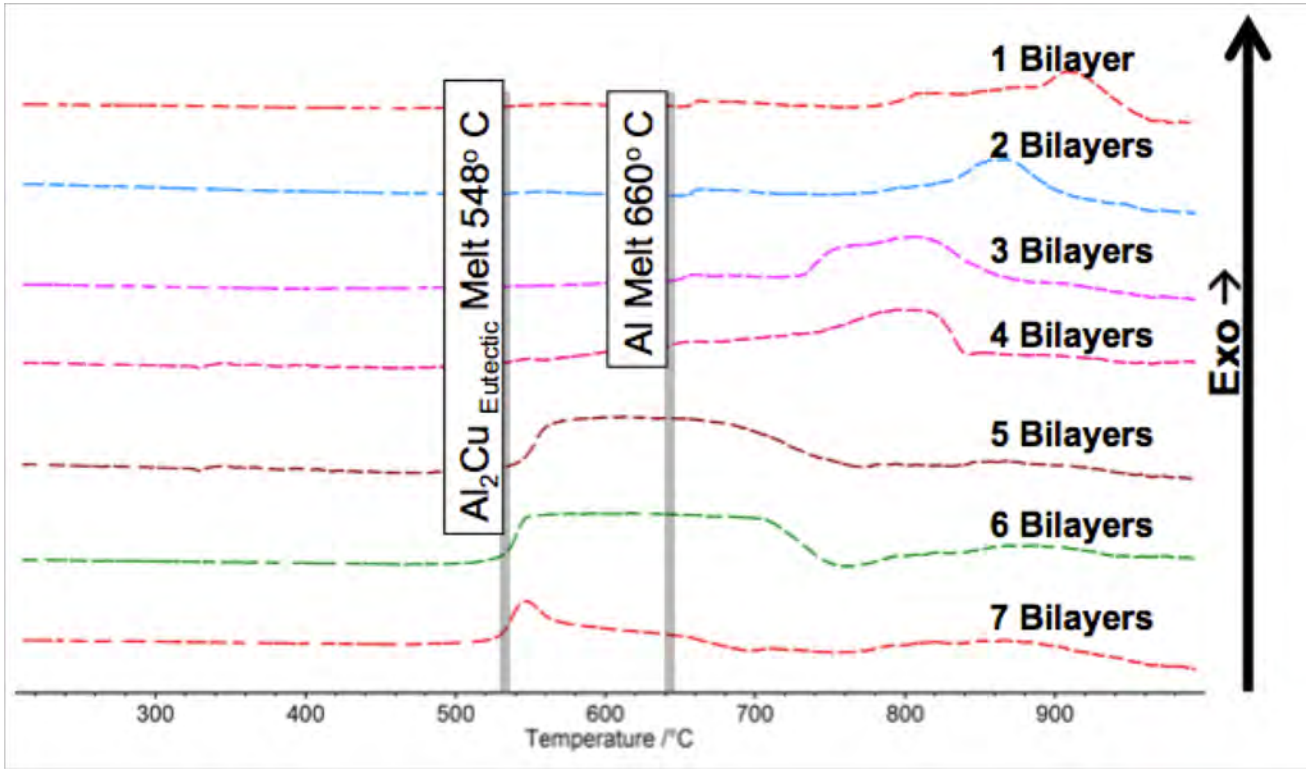

E.J. Mily. Thermite on the Nano-Scale, 2015

Goal: obtain evidence of intermetallic formation

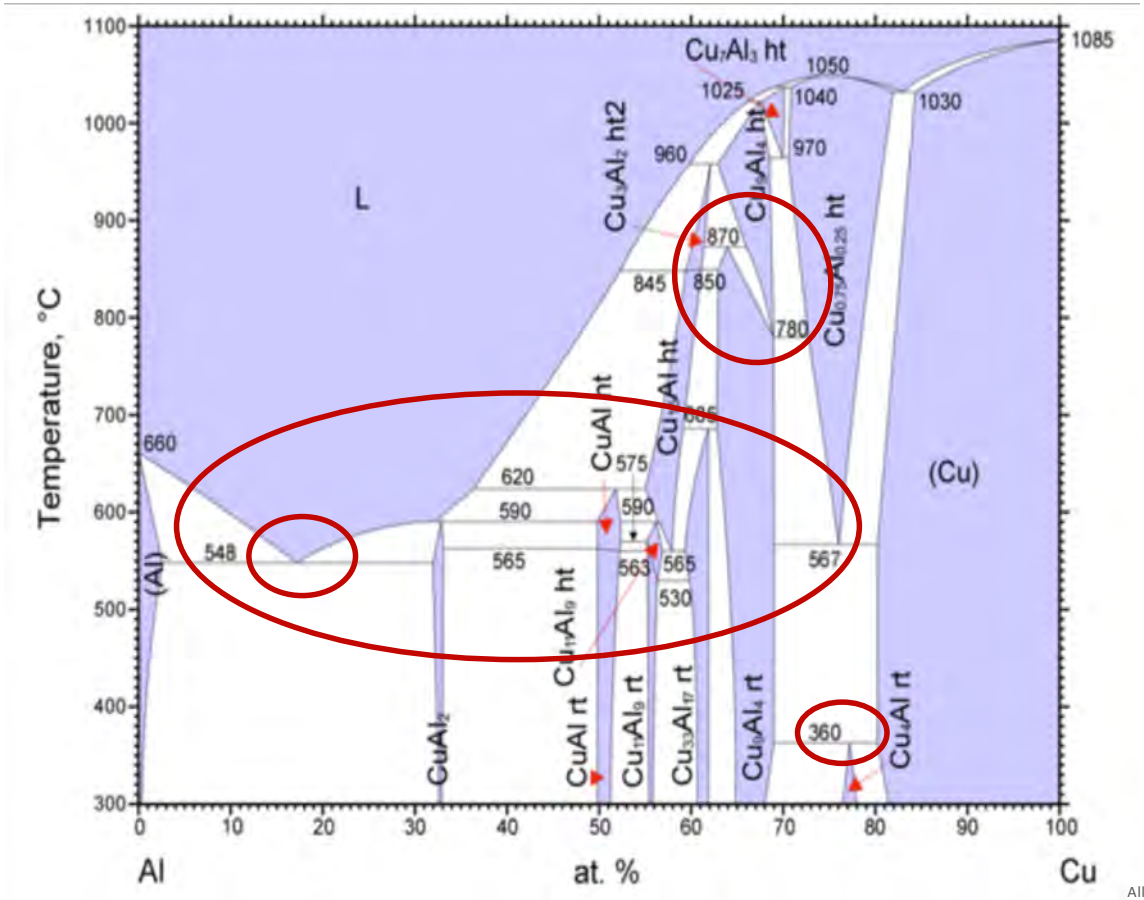

Alloy Phase Diagram Database, Al-Cu Diagram No. 9006

In Situ XRD measurements

- 20 bilayer sample on sapphire (Al: 37 nm, CuO: 63 nm)
- 20 bilayer sample heated in XRK 900 reactor chamber, in 20 sccm N_2 environment
- Heated at 5 °C/min to 900 °C, held for 30 minutes, then cooled at 5 °C/min back down to RT

In Situ XRD of 20 bilayer Al/CuO RNL

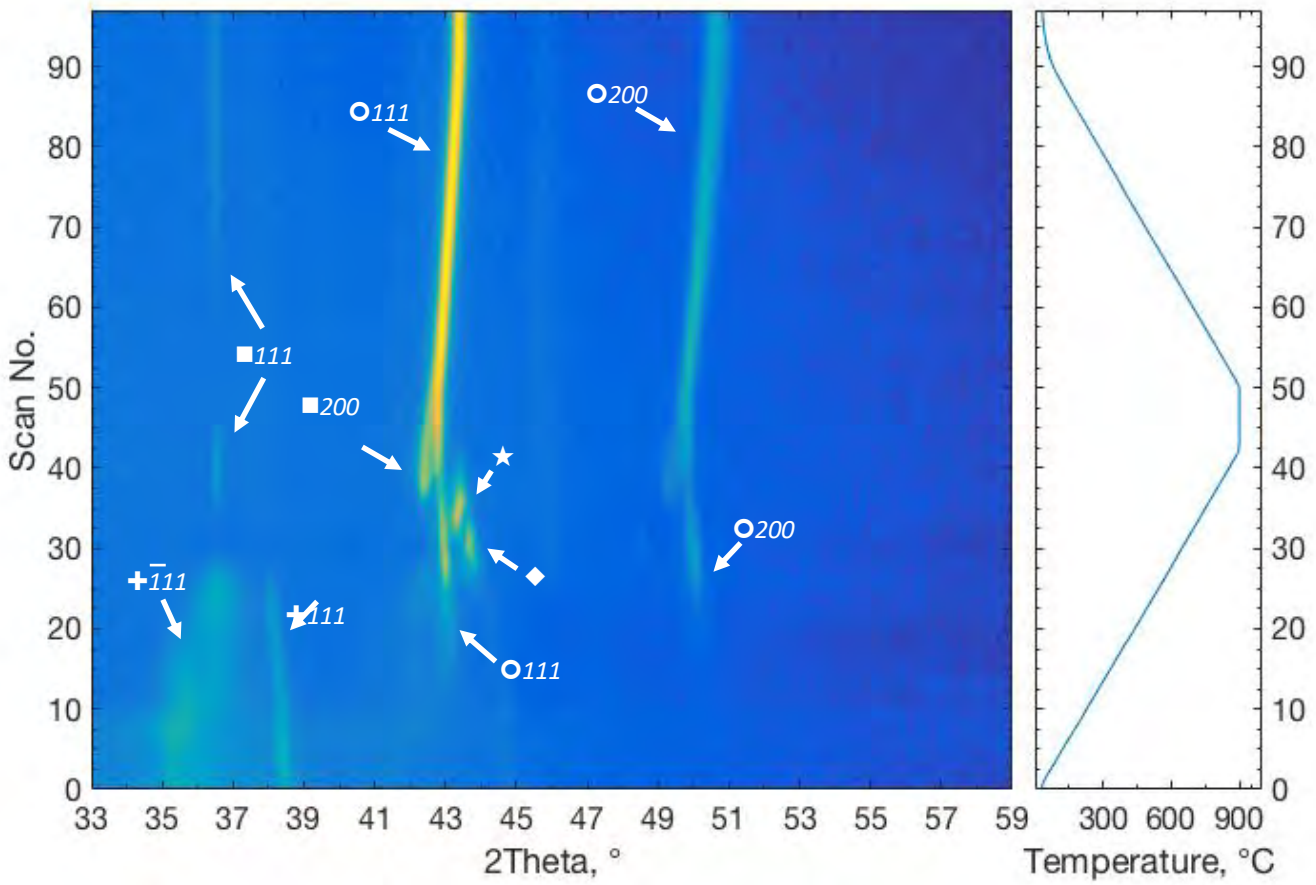

✚ CuO
■ Cu_2O
O Cu
★ unknown
◆ unknown

In Situ XRD of 20 bilayer Al/CuO RNL

- Cu formation begins around 300 °C, and becomes prominent around 540 °C, consistent with temperatures of the eutectic melting point of the Al-Cu system
- Cu peaks shift through thermal expansion and relaxation

✚ CuO
■ Cu_2O
O Cu

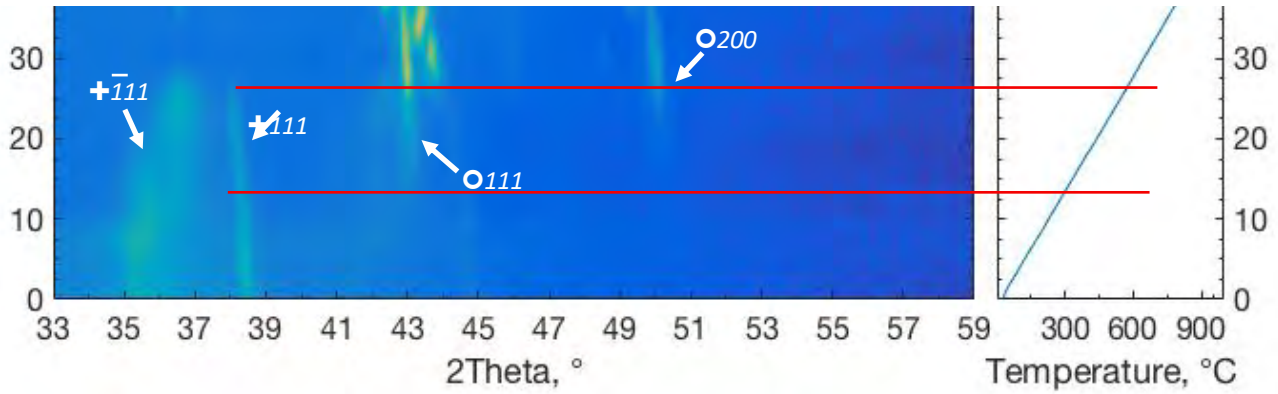

In Situ XRD of 20 bilayer Al/CuO RNL

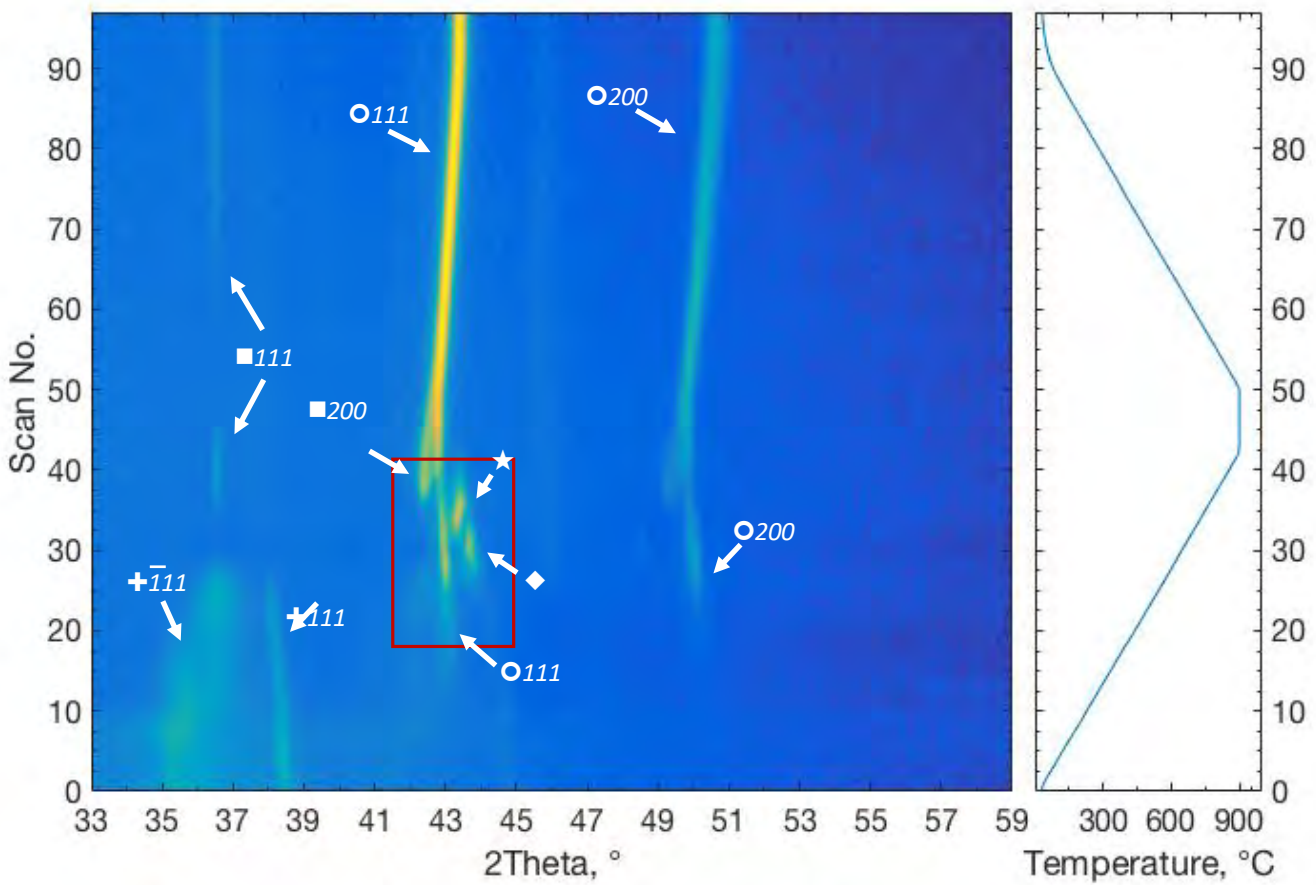

✚ CuO
■ Cu_2O
O Cu
★ unknown
◆ unknown

In Situ XRD of 20 bilayer Al/CuO RNL

★ transient: range of 43.2⌗- 43.6⌗ at ~680 ⌗C to 810 ⌗C
- Likely Al_3Cu_2 (reflection at 43.67⌗)
- Forms between 560⌗-960⌗

◆ transient: range of 43.6 ⌗-43.8⌗ at 600 ⌗C to 680 ⌗C
- Likely $AlCu_3$ (reflection 43.97⌗)
- Forms between 567⌗-1050⌗

Strong intensity indicates metallic in nature

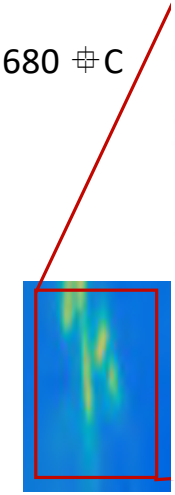

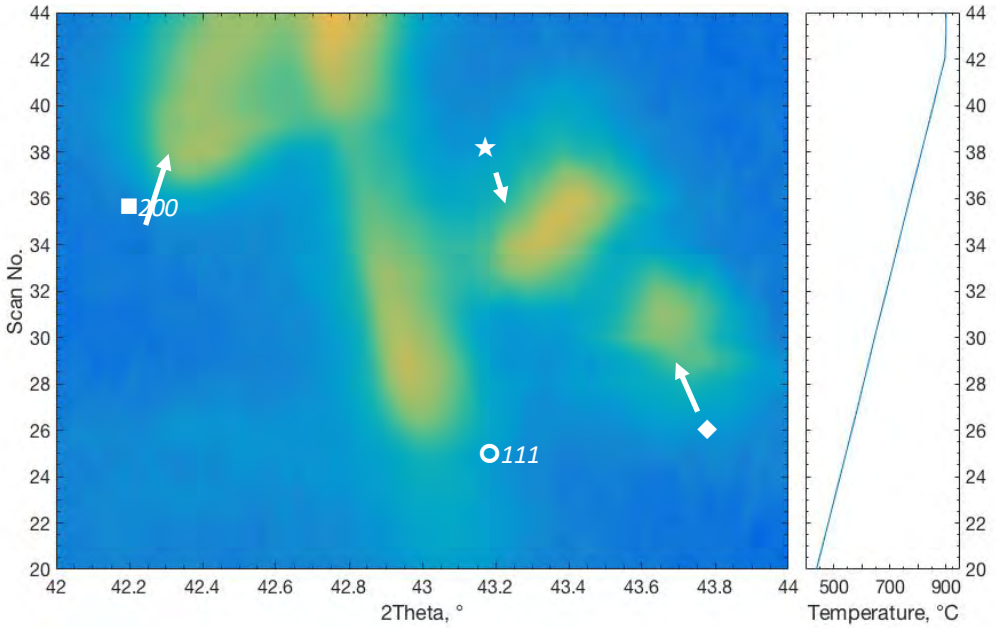

✚ CuO
■ Cu_2O
O Cu
★ Transient
◆ Transient

Applications of intermetallics in RNLs

- Introducing thin-film of terminal metal to enhance or dampen reactivity
- Alloying metal to increase or decrease density to enhance/dampen energy density
- Ternary RNL systems

Outline

I. Introduction & Motivation

II. Intermetallic Formation in Nano-Thermite

I. Geometry of Thermite RNLs

I. Reactants of Thermite RNLs

I. Concluding Remarks

Thermite Reactive Nano-Laminates (RNLs)

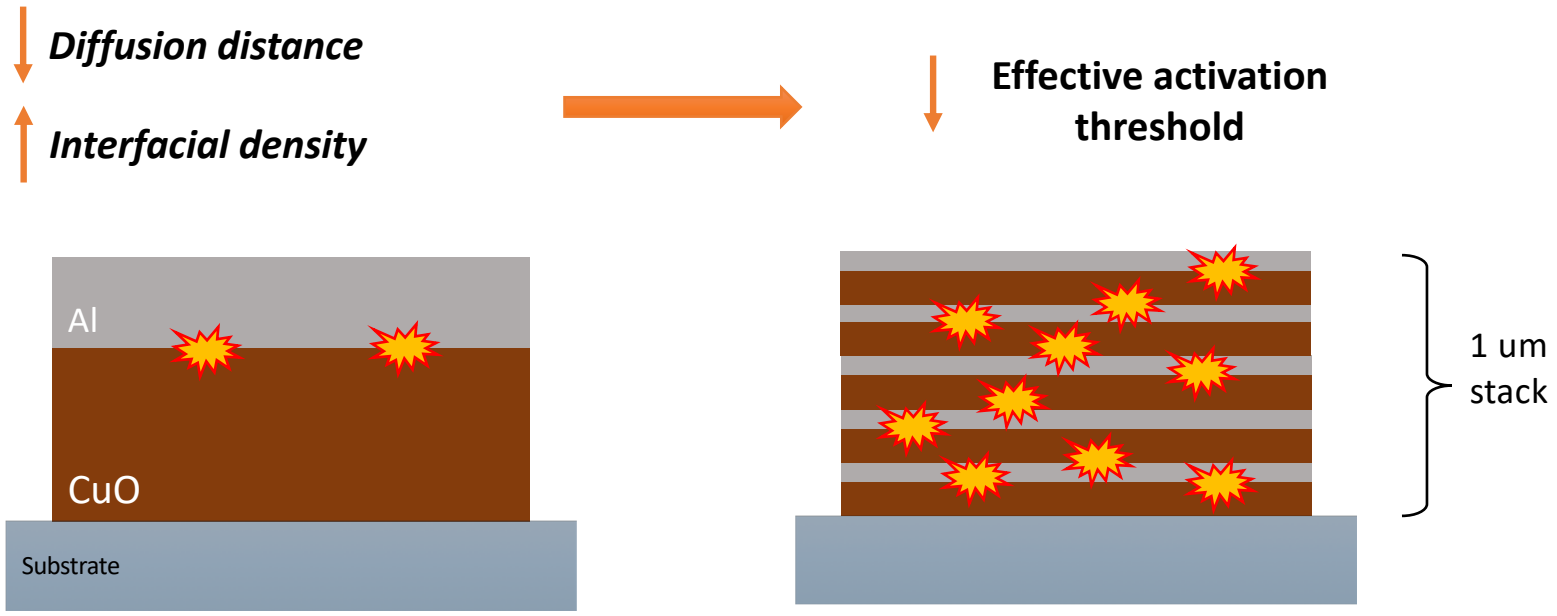

- **Bilayer:** Metal/CuO pair

Dependence on film thickness

- Previous work: Calorimetry data for Al/CuO system under slow heating
  - Monitor T_{exo} as function of BL
  - Exothermic peak temperature dependence on bilayer thickness

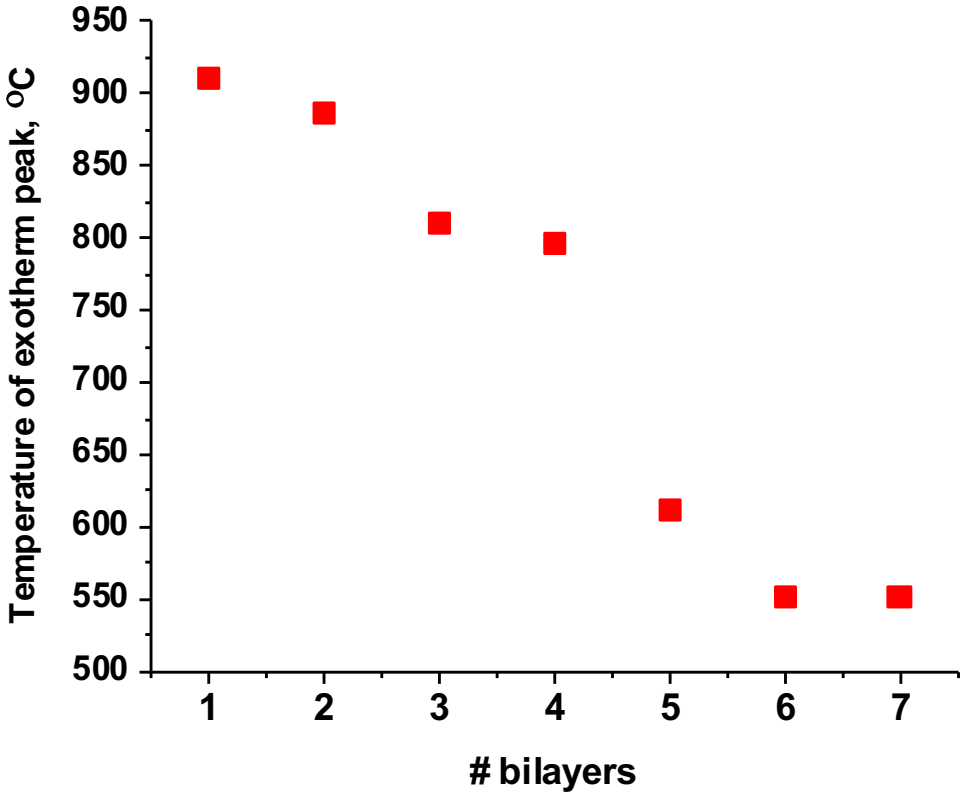

Geometry of Thermite RNLs

- We have seen previously that temperatures of exothermic activity are dependent on bilayer thickness
  - How does the system react to mechanical shock?
  - To what extent does the exothermic activity change with interfacial density?

Zr/CuO: flyer plate studies

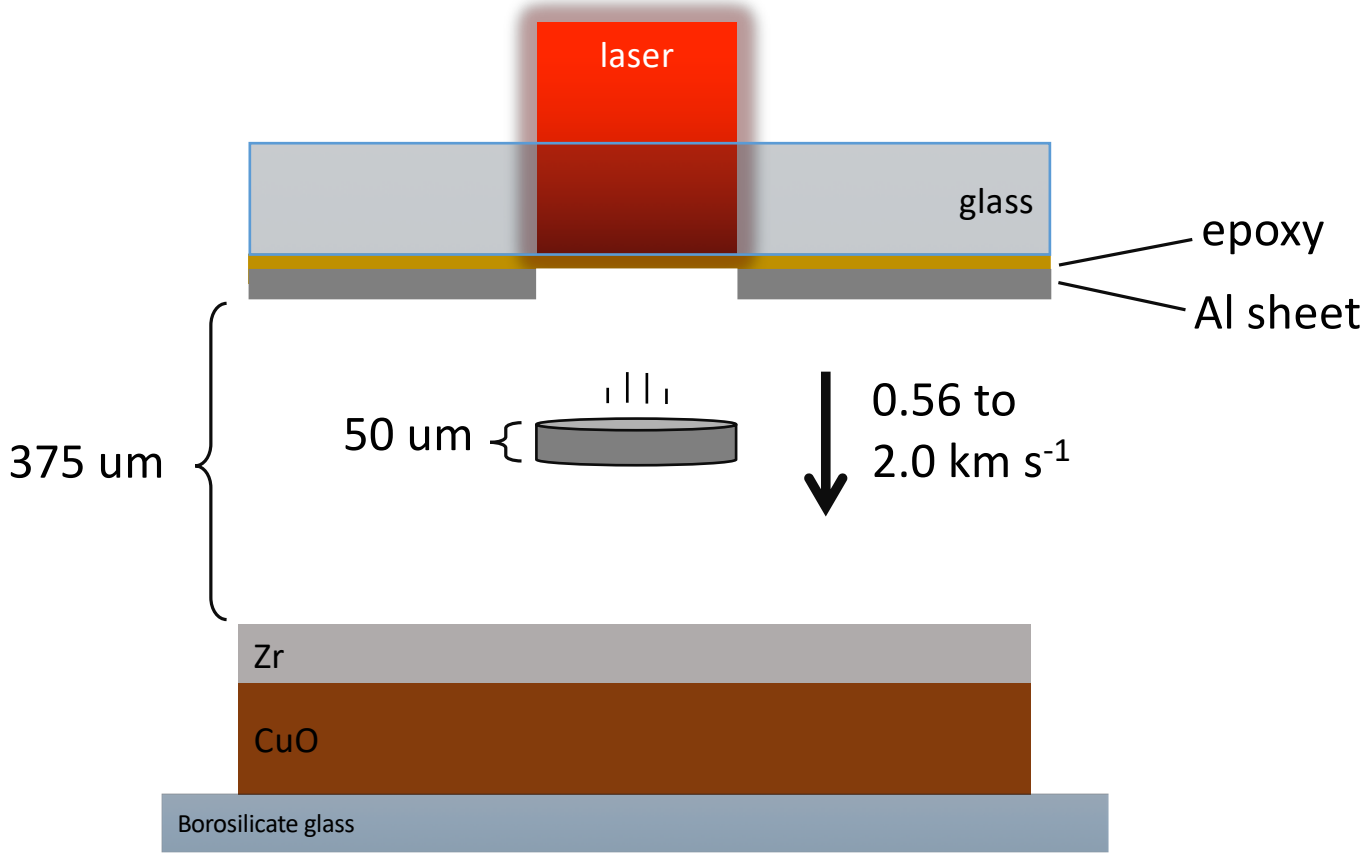

W. L. Shaw, D. D. Dlott, R. A. Williams, and E. L. Dreizin, Propellants, Explos. Pyrotech. **39**, 444 (2014).

RNL Reactivity

- Zr/CuO system
  - Fast reaction, sensitive to fabrication
  - Flyer plates: shock studies, measuring reaction output from mechanical work on short time scales
  - Constant thickness with 1-3 BL
  - Measurements at time scales that the reaction is occurring

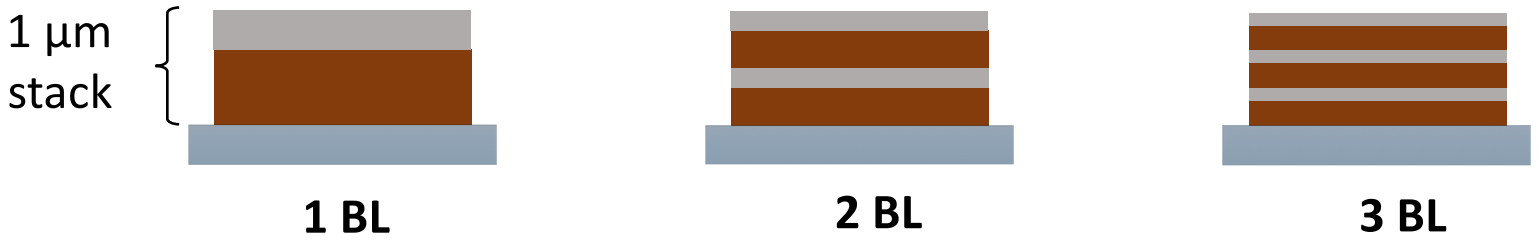

- 0.89 km s^{-1}
- 1,2,3 BL & CuO standard

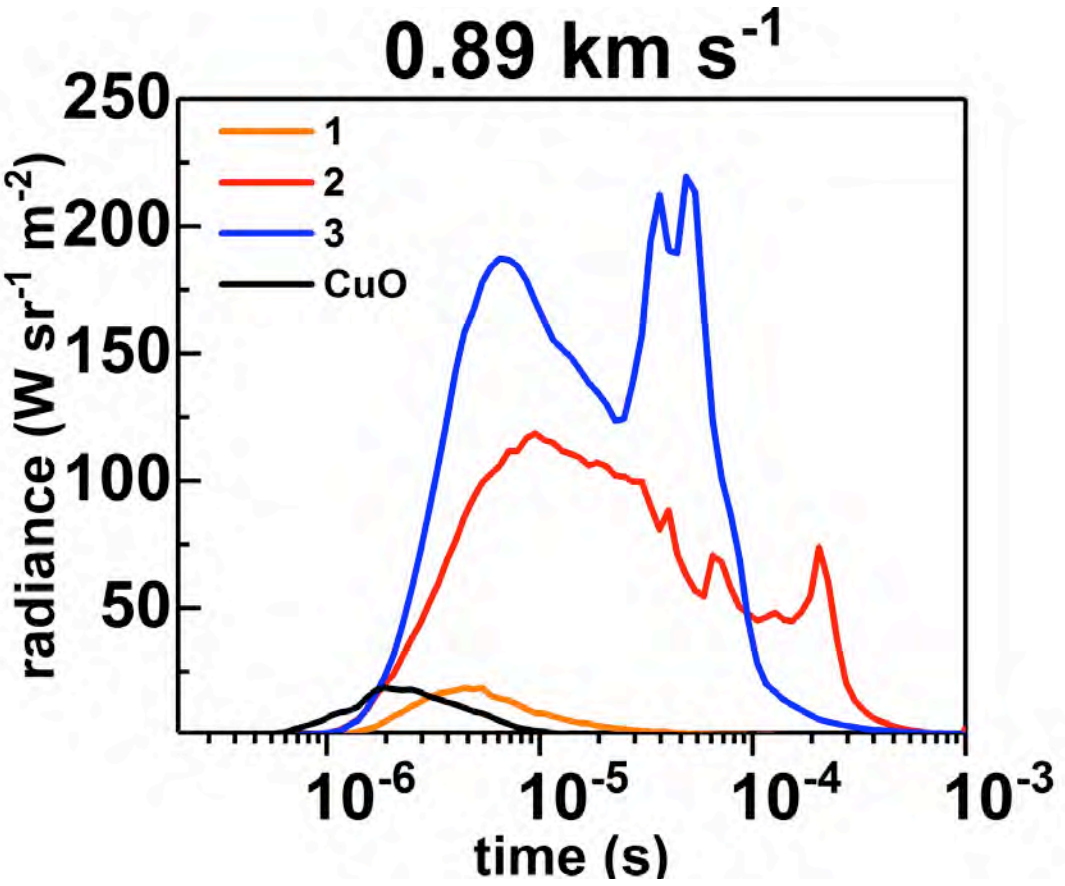

S. Matveev, E.L. Routh, D. Dlott, J-P. Maria, *In Preparation*

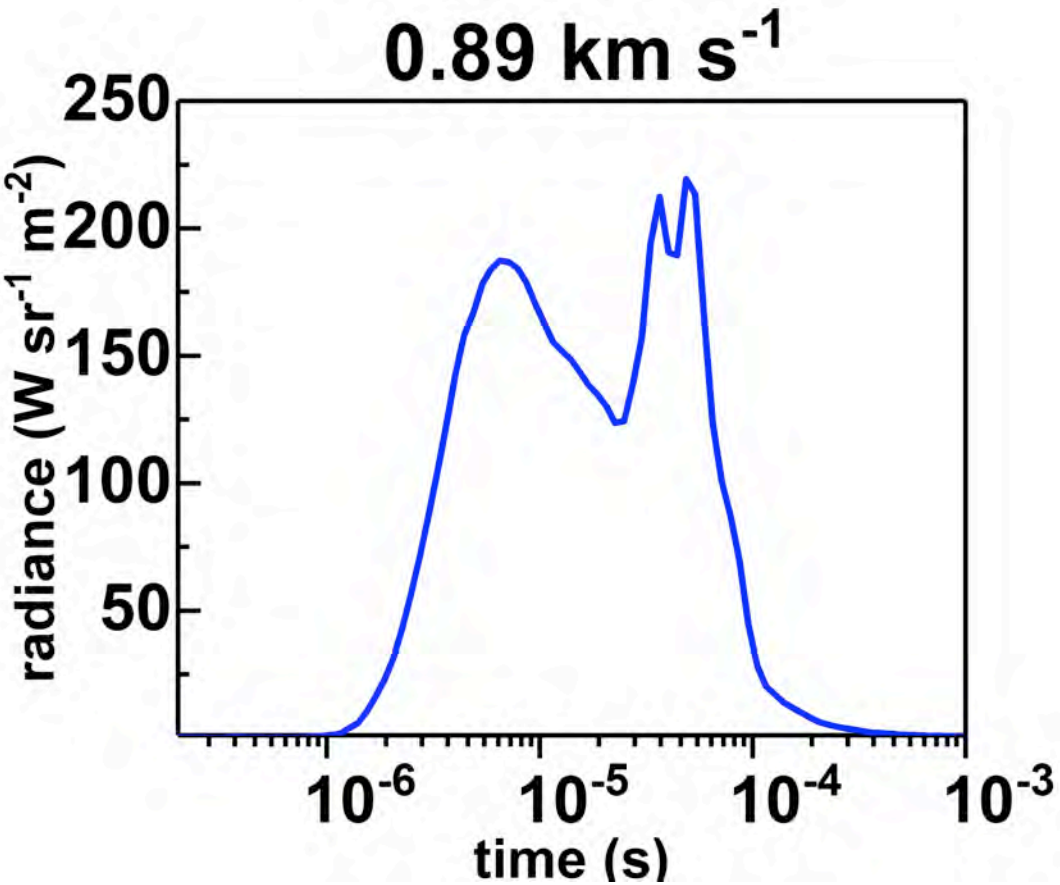

S. Matveev, E.L. Routh, D. Dlott, J-P. Maria, *In Preparation*

Total radiance:
Radiant emission over time

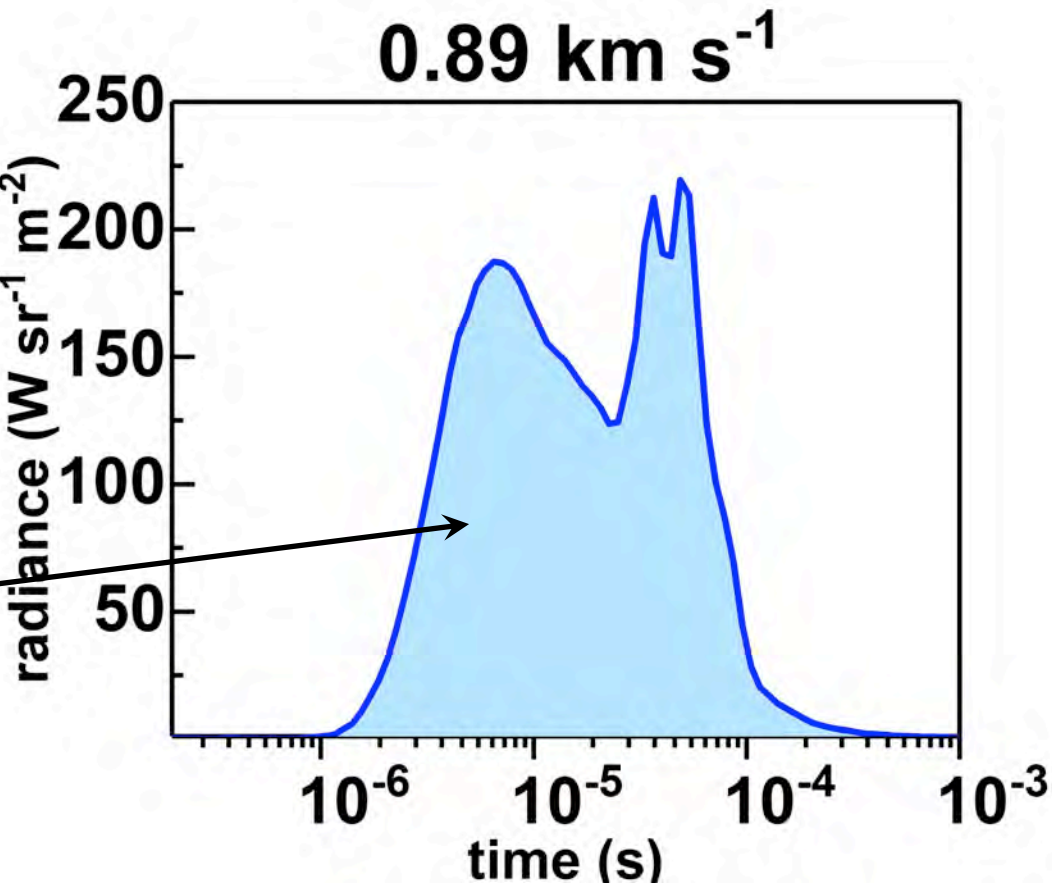

S. Matveev, E.L. Routh, D. Dlott, J-P. Maria, *In Preparation*

1-3 BL comparison of total radiance

- Total radiance: integrating measured radiance v. time
- Reactivity increases an order of magnitude with increasing number of bilayers
- Suggests higher bilayer stack going to completion
- Consistent with trends from heating experiments

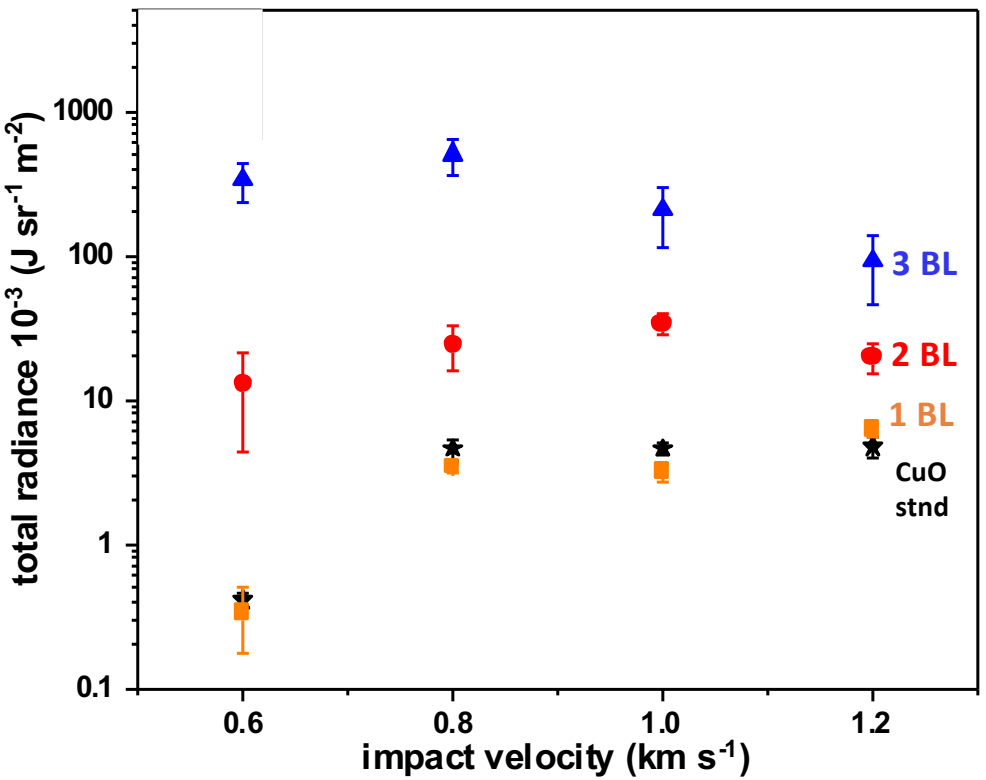

S. Matveev, E.L. Routh, D. Dlott, J-P. Maria, *In Preparation*

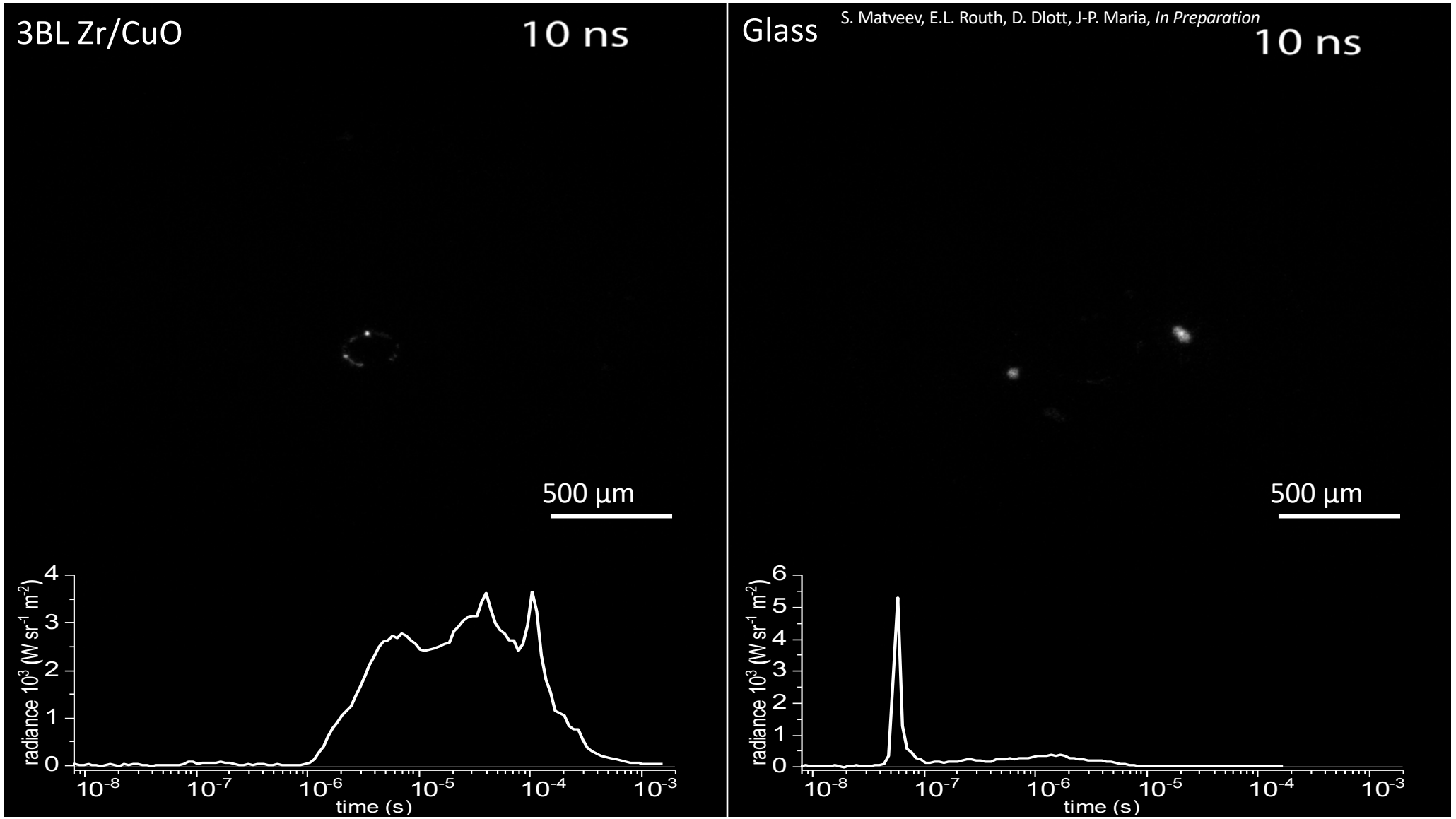
3BL Zr/CuO
10 ns
500 µm
radiance 10^3 (W sr^-1 m^-2)
time (s)
Glass
S. Matveev, E.L. Routh, D. Dlott, J-P. Maria, In Preparation
10 ns
500 µm
radiance 10^3 (W sr^-1 m^-2)
time (s)

0.89 km s^{-1}

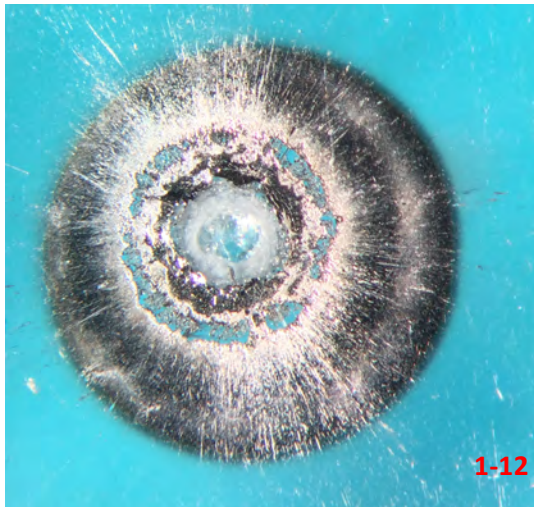

1 BL

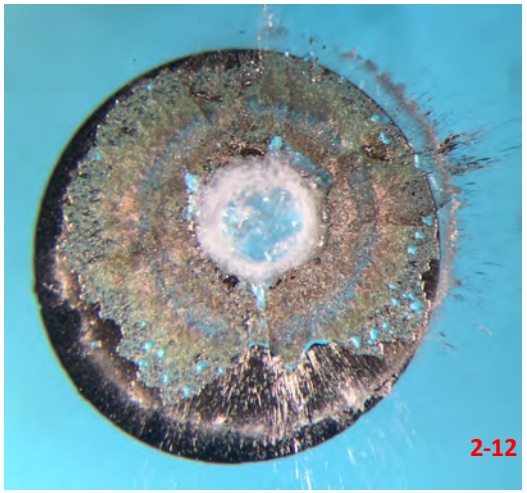

2 BL

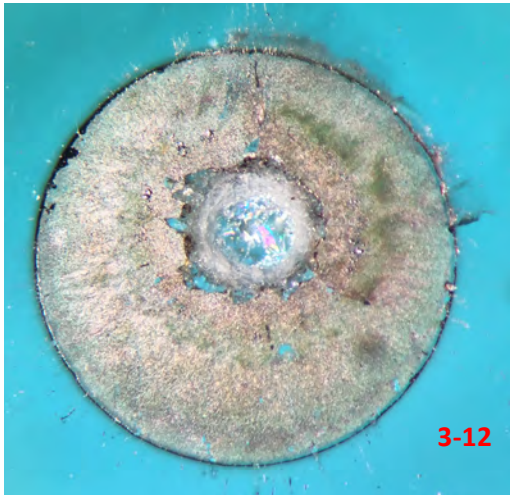

3 BL

S. Matveev, E.L. Routh, D. Dlott, J-P. Maria, *In Preparation*

Outline

I. Introduction & Motivation

II. Intermetallic Formation in Nano-Thermite

I. Geometry of Thermite RNLs

I. Reactants of Thermite RNLs

I. Concluding Remarks

Why change the reactants of RNLs?

- Different applications of the material
  - Take into account sensitivity, stability, and reactivity needed
  - Different material properties can be utilized in different systems
    - ex: conductivity of thermite
- **Tunable energy density → tunable power density**

Energy density

$$\left[\frac{kJ}{cm^3}\right] = \left[\frac{kJ}{g}\right]\left[\frac{g}{cm^3}\right]$$

Specific energy Density of system

Chemical composition of thermite RNLs

Energy density comparison

Thermite System	Specific Energy [-kJ/g]	Energy Density [-kJ/cm^3]
$2Be + PbO_2$	3.16	26.7
$2Al + 3PdO$	3.67	23.0
$2Al + 3CuO$	4.08	20.8
$Zr + 2CuO$	3.15	20.2
$Hf + 2CuO$	2.38	19.8
$Mg + CuO$	4.61	18.2
$2Al + Fe_2O_3$	3.96	16.5
$Zr + 2ZnO$	1.56	9.16

S. H. Fischer and M. C. Grubelich, *Theoretical Energy Release of Thermites, Intermetallics, and Combustible Metals* (1998).
*ZnO/Zr Calculated

Theoretical energy density range: 9.16-26.7 kJ/cm^3

Dependence on film constituents

3 BL Al/CuO

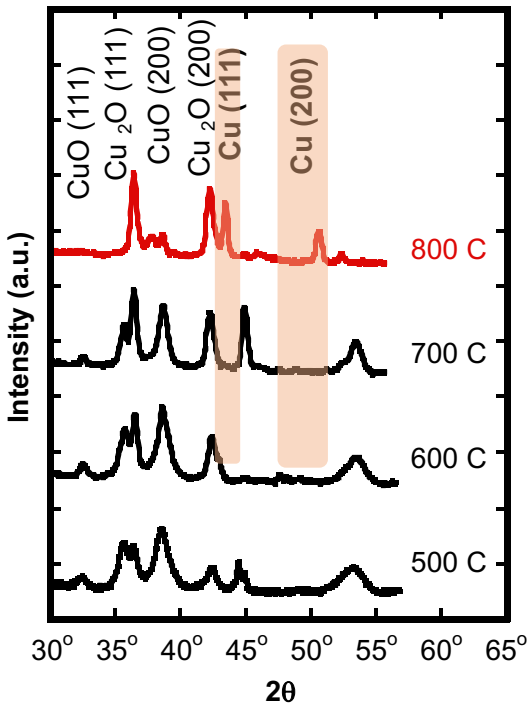

Cu formation ~800 ºC

3 BL Zr/CuO

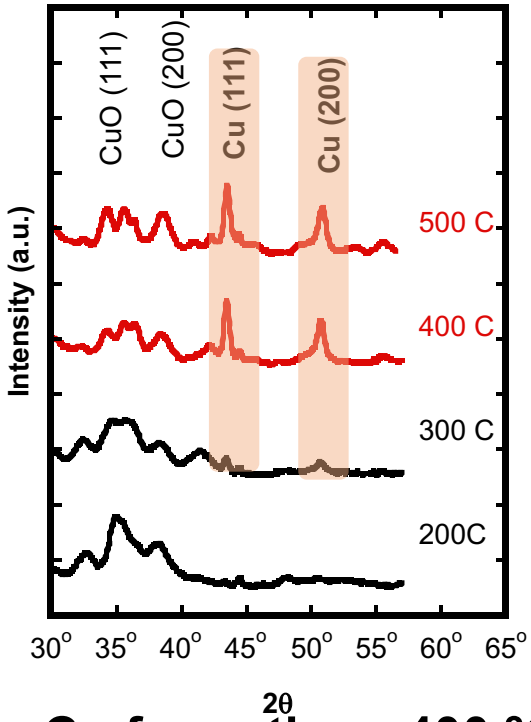

Cu formation ~400 ºC

E.J. Mily, PhD Defense, 2015

Can we tune reactivity by changing the oxidizer?

- Previous work:
  - Studied CuO paired with Al, Mg, Zr
  - Have seen Zr/CuO system is more sensitive than Al/CuO

- Ideal candidate: ZnO

ZnO Advantages

- Transparent film
  - For shock studies, advantageous
    - CuO acts as neutral density system
- Preferred growth orientation and crystallinity
- Zinc only has one oxidation state
  - Leads to robust computational models

Zr/ZnO 1-5 bilayer *ex situ* heating

- 1-5 bilayer Zr/ZnO on Si
  - 1 micron stack thickness
- Heated at 250 ºC, 350 ºC, 450 ºC, 550 ºC
- XRD for Zn

5 BL

- Zn onset at 350 ºC
  - seen in 2-5 BL at 350 ºC
  - Needs 550 ºC for 1 BL

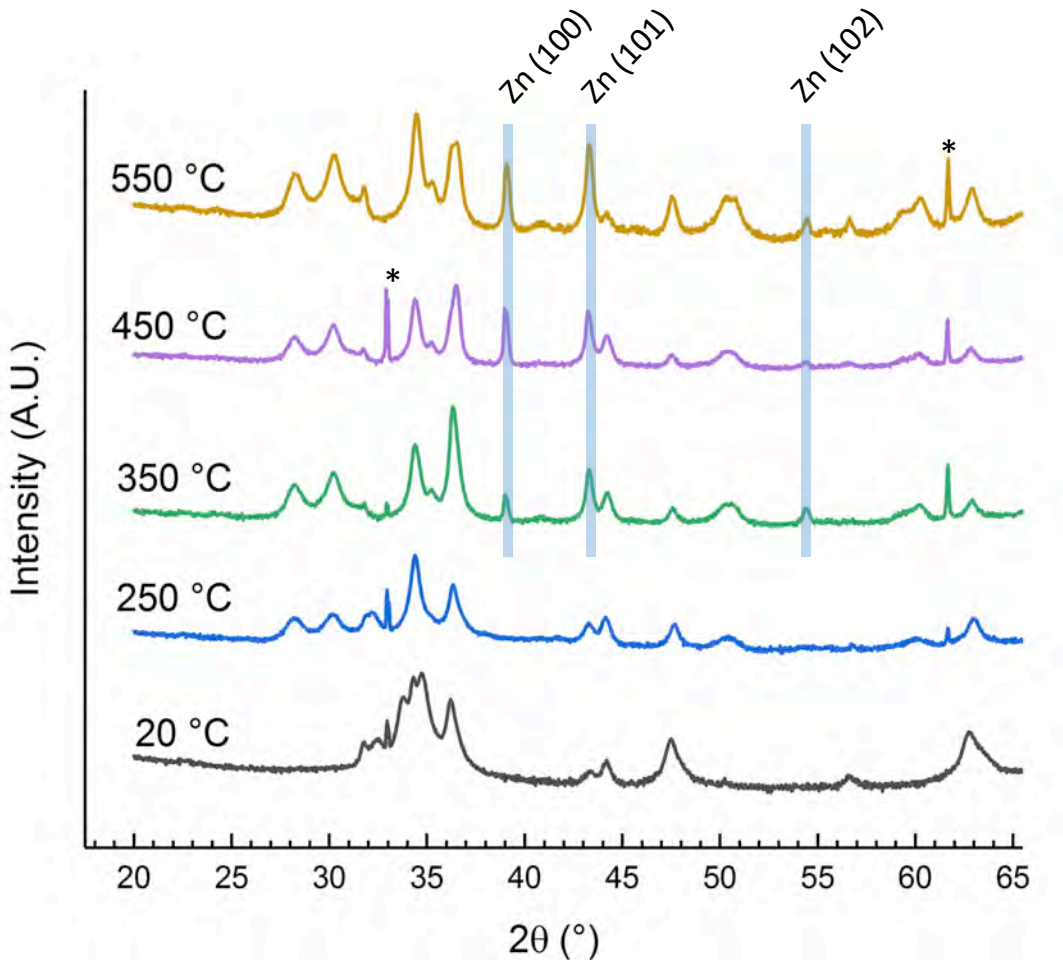

Zr/ZnO

- Formation of Zn means the system is reacting
- More stable than Zr/CuO
  - Currently, 4 BL Zr/CuO too reactive to remove from vacuum chamber
- Future work:
  - Higher bilayer samples, to find geometry threshold
  - DSC studies
  - Crystalline ZnO in 1 BL sample
  - *In situ* XRD

Outline

I. Introduction & Motivation

II. Intermetallic Formation in Nano-Thermite

I. Geometry of Thermite RNLs

I. Reactants of Thermite RNLs

I. Concluding Remarks

Concluding remarks

- Intermediate reaction mechanism possible in thermite RNL
- Thermite system more reactive with more bilayers present
- The Zr/ZnO system is reactive

Thermite reactivity can be engineered via geometry and constituents present in the system

Acknowledgements

- Special thanks to Dr. Donald Brenner and Dr. Michael Dickey for their time serving on the committee
- Dr. Jon-Paul Maria
- Dr. Sergey Matveev and Dr. Dana Dlott, Flyer Plate studies
- Dr. Christina Rost and Dr. Patrick Hopkins, TDTR
- Dr. Everett Grimley, Rachel Jackson, and Dr. James LeBeau, STEM
- Army Research Office
- Current and past Maria group members: Kyle Kelley, Kevin Ferri, George Ktsonis, Trent Borman, Delower Houssain, Richard Floyd Jr., Dr. Xiaoyu Kang, Dr. Christina Rost, Sarah Lowum, Dr. Evan Runnerstrom, Dr. Christopher Shelton, Dr. Edward Sachet, and Dr. Petra Hanusova


HAPPY
VALLEY
PENN
STATE
PSU

Thank you!

Thank you!

Thank you!

CuO laminate absorbance

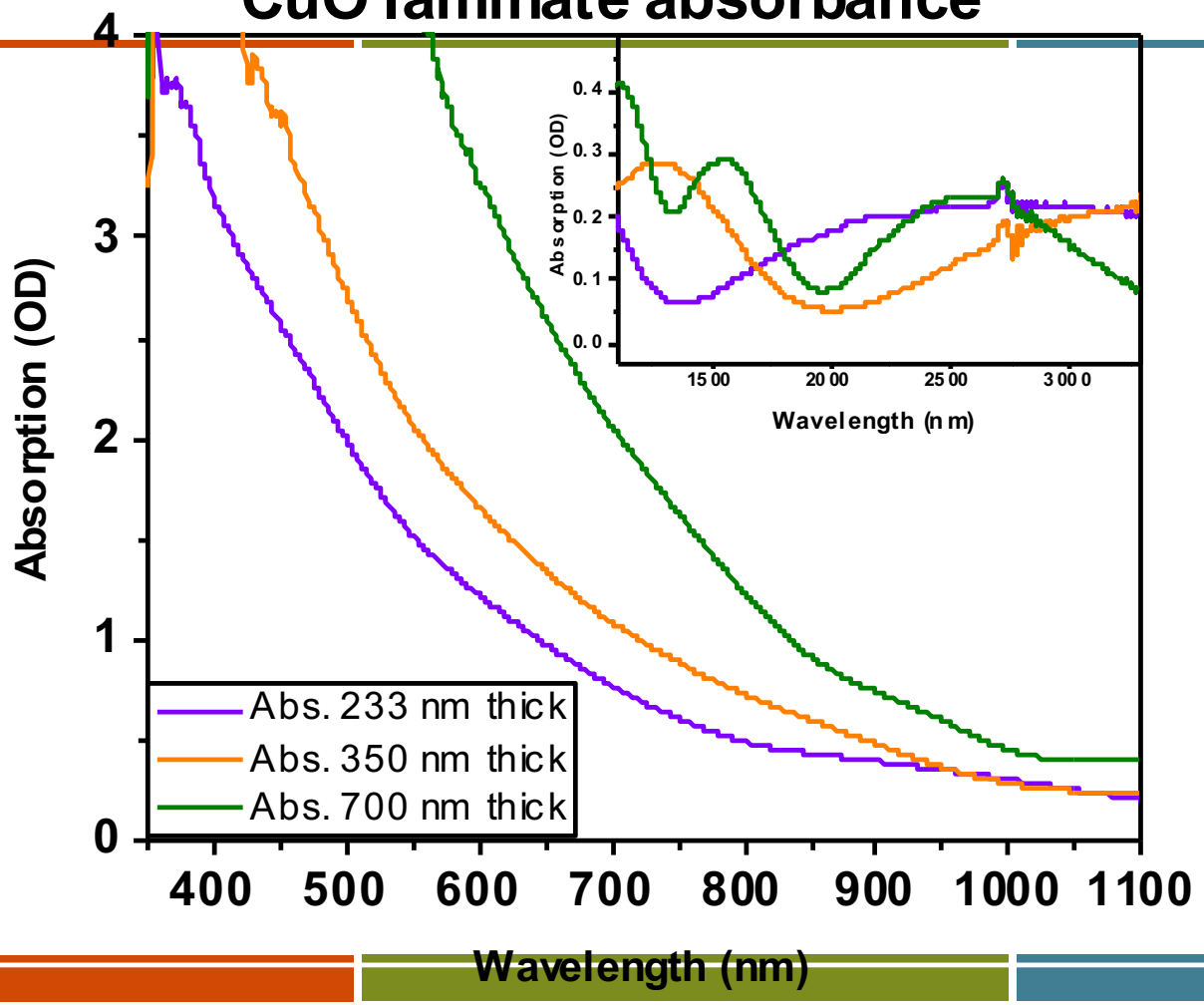

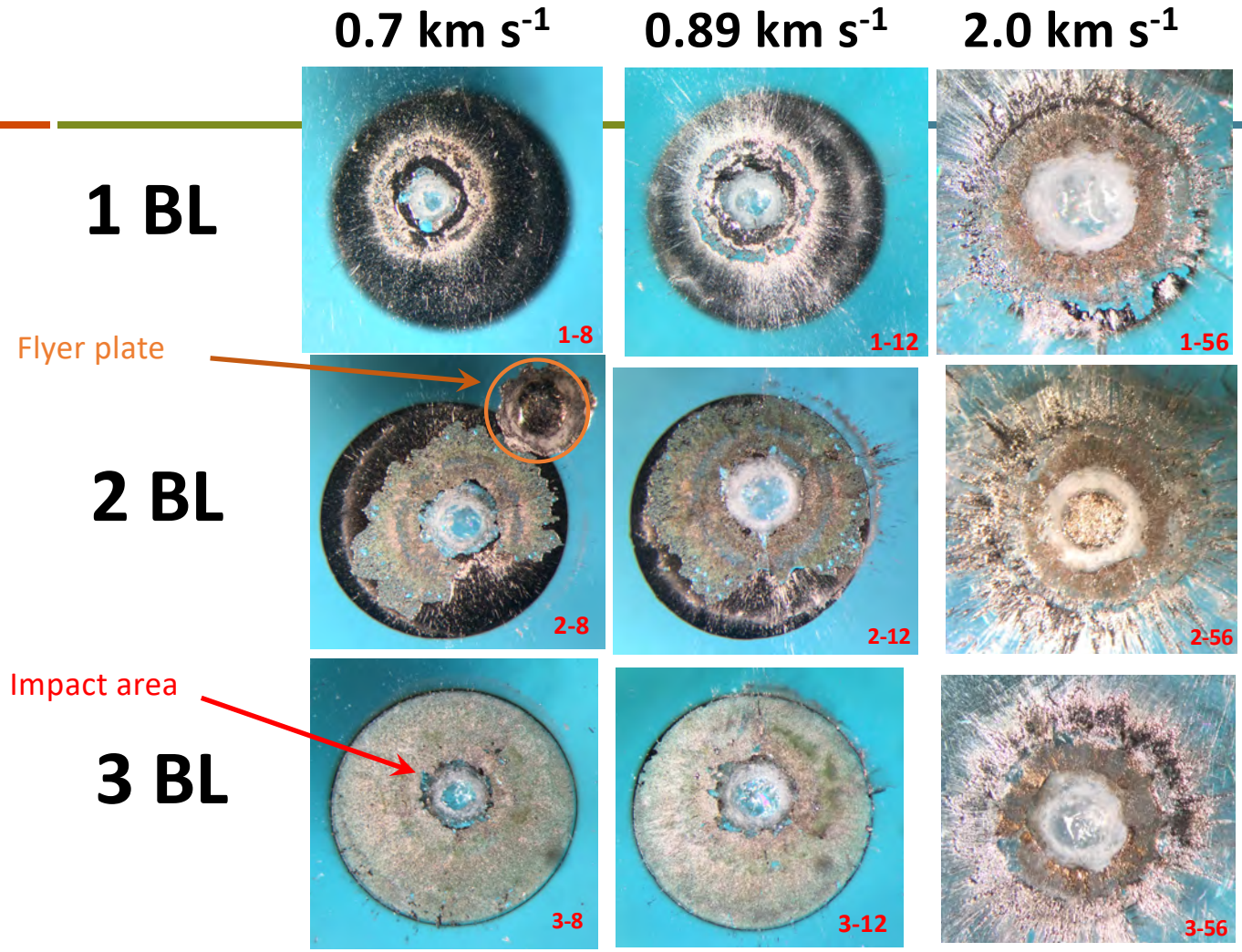
0.7 km s-1
0.89 km s-1
2.0 km s-1
1 BL
2 BL
3 BL
Flyer plate
Impact area
1-8
1-12
1-56
2-8
2-12
2-56
3-8
3-12
3-56

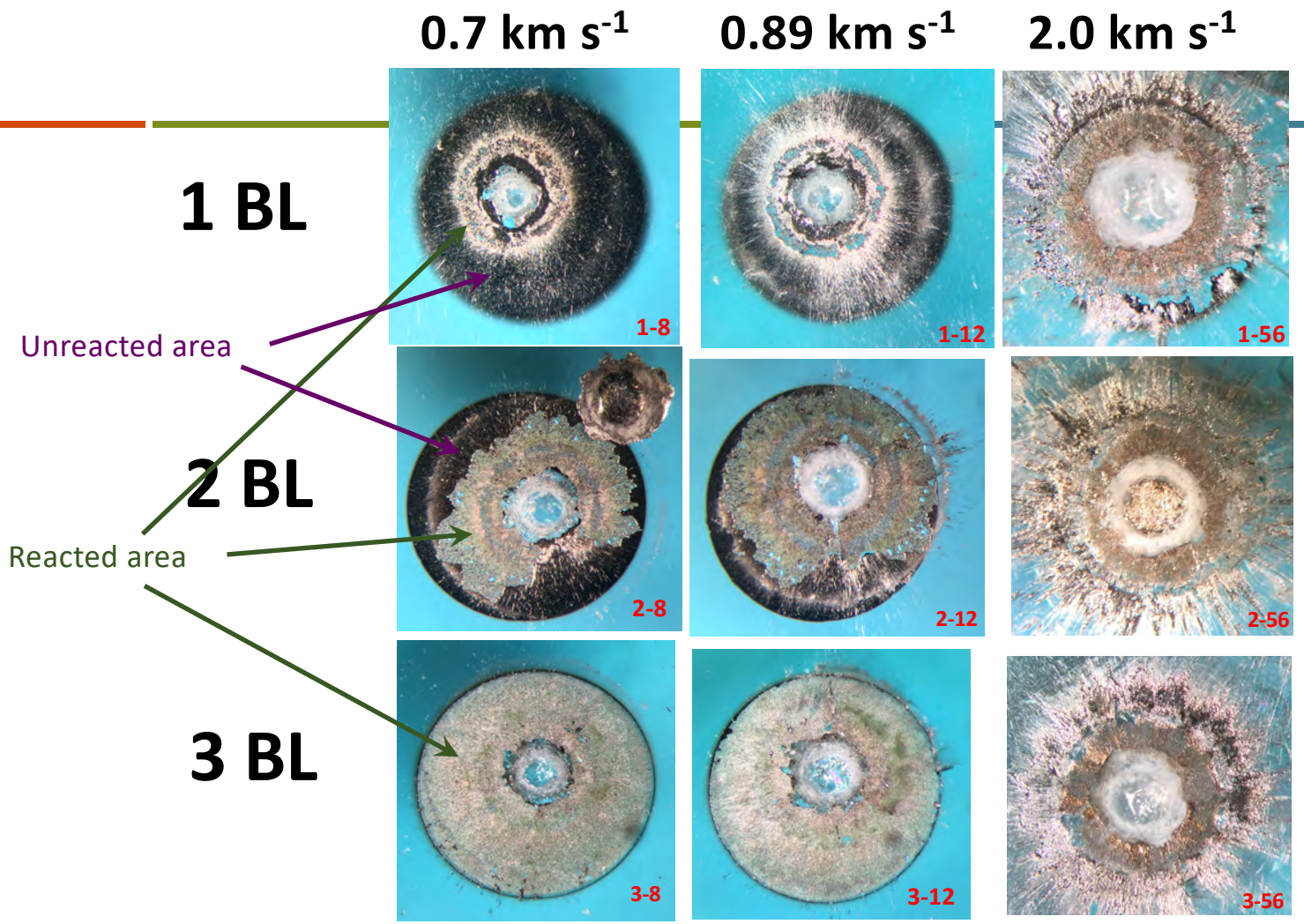
0.7 km s-1
0.89 km s-1
2.0 km s-1
1 BL
2 BL
3 BL
Unreacted area
Reacted area
1-8
1-12
1-56
2-8
2-12
2-56
3-8
3-12
3-56

Thermal Transport- move to end

- Previous work has given us information on heat generation
  - But what about heat dissipation?
  - To what extent does the increased interfacial density affect thermal conductivity of the stack?

Thermal Transport

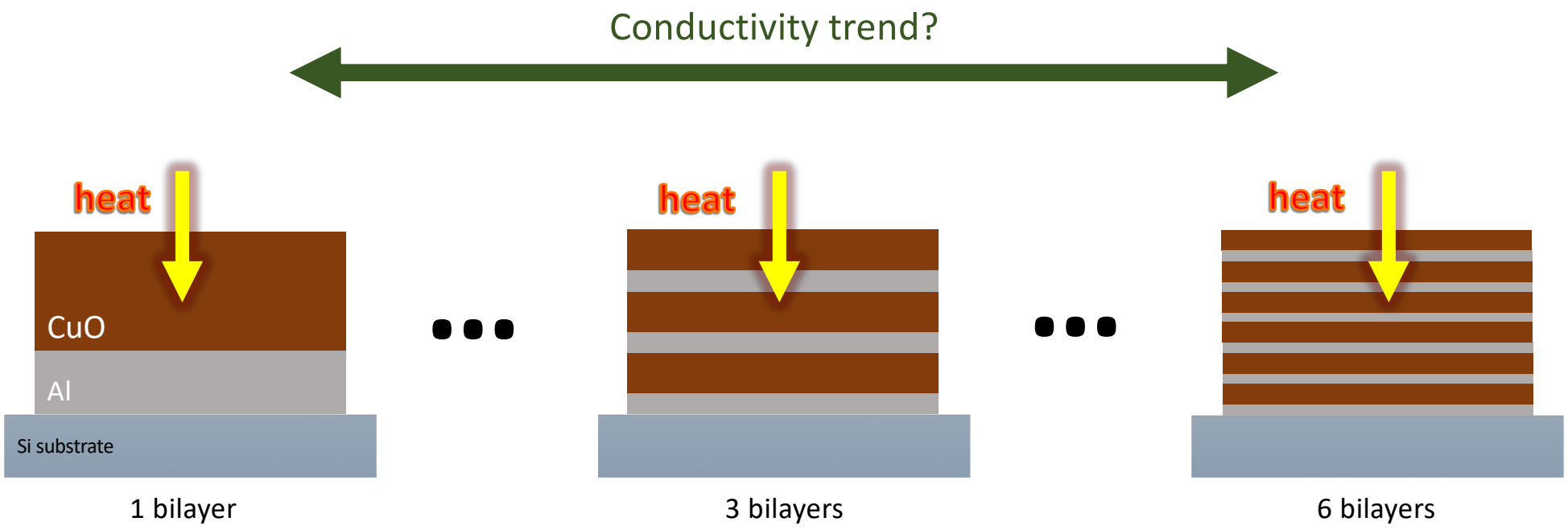

Time Domain Thermoreflectance TDTR

- Conducted by Hopkins group, measured by Dr. Christina Rost, University of Virginia
  - Relating thermal conductivity and interfacial density

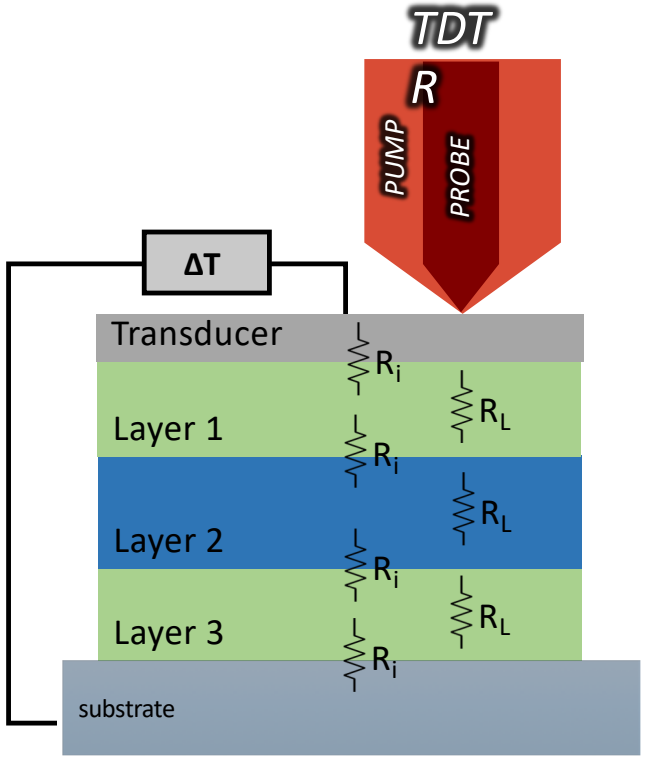

TDTR: TEM imaging Al/CuO RNL

- TDTR requires accurate thickness measurements

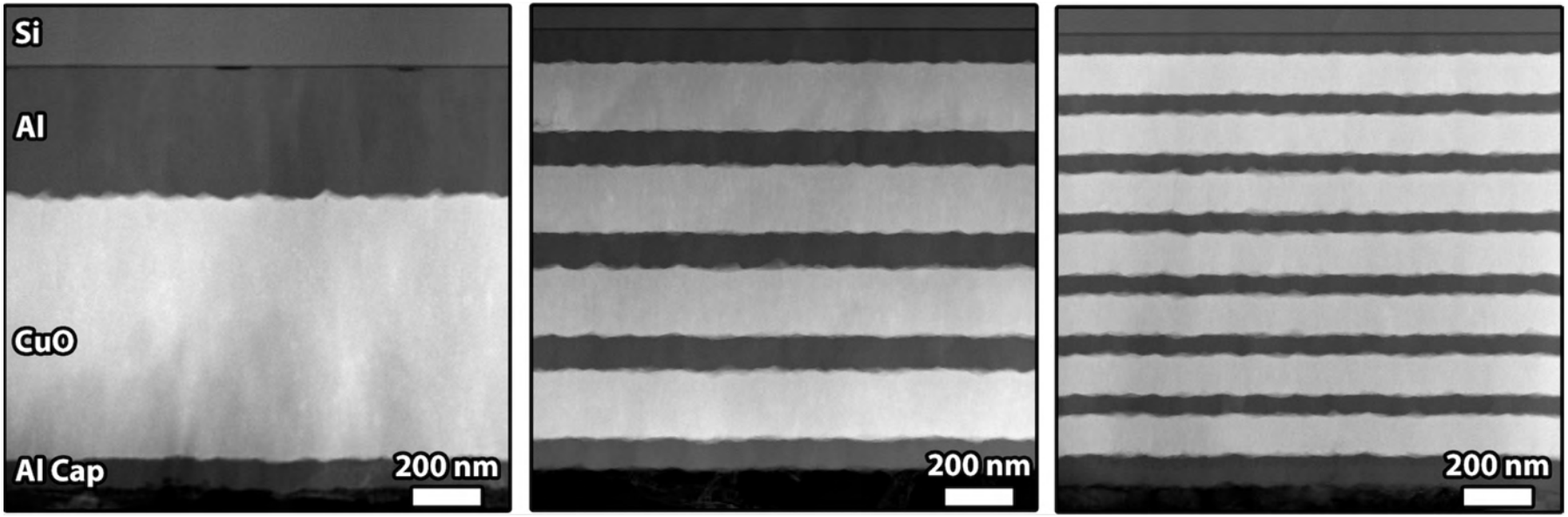

E. Grimley, R. Jackson, J. LaBeau, NCSU MSE 2017

Thermal analysis: Al/CuO stack

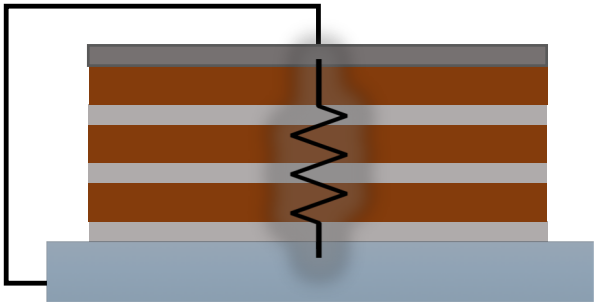

- **Thermal conductivity (k2)**: thermal conductivity of system as one collective layer
- k2- decreasing trend with increasing number of bilayers ~20%
- Roughness increases with more BL… source of decrease?

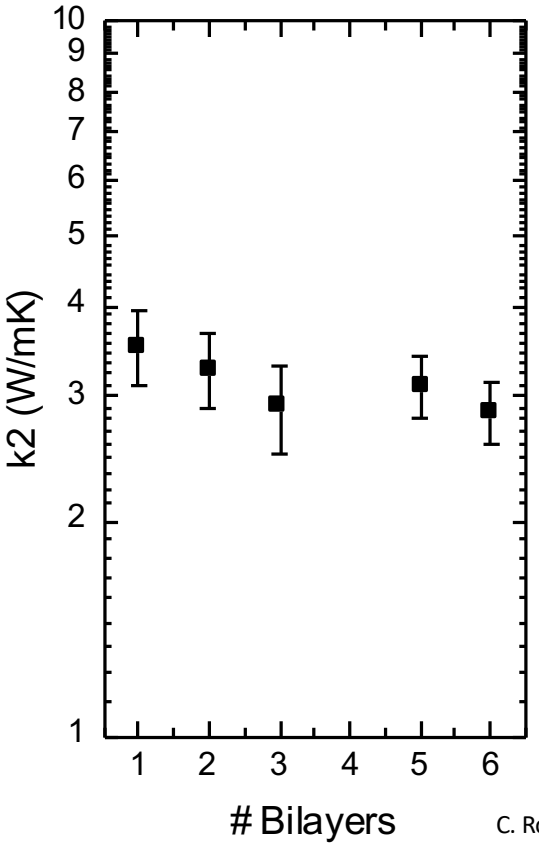

C. Rost, 2017

Thermal Analysis: Al transducer-CuO interface

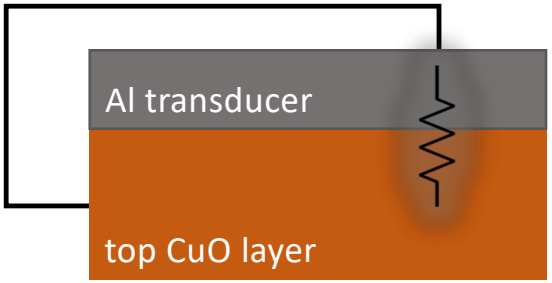

- **Interface conductance (G1):** between Al transducer and 1st CuO layer
- G1 is constant

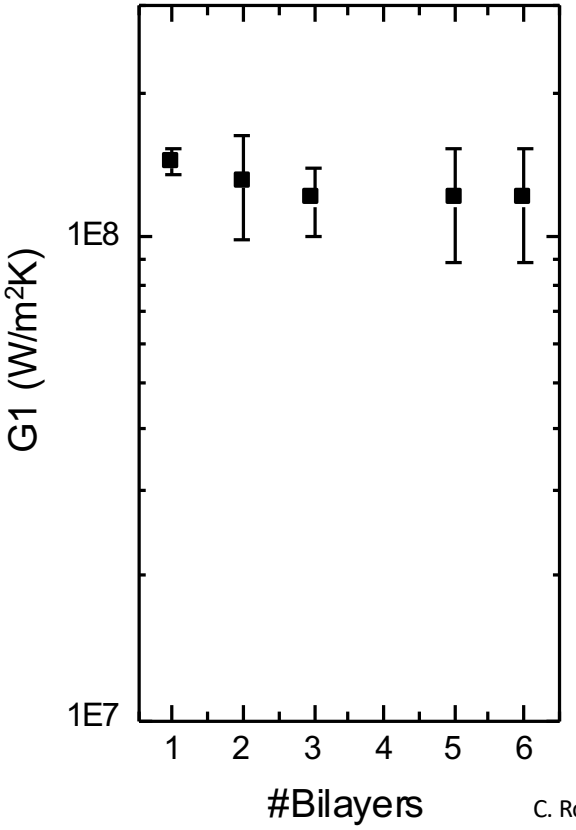

C. Rost, 2017

- Excess ZnO in all samples at 550 ºC
- Zn formation in all samples